GEOCHRONOLOGY AND GEOCHEMISTRY OF MID-MIOCENE BONANZA

LOW-SULFIDATION EPITHERMAL ORES OF THE

NORTHERN GREAT BASIN, USA

Except where reference is made to the work of others, the work described in this thesis is my own or was done in collaboration with my advisory committee. This thesis does not include proprietary or classified information.

_____
Derick Lee Unger

Certificate of Approval:

_____
James Saunders, Co-Chair
Professor
Geology and Geography

_____
Willis Hames, Co-Chair
Professor
Geology and Geography

_____
Robert Cook
Professor Emeritus
Geology and Geography

_____
Joe F. Pittman
Interim Dean
Graduate School

GEOCHRONOLOGY AND GEOCHEMISTRY OF MID-MIOCENE BONANZA

LOW-SULFIDATION EPITHERMAL ORES OF THE

NORTHERN GREAT BASIN, USA

Derick Lee Unger

A Thesis

Submitted to

the Graduate Faculty of

Auburn University

in Partial Fulfillment of the

Requirements for the

Degree of

Master of Science

Auburn, Alabama
May 10, 2008

GEOCHRONOLOGY AND GEOCHEMISTRY OF MID-MIOCENE BONANZA

LOW-SULFIDATION EPITHERMAL ORES OF THE

NORTHERN GREAT BASIN, USA

Derick Lee Unger

_____

Signature of Author

_____

Date of Graduation

iii

VITA

Derick Unger, the son of David and Sherri Unger, was born July 23, 1982 in Sullivan, Indiana. He graduated from Sullivan High School in 2000 and continued on to Indiana State University were he received his Bachelor's of Science degree in spring 2005. He entered the Graduate School at Auburn University in fall 2005. In the summer of 2007 he began working as an exploration geologist for Victoria Resources Corporation in northern Nevada.

THESIS ABSTRACT

GEOCHRONOLOGY AND GEOCHEMISTRY OF MID-MIOCENE BONANZA

LOW-SULFIDATION EPITHERMAL ORES OF THE

NORTHERN GREAT BASIN, USA

Derick Lee Unger

Master of Science, May 10, 2008
(B.S. Indiana State University, 2005)

152 Typed pages

Directed by James Saunders and Willis Hames

Ore petrography, geochemistry, and geochronology data collected for some low-sulfidation epithermal precious metal deposits in the northern Great Basin indicate that the mid-Miocene deposits have consistent ore mineralogy, geochemistry that varies between two end members, and a narrow range of ages. These deposits are coeval with bimodal volcanism and often classified as "volcanic-hosted." However, a number of deposits in this study are not hosted by volcanic rocks and it appears that the host rock may significantly affect gangue mineralogy. New high precision $^{40}Ar/^{39}Ar$ geochronology

conducted on previously undated deposits (or deposits with older, less precise K/Ar dates only), indicates that low-sulfidation epithermal Au-Ag mineralization in the northern Great Basin began around 16.5 Ma and continued until at least 15.6 Ma. This time frame adds further support to the hypothesis that these deposits are genetically related to the emergence of the Yellowstone hotspot near the present day intersection of the Idaho, Nevada and Oregon boarders. High-grade bonanza ores in these deposits consist of precious metal minerals inter-grown with quartz and adularia ($KAlSi_3O_8$). The intimate association of precious metals with adularia, an ideal mineral for use in $^{40}Ar/^{39}Ar$ geochronology, allows for unambiguous dating of the precious metal mineralization event. For this study, five adularia crystals from each sample location were analyzed individually rather than as a bulk sample. The effects of argon loss or gain are much more evident in single crystal analysis and thus can be mitigated during the final age calculation.

Deposits in or near the Slumbering Hills (Jumbo, New Alma, Sandman and Ten Mile) northwest of Winnemucca, Nevada as well as two locations on War Eagle Mountain, Silver City District, Idaho, were selected for geochronologic study. A new younger age of 16.53 ± 0.04 Ma at the 1σ confidence level was determined for the Jumbo deposit. Evidence for excess Ar was found in the samples from Jumbo, which likely explains an anomalously old date of 17.3 Ma that was previously determined using K/Ar methods. The youngest deposit in the Slumbering Hills area is the New Alma deposit (16.03 ± 0.07 Ma), which sits just south of the Jumbo deposit. The Ten Mile and Sandman deposits fall in between with ages of 16.52 ± 0.04 Ma and 16.17 ± 0.04 Ma respectively. The presence of the recently mined Sleeper deposit and the Sandman

deposit, which is a current exploration target, indicates the Slumbering Hills area may host other significant bonanza ores. War Eagle Mountain vein samples yielded ages of 16.31 ± 0.04 Ma and 15.61 ± 0.10 Ma. The geochronology data as a whole indicate that precious metal mineralization occurred in the region for a period of at least 1 Ma.

Suites of ore samples from several low-sulfidation deposits in the northern Great Basin were collected to examine similarities and contrasts in the mineralogy and geochemistry. Polished thin section petrography and geochemical data indicate that the most common precious metal minerals are electrum and Ag-selenides, Ag-sulfides, and Ag-sulfosalts. A new classification scheme, the "epithermal trilinear diagram," based on metal and metalloid contents in these ores, was devised to examine geochemical properties within and amongst deposits. Each geochemical sample plots as a point on a trilinear diagram based on certain metal (Au, Ag, Pb) and metalloid (As, Sb, Te, Se) molar ratios. For the sake of comparison, some low-sulfidation ores from Colorado and Japan were included in this portion of the study. This new classification scheme indicates deposits fall between two end members being either Ag-Se or Au-Te rich. The Colorado ores analyzed all fall in or near the Au-Te field, whereas samples from the northern Great Basin and Japan generally plot in or near the Ag-Se field. The greatest determining factor in where a sample falls in this technique is the metalloid content.

The high-grade nature of low-sulfidation epithermal precious metal deposits makes them attractive for mining. However, their relatively small deposit footprint and susceptibility to erosion makes them difficult exploration targets. A better genetic and exploration model can be developed by understanding factors such as the limited age

range for formation, the broader range of host rocks than generally recognized, and the

typical geochemical signature of these deposits.

ACKNOWLEDGEMENTS

Style manual or journal used: <u>Economic Geology</u>

Computer software used: Microsoft Word, Microsoft Excel, Microsoft Powerpoint,

Isoplot, Minitab, Adobe Illustrator, Adobe Photoshop

TABLE OF CONTENTS

LIST OF FIGURES

LIST OF TABLES

INTRODUCTION

The complex geologic history of the northern Great Basin has resulted in a wealth of mineral resources including huge endowments of Au and Ag. The mid-Miocene low-sulfidation epithermal precious metal deposits of the northern Great Basin are attractive for mining because they frequently contain bonanza grades and can have Au contents of several million ounces (Simmons et al., 2005). However, due to their small size and susceptibility to erosion, this type of deposit remains a difficult exploration target. A better understanding of the genesis of low-sulfidation epithermal precious metal deposits could lead to new and more effective methods of exploration.

Worldwide, low-sulfidation epithermal precious metal deposits have been attributed to a variety of extensional tectonic settings (Sillitoe and Hedenquist, 2003). During the mid-Miocene the northern Great Basin experienced extension and rifting-related bimodal volcanism that has been linked to the formation of the low-sulfidation epithermal precious metal deposits in the region (John, 2001). The first volcanism related to the Yellowstone hotspot also occurred in the region during this time (Brueseke et al., 2007). The genetic link between the mid-Miocene Au-Ag deposits and the initiation of the Yellowstone hotspot was first proposed by Saunders et al. (1996). A strong temporal and spatial relationship exists between the first volcanism of the Yellowstone hotspot and the mid-Miocene deposits (see below). However, a number of questions about the genesis

of these deposits remain including: what role (if any) the Yellowstone hotspot played in their formation and, from what source the Au, Ag, and other epithermal suite elements were derived?

The lack of exploration activity in the northern Great Basin during the late 1990's and early 2000's has meant very few new deposits of this type have been discovered or researched. Thus, only a small number of deposits have been evaluated using modern methods of geochronology and geochemistry. This study sought to provide new geochronology data for low-sulfidation epithermal precious metal deposits in the northern Great Basin that had either been significant historic producers or are the target of current exploration. Additionally, a broader look at other northern Great Basin mid-Miocene low-sulfidation deposits was preformed, along with ores from deposits in Colorado and Japan for comparison, to contrast ore mineralogy and geochemistry.

The possibility that these deposits could be related to a mantle plume has important exploration implications. Not only would other areas worldwide with past or present mantle plume activity represent prospective targets but, the areas further east of the northern Great Basin within the Yellowstone hotspot track may also represent areas of potential.

PREVIOUS WORK

Low-sulfidation Epithermal Precious Metal Systems

Epithermal systems form at shallow depths (<2 km) and low temperatures (< 300º C) and are classified as high-sulfidation, intermediate-sulfidation, and low-sulfidation based on ore mineralogy, alteration, and gangue mineral assemblages (Hedenquist and Lowenstern, 1994; Simmons et al., 2005). Low-sulfidation hydrothermal systems are generally associated with bimodal (basalt-rhyolite) or intermediate composition volcanism in a wide range of extensional tectonic settings (e.g., Sillitoe and Hedenquist, 2003). The ore-forming fluids in low-sulfidation hydrothermal systems are low-salinity, near-neutral pH, sulfide-dominated, and reducing (Hedenquist and Lowenstern, 1994). Low-sulfidation deposits most often form distal from the magmatic heat source (Sillitoe 1989). These deposits are shallowly emplaced and easily eroded, thus few deposits older than Tertiary age are known.

A number of larger low-sulfidation epithermal Au-Ag deposits in the northern Great Basin have been the subject of one or more papers including: Midas (Goldstrand and Schmidt, 2000; Leavitt et al., 2004), Hollister (Bartlett et al., 1991; Wallace, 2003), Mule Canyon (John et al., 2003), Ten Mile (Bowell et al., 2000), Sleeper (Saunders, 1990; Conrad et al., 1993; Saunders, 1994; Saunders and Schoenly, 1995; Nash et al., 1995), National and Buckskin-National (Vikre, 1985; Vikre 1987; Vikre 2007).

3

Epithermal precious metal deposits have also been examined in a regional context by John (2001) and John et al. (1999). These studies have established a number of general characteristics of low-sulfidation epithermal precious metal deposits in the region, including their relationship to extensional tectonism and bimodal volcanism.

The ore textures for low-sulfidation epithermal precious metal deposits in the northern Great Basin and abroad have been well documented by a number of deposit-specific and overview studies (see above). Colloform banded-veins, attributed to multiple pulses of mineralizing fluids, have been reported at many well-known deposits. Alternating layers of quartz, chalcedony, adularia, calcite, clay, electrum, Ag-selenides, Ag-sulfides, Ag-sulfosalts, and/or base metal sulfides have been noted at: National and Buckskin National (Vikre, 1985; Vikre, 2007), Hishikari (Izawa et al., 1990), Sleeper (Saunders, 1994; Saunders et al., 1996), Hog Ranch (Bussey, 1996), Midas (Goldstrand and Schmidt, 2000), and Mule Canyon (John et al., 2003). Adularia has long been recognized as a common gangue mineral in these deposits and was first reported in the region by Lindgren (1898) in the Black Jack-Trade Dollar vein on Florida Mountain in the Silver City district, Idaho. Adularia encrustations on open fractures are a common texture at the Jumbo, New Alma, Sandman and Ten Mile deposits in this study, and similar textures have been reported at Martha Hill, New Zealand (Simmons et al., 2005). Electrum dendrite textures were reported and shown to vary according to depth and temperature at the Jumbo, Midas, National, Seven Troughs, Sleeper, and Ten Mile deposits by Saunders et al. (1996). This texture indicates that Au and Ag were transported as colloids and deposited rapidly from supersaturated fluids (Saunders 1994; Saunders et al., 1996). Bladed calcite and its psuedomorphic replacement by quartz are considered

indicators of boiling in an epithermal system (Simmons and Christensen, 1994). Such textures have been observed at National and Buckskin National (Vikre, 1985), Sleeper (Saunders, 1994), Midas (Goldstrand and Schmidt, 2000), Mule Canyon (John et al., 2003), and Martha Hill, New Zealand (Simmons et al., 2005). Additionally, at Midas, Goldstrand and Schmidt (2000) reported the deposition of Au/Ag-minerals on the leeward side of quartz, suggesting they were transported as colloids. That study also found Au/Ag-mineral deposition at or near quartz-adularia boundaries, similar textures are present in some samples collected for this study.

Precious Metal Source

  The ultimate source of the precious metals in low-sulfidation epithermal systems is an issue that has been debated for over one hundred years. The two most common theories propose metals are either leached from local host rocks or derived from magmas. A previous study by John (2001), of mid-Miocene low-sulfidation epithermal deposits in the northern Great Basin, determined these deposits are related to a bimodal volcanic assemblage of mid-Miocene age. However, John (2001) states that the precise role that magmas had in the formation of these deposits "remains ambiguous." As recently as the 1990's some deposit models suggested that metals were sourced from leaching of local host rocks (e.g., Sleeper, Nash et al., 1995). The Hedenquist and Lowenstern (1994) model links epithermal precious metal deposits to porphyry systems; and indicates magmatic fluids are important contributors to epithermal hydrothermal systems (Fig. 1).
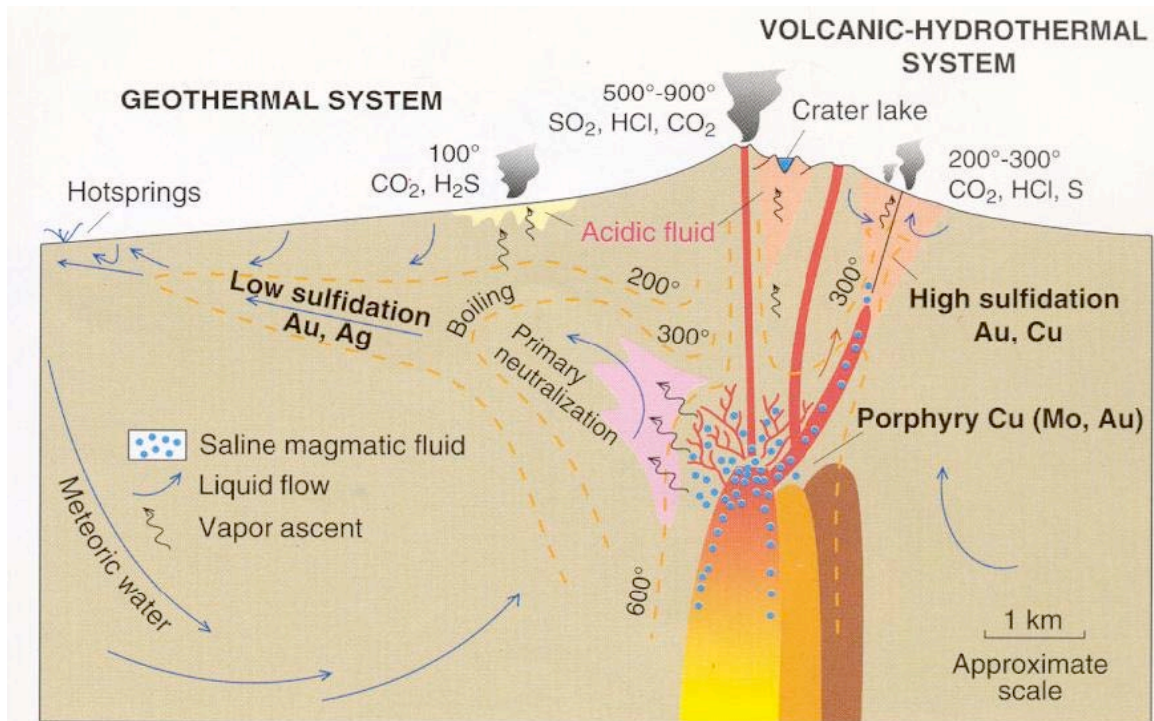
FIG. 1. Diagrammatic illustration of the "porphyry-epithermal" transition and possible associated deposit types, modified form Hedenquist and Lowenstern (1994).

Later work has shown that magmatic fluids can transport Au from the porphyry environment into shallower epithermal systems (Heinrich et al., 2004; Heinrich, 2005). Deep hydrothermal waters at an actively-forming low-sulfidation Au deposit at Lihir Volcano, contain extremely high levels of dissolved Au as bisulfide complexes (Simmons and Brown, 2006), which suggests that epithermal Au deposits could form in time spans of tens of thousands of years, or less (Heinrich, 2006). Lead-isotope data from the same deposit (Ladolam, Lihir Island) also indicates that ore metals were derived from a single volatile-rich magma pulse, rather than hydrothermal leaching of the local volcanic host rocks (Kamenov et al., 2005). It has also been suggested that basaltic rather than rhyolitic magmas maybe responsible for Au-bearing fluids. There are some geochemical and isotopic data to support this theory (Noble et al., 1988; Connors et al., 1993; Kamenov et

al., in press), as well as petrography from another study that found native gold and copper blebs present in olivine phenocryst in a picrite lava (basalt) (Zhang et al., 2006).

Regional Geology

The complex geologic history of the northern Great Basin has resulted in numerous mineralizing events and deposit types. During the Nevadan, Elko, Sevier, and Laramide orogenies (Mesozoic to early Cenozoic), east-dipping subduction beneath western North America resulted in accretion of island arc terranes to the west in California, Cordillera-wide contraction from west to east, and widespread calc-alkaline magmatism throughout the northern Great Basin (John, 2001). A transition to extension occurred in the late Eocene, possibly due to the removal of the subducted Farallon plate from the North American lithosphere (Cline et al., 2005). Concurrent initiation of high-K calc-alkaline magmatism and formation of most Carlin-type Au deposits occurred between 42 and 36 Ma (Cline et al., 2005). Although strong temporal and spatial relationships exist, the role of magmatism in the formation of Carlin-type deposits is still debated (see discussion in Muntean et al., 2004). Beginning about 17 Ma, extension became more widespread and along with coincident bimodal volcanism created the Basin and Range physiography of the region today (John, 2001).

The earliest stages of bimodal volcanism, including that associated with the northern Nevada rift, have been attributed to either back-arc extension and/or the impingement of the Yellowstone hot spot with the upper crust (Brueseke et al., 2007). Early workers noted the association of basalt dike swarms with a single prominent magnetic anomaly, which represents the northern Nevada rift (Zoback and Thompson,

1978; Zoback et al., 1994). Further work by Ponce and Glen (2002) identified three additional linear aeromagnetic highs, which they interpret to be subparallel rifts similar in composition and genesis to the northern Nevada rift. All of these rifts are spatially associated with mid-Miocene bimodal volcanic centers. A strong spatial link between the rifts and mid-Miocene epithermal Au-Ag deposits exists (Ponce and Glen, 2002) and rift related igneous activity is reported to have occurred predominately between 16.5 and 15 Ma (John et al., 2000). It has also been suggested that the development of the northern Nevada rift and a number of other large-scale fractures in northern Nevada is related to the Yellowstone hotspot (Zoback and Thompson 1978; Zoback et al., 1994; Pierce et al., 2000; Glen and Ponce, 2002). However, there is no consensus on where the Yellowstone hotspot originated, and by what mechanism it formed the large-scale fractures. Recent detailed studies of the Santa Rosa-Calico Range, the host of the National district, suggest that volcanism (at least in that study area) contains numerous intermediate compositions and therefore is not strictly bimodal as previously thought (Brueseke and Hart, 2004). Basaltic volcanism in the Santa Rosa-Calico range and at Steens Moutain occurred from about 16.73 ± 0.04 to 14.35 ± 0.38 Ma and 16.58 ± 0.18 to 15.51 ± 0.28 Ma respectively (Brueseke et al., 2007). These ages are some of the earliest for mid-Miocene bimodal volcanism in the Great Basin and may reflect the initiation of the Yellowstone hotspot in the region.

Geology of Mining Districts

Slumbering Hills: The Slumbering Hills and surrounding pediment contain a number of low-sulfidation Au-Ag deposits that have been significant recent or historic

producers including the Jumbo, New Alma, Sleeper, and Ten Mile deposits as well as the

Sandman deposit, which is currently being evaluated for resource potential. The

Slumbering Hills consist primarily of Mesozoic slates and phyllites of the Auld Lang

Syne Group as well as a Cretaceous granitoid stock (Willden, 1964). Unconformably

overlying these are Tertiary volcanics including ash-flow tuffs that correlate with tuffs of

the McDermitt volcanic field to the north (Rytuba and McKee, 1984; Rytuba, 1989).

The Awakening district is located in the northern half of the Slumbering Hills and

hosts a number of mineral deposits including the historically mined Jumbo and New

Alma deposits as well as the recently mined Sleeper deposit. The gold-bearing quartz-

adularia stockwork-veins at Jumbo and New Alma are primarily hosted in Mesozoic

metamorphosed argillaceous rocks (Willden 1964). Production at the Jumbo deposit up to

1963 approached $1,000,000 (Willden, 1964). The Sleeper deposit sits just northwest of

Jumbo in the pediment and was originally covered by 10 to 50 m of alluvium (Conrad et

al., 1993). Production at the mine occurred from 1986 to 1996 with over 1.6 Moz. of Au

recovered (Conrad and McKee, 1996; John, 2001). Tertiary volcanics in the Sleeper

mine area consist of a basil unit of volcaniclastic rocks followed by intermediate

composition lava flows and lapilli tuff (Conrad et al., 1993). These units are overlain by

the major ore host at the Sleeper deposit, rhyolite porphyry emplaced from 16.5 to 16.3

Ma just prior to eruption of peralkaline volcanics from the McDermitt volcanic field to

the north (Conrad and McKee, 1996). The main period of high-grade Au/Ag vein

formation began around 16.1Ma and is though to have continued for about 700,000 yrs.

(Conrad and McKee, 1996). The other volcanic rocks in the Slumbering Hills are

significantly younger than the Sleeper veins and rhyolite porphyry host rock; these units

do not appear to have a connection with any mineralization or alteration at the Sleeper deposit (Conrad and McKee, 1996).

To the south of the Slumbering Hills and 15 km northwest of Winnemucca, Nevada is the Ten Mile district. The Ten Mile district contains low-sulfidation adularia-sericite type deposits hosted in argillaceous-arenite rocks of the Triassic Raspberry Formation (Bowell et al., 2000). These deposits are unique in that unlike the other northern Great Basin deposits in this study, they share no known temporal or spatial relationship to Miocene rhyolites, and none are present within the district (Nash, 1972; Saunders et al., 1996). Production in the district is believed to have been about 20,000 oz. Au from 1900 through 1942 (Bowell et al., 2000). Just north of the Ten Mile district is the Sandman deposit previously drill by Newmont Gold and currently the subject of exploration activity by Fronteer Development Group (acquired from New West Gold) (www.fronteergroup.com). Current measured and indicated resources at the property are 271,000 oz. Au (Fronteer press release, Nov. 6, 2007).

Northern Carlin Trend: The Carlin Trend is an approximately 37 mile long north-northwest alignment of Eocene sediment-hosted gold deposits, located near the town of Carlin, Nevada (Teal and Jackson, 1997). Unlike the rest of the Carlin Trend, the northern Carlin Trend hosts the Midas and Ivanhoe mining districts, which contain Miocene low-sulfidation epithermal precious metal deposits. These deposits differ considerably from the Eocene age Carlin-type deposits, which tend to be large low-grade disseminated gold-silver deposits (Cline et al., 2005). The relationship between the Eocene and Miocene deposits is not clear. It has been suggested that the Midas district could represent the northern extension of the Carlin Trend and, that the deposits there

formed during Miocene reactivation of a regional dextral and normal slip fault zone (Goldstrand and Schmidt, 2000). The Midas and Ivanhoe districts also are located near the eastern margin of the Northern Nevada Rift, which shares a strong temporal and spatial relationship with many of the low-sulfidation epithermal precious metal deposits of the northern Great Basin (see above).

The Midas district hosts numerous historic workings along with the currently active Ken Snyder mine. Host rocks in the Midas district consist of a bimodal suite of felsic ash-flow tuffs, flows, plugs, volcaniclastic sediments along with mafic sills and dikes (Goldstrand and Schmidt, 2000). Hydrothermal activity at Midas appears to have begun around 15.6 Ma at the earliest and continued until 15.2 Ma (Leavitt et al., 2004). Volcanics associated with mineralization in the Midas area include the red rhyolite and Sawtooth dike, which have ages of 15.6 and 15.4 Ma respectively (Leavitt et al., 2004). Ages for high-grade veins in the district range from 15.4 to 15.3 Ma (Leavitt et al., 2004).

The Ivanhoe district sits approximately 15 km to the southeast of the Midas district. It contains very similar epithermal precious metal deposits along with related mercury deposits. Early mining activity focused on cinnabar-bearing hot spring-type sinter and silica replacement deposits hosted in volcanic and sedimentary rocks (Wallace, 2003). Later exploration activities identified several disseminated gold resources beneath the mercury deposits, one of these being the Hollister deposit (Wallace, 2003). During the early 1990s low-grade disseminated gold ores were mined from two open pits (Hollister et al., 1992; Tewalt, 1998). Later deep drilling by Great Basin Gold Ltd. (www.greatbasingold.com) identified a series of high-grade gold-silver veins, hosted in Ordovician sedimentary rocks, near the Hollister open pits (Price, 2001). The

disseminated ores have been dated at 15.1 ± 0.4 Ma with K-Ar (Barlett et al., 1991) and the nearby vein deposits are 15.16 ± 0.05 Ma (Peppard, 2002). This overlap in uncertainties along with oxygen isotope data suggests that both deposits, along with the overlying mercury sinter deposits, are related to the same hydrothermal system and, that the veins served as feeders for the near-surface mercury and disseminated gold deposits (Peppard, 2002; Wallace, 2003). Mercury-gold mineralization in the district occurred from about 15.2 to 14.9 Ma along with rhyolitic volcanism and high-angle faulting (Wallace, 2003).

Silver City, Idaho: The area surrounding Silver City in southwest Idaho contains the War Eagle Mountain and Florida Mountain deposits in the Silver City district and neighboring DeLamar deposit in the DeLamar district. Historic production first began in the Silver City area on War Eagle Mountain in the 1860's, followed by production at DeLamar in 1890, and Florida Mountain in 1892 (Lindgren, 1900). Production at War Eagle Mountain had nearly ceased and many of the old workings were inaccessible by the time Lindgren examined the area in 1897 (Lindgren, 1900). The Oro Fino vein system is credited as the most productive on War Eagle Mountain and produced $7 million in gold and silver ore (Lindgren, 1900). Adularia (called valencianite by Lindgren) is also noted as common gangue mineral in some of the veins at War Eagle Mountain, Florida Mountain and DeLamar (Lindgren, 1898; Lindgren 1900). Lindgren's 1898 report is the first published account of adularia in the northern Great Basin.

More recently, the DeLamar silver mine to the west of Silver City produced 17 million ounces of silver and 230 thousand ounces of gold from 1977 to 1987 (Halsor et al., 1988). The deposits in both the DeLamar and Silver City districts share a temporal

and spatial relationship with the western Owyhee volcanic field, which consists of middle Miocene basalts and younger middle Miocene rhyolites (Halsor et al., 1988). These volcanics are underlain by granite of quartz monzonite to granodiorite composition that appears to correlate with the Idaho batholith based on petrologic similarities and a radiometric age of 65 Ma (Asher, 1968; Pansze, 1975). The middle Miocene volcanics of the Owyhee volcanic field are mostly absent on War Eagle Mountain but are abundant to the west in the area surrounding the DeLamar mine (Halsor et al., 1988). Basalts up to 800 m thick form the basal unit and have been dated using whole rock K-Ar methods to be 16.6 ± 4.3 Ma (Asher, 1968; Pansze, 1975). Overlying the basalts are pre- and postmineralization rhyolites. Premineralization rhyolites consist of coalescing flows from multiple volcanic sources and include the Silver City rhyolite (Asher, 1968). Ages for this unit cluster around 16.0 Ma (Pansze 1975). Postminerlization units exposed in the area include the Swisher Mountain tuff (Ekren et al., 1981), which is believed to be around 14 Ma based on ages for a correlative rhyolite at Poison Creek (Neill, 1975). North to northwest trending high-angle faults host veins at DeLamar and War Eagle Mountain (Halsor et al., 1988). Movement of up to several hundred meters is predominately vertical and pre- and postdates the emplacement of the basalts and rhyolites (Pansze, 1975; Ekren et al., 1981; Thomason, 1983). These faults are thought to be related to Basin and Range extension and rifting in the Snake River Plain (Pansze, 1975).

National: The National district is located in northern part of the Santa Rosa Mountains in north central Nevada, 20 miles southeast of McDermitt. The district hosts the National and Buckskin National deposits. As a whole the district produced 200,000

oz. gold and 750,000 oz. silver from 1906 to 1941 (Vikre, 1985). The area was first described in detail by Lindgren (1915) when production in the district was near its peak. Lindgren (1915) noted that although a few small ore shoots such as the "Stall Brothers" stope contained spectacularly high gold grades, the deposits as a whole contained much larger amounts of silver. Production of Hg also occurred from Hg-bearing silica sinter near the top of Buckskin Mountain (Roberts, 1940). Since the 1970's a number of companies have explored the area around Buckskin National for vein-type deposits similar to those mined in the past. The area is currently being explored by Romarco Minerals Inc. (www.romarco.com).

Host rocks in the National district consist of a 3,000 ft. thick section of mostly Miocene volcanics that unconformably overlie Mesozoic metasedimentary rocks (Vikre, 1985). The oldest lithology with hydrothermal alteration is the rhyolite of Buckskin Mountain, with a sanidine age of 16.57 ± 0.03 Ma (Vikre, 2007). This unit overlies basalt and basaltic-andesite flows (ca. 16.7 Ma) similar to those of Steens Mountain (Brueseke et al., 2007). Overlying and intruding the rhyolite of Buckskin Mountain is porphyritic rhyolite (16.31 ± 0.03 Ma) that is overlain by lithophysic rhyolite (16.11 ± 0.03 Ma) (Vikre, 2007). The sinter and banded veins at Buckskin Mountain have been dated at 16.06 ± 0.03 Ma (Vikre, 2007). At National the large porphyritic intrusion that forms Charleston Hill and serves as the primary host rock has a sanidine age of 16.01 ± 0.15 Ma (Vikre, 2007). Emplacement of the vein and sinter deposits at Buckskin Mountain is thought to have occurred over several hundred thousand years and the entire hydrothermal system was active for about 500,000 years (Vikre, 2007).

Geochronology of Low-Sulfidation Epithermal Deposits

In the northern Great Basin a mid-Miocene (17-13 Ma) time frame for ages of mineralization and volcanism related to low-sulfidation epithermal Au-Ag deposits has been measured by a number of studies using K/Ar and Ar/Ar methods (Table 1).

Table 1. Geochronology of Mid-Miocene Au-Ag Deposits in the Northern Great Basin Preformed Prior to this Study

Deposit	Age ± 1σ (Ma)	Dating Method	Predominant Host Rocks	Reference
Jumbo	17.3±0.5	K/Ar	metasediments	Conrad et al., 1993
War Eagle Mtn.	16.6-15.2	K/Ar	granite	Halsor et al., 1988
Sleeper	16.1±0.07	Ar/Ar	rhyolite	Conrad and McKee, 1996
Buckskin National	15.8-15.4±0.2	K/Ar	rhyolite	Vikre, 1985
Mule Canyon	15.6±0.04	Ar/Ar	rhyolite	John et al., 2003
DeLamar	15.7±0.5	K/Ar	rhyolite	Halsor et al., 1988
McDermitt (Hg)	15.6±0.4	K/Ar	rhyolite	Noble et al., 1988
Midas	15.4-15.3±0.08	Ar/Ar	rhyolite	Leavitt et al., 2004
Hog Ranch	15.2-14.8±0.4	K/Ar	rhyolite	Bussey, 1996
Hollister	15.19±0.05	Ar/Ar	rhyolite	Peppard, 2002
Seven Troughs	13.82±0.02	Ar/Ar	rhyolite	Hudson et al., 2006

Saunders et al. (1996) proposed that these deposits are related to the initial development of the Yellowstone hotspot. Other studies suggest that the Yellowstone hotspot, and flood basalt magmatism similar in age and composition to the Columbia River flood basalts, originated in the Nevada-Oregon-Idaho tri-state region between 17.5 and 16.5 Ma (Fig. 2; Hooper, 1997).
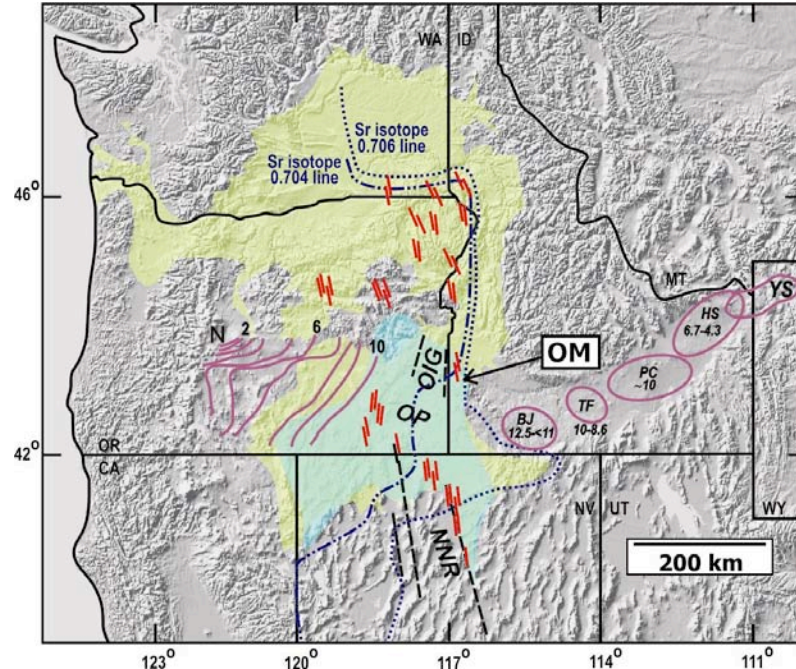
FIG 2: Shaded relief map of the northwestern United States depicting selected Cenozoic tectonomagmatic features. Green shading depicts the region where mid-Miocene Columbia River (WA-OR-ID) and Steens (OR-NV-ID-CA) flood basalt lava flows crop out (after Hart and Carlson, 1985; Camp and Ross, 2004; Brueseke et al., 2007). The major flood basalt dike swarms/eruptive loci are depicted as red lines, the Oregon-Idaho graben (OIG) and magnetic anomalies corresponding to zones of lithospheric extension/mafic magma emplacement (NNR; northern Nevada rift) are depicted as black dashed lines (Cummings et al., 2000; Glen and Ponce, 2002). The Owyhee Mountains are labeled (OM) and denoted by an arrow. The purple ovals are the silicic-dominated volcanic systems of the Snake River Plain-Yellowstone province; BJ, Bruneau-Jarbidge (~12.5 to <11 Ma); TF, Twin Falls (~10 to 8.6 Ma); PC, Picabo (~10 Ma); HS, Heise (~6.7 to 4.3 Ma); and YS, Yellowstone (<2.5 Ma), and the purple lines are the age isochrons associated with Oregon High Lava Plains silicic activity (N, Newberry Volcano; after Jordan et al., 2004). The initial $^{87}Sr/^{86}Sr$ 0.706 and 0.704 isopleths are depicted (after Armstrong et al., 1977; Kistler and Peterman, 1978; Leeman et al., 1992; Crafford and Grauch, 2002) and are interpreted to define the western edge of the Precambrian North American craton (the 0.706 isopleth), and a zone of transitional lithosphere between the older craton and Mesozoic accreted terranes to the west (between the two isopleths). The blue shaded region depicts the portion of the Owyhee Plateau (OP) characterized by mid-Miocene silicic magmatism.

Whereas the greatest degree of Columbia River flood basalt magmatism occurred to the

north in northeastern Oregon and southwestern Washington, flood basalts at Steens

Mountain in southern Oregon were coeval with eruption of the earliest and most

voluminous Columbia River basalts (Brueseke et al., 2007), and overlap with the age of

large silicic calderas at McDermitt (Fig. 2). Thus, the mid-Miocene bonanza deposits of

16

the northern Great Basin are not only closely associated with magmatism and extension that formed the northern Nevada rift, but they also may be broadly associated with the inception of Yellowstone hotspot magmatism, and perhaps flood basalt magmatism.

Previous studies, including Conrad et al. (1993) and John (2001), have established the general timing and age relationships for a few bonanza ores of northern Nevada. However, the bulk-sample total fusion (K/Ar and Ar/Ar) techniques used in most of the published studies yield relatively broad age constraints, due to their inability to resolve problems posed by the presence of extraneous argon or partial degassing following initial trapping. Given the mounting evidence that these deposits form during rapid deposition events over periods of tens to hundreds of thousands of years (Sanematsu et al., 2006; Simmons and Brown 2006; Heinrich, 2006), well constrained dates for deposit formation are needed to fully understand what geologic processes are involved.

METHODOLOGY

Field Methods

Field work was carried to out to collect samples suitable for this study in northern Nevada and southern Idaho during the summer of 2006. Samples of probable mid-Miocene deposits, including historic mines, prospects and outcropping mineralization, were collected. Samples of ore-bearing quartz and/or adularia veins along with host rocks were described in the field and locations were recorded using a GPS receiver. Emphasis was placed on obtaining samples with visible precious metal minerals and adularia. Field work was mainly conducted by a team of three, the author, Willis Hames, and James Saunders, of Auburn University. Considerable advice on sampling sites, additional samples with maps of collection localities, and some field assistance was provided by Bill Utterback, a local expert on epithermal gold deposits based in Winnemucca, Nevada. Robert Cook also provided some samples and advice on sampling locations for the National district.

Ore Petrography

Both standard and polished thin sections were prepared for determination of suitable material for $^{40}Ar/^{39}Ar$ dating and to examine ore mineralogy and textures (Fig. 3).
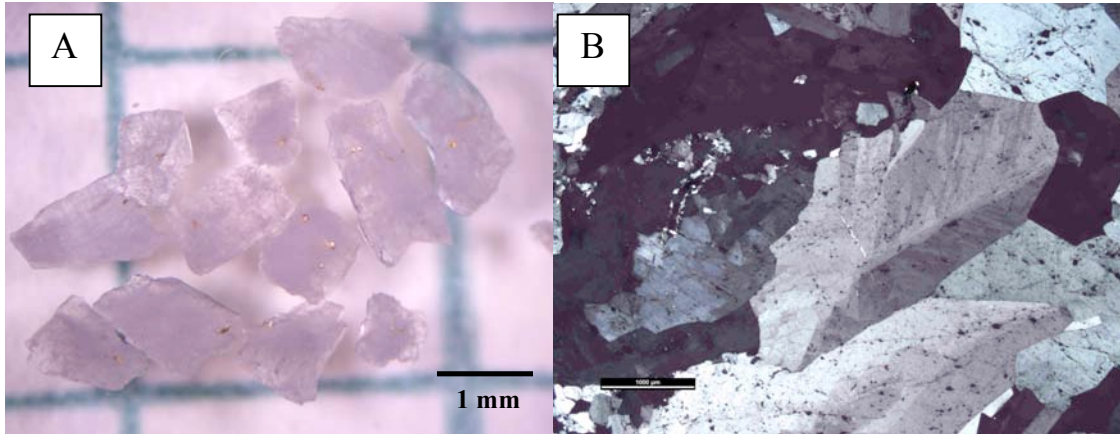
FIG. 3. Photograph and photomicrograph of ore-bearing adularia used for ^{40}Ar/^{39}Ar geochronology. A. Binocular microscope view of adularia grains with visible electrum. B. Photomicrograph (cross-polarized light) of euhedral adularia crystals with characteristic feather-like extinction (Photomicrograph scale bar = 1 mm).

Standard thin sections were prepared in Auburn University's thin section lab and polished thin sections were prepared by Vancouver GeoTech Labs. Thin section off-cuts were stained for K-feldspar. Petrography was preformed using a transmitted and reflected light microscope. Mineral identification was aided by the accompanying geochemical data for each sample.

Geochemistry

The majority of the geochemistry samples were obtained by field collection. A few samples (e.g., HCN 1-4) were collected and provided by Bill Utterback. For comparison, additional samples representing well known low-sulfidation Au/Ag-deposits from northern Nevada (Sleeper and National), Colorado (Bessie G, Sunnyside, Cresson, Vindicator, and Black Rose), and Japan (Koryu), were provided by James Saunders and Robert Cook. All samples were analyzed by ACME Analytical Labs LTD.

Before samples were sent to ACME, each was sawed in half, with one split used for geochemical analysis. The other half was retained as reference or made into a polished thin section. Geochemical samples were prepared to contain a minimum of host rock, and ideally contain a high ratio of ore minerals to gangue vein material. Thus, precious metal concentrations were maximized and are not necessarily representative of mining grades. Once the samples were sent to ACME, a sample of up to 1 kg was crushed to 70% passing at 10 mesh followed by a 250 g split being pulverized to 95% passing at 150 mesh. A multi-element assay for 34 elements including: Mo, Cr, Ba, Hg, Cu, Pb, Zn, Ag, Ni, Co, Fe, As, Sb, Sr, Se, and Te, was preformed by hot aqua regia digestion of a 1 g sample split followed by ICP-ES and ICP-MS analysis. Analysis for Au was preformed by fire assay.

A Pearson correlation plot was created using MINITAB and used to evaluate elemental relationships using both log normalized and "raw" concentration data. Only data from the northern Great Basin deposits was input into the correlation matrix. Any data that was below detection limits was reduced to one half of the detection limit as is the standard practice.

A modified trilinear plot was devised to serve as a visual way to compare the chemical attributes of each deposit. The modified trilinear plot, henceforth called the epithermal trilinear diagram, was created by plotting the molar ratios of Au, Ag, and Pb/10 on a cation trilinear diagram, and plotting the molar ratios of Sb/10+As/10, Se and Te on the anion trilinear diagram. These points were then projected onto the quadrilateral field of the trilinear diagram as normal. The concentrations of Pb, Sb, and As were

20

divided by a factor of ten to compensate for the fact that they have higher average abundances relative to the other elements.

Geochronology

All $^{40}Ar/^{39}Ar$ dating was preformed in the Auburn Nobel Isotope Mass Analysis Lab (ANIMAL) under the direction of Dr. Willis Hames. The mineral adularia ($KAlSi_3O_8$) was dated because it is rich in K, and a common gangue mineral that is often intimately associated with the Au/Ag-minerals. Each sample was crushed and sieved to 14-20 and 20-60 mesh size fractions for hand picking. Hand picking of each sample was preformed to select individual crystals or cleavage fragments, free from visible inclusions of other phases, and generally free from alteration. All samples were washed in dilute HF prior to analysis to remove any oxide coatings. Neutron irradiation at the central core facility of the McMaster Nuclear Reactor in Hamilton, Ontario was used for the production of ^{39}Ar and followed standard procedures as described by Dalrymple et al. (1981). Crystals were placed in aluminum disks with the monitor FC-2 (for J-value determination, age = 28.02 Ma, Renne et al., 1998) along with reagent grade K_2SO_4 and CaF_2 as flux monitors. Following irradiation, the best technique for Ar extraction was determined by heating single adularia crystals with a CO_2 laser by the following methods: 1) total fusion, 2) two-step release, and 3) incremental heating. Incremental heating produced the most precise results and proved to be the best way to deal with the high radiogenic yields and extraneous ^{40}Ar typical of these samples. Heating schedules of 10-20 steps were used for 5 adularia crystals from each sample location. The first several heating steps were preformed at low laser power and served to remove extraneous ^{40}Ar

contained on surface defects or in fluid inclusions. The middle steps tended to release the

majority of Ar contained in the crystal lattice, while the final steps served to totally fuse

the crystal and insure all the Ar had been extracted. An Excel spreadsheet and the Excel

add-on Isoplot (Ludwig, 2003) was used for data reduction and to create model-age

spectrum and isotope correlation diagrams. See appendices 1, 2, and 3 respectively for

additional lab descriptions, incremental heating data for each sample, and monitor and air

data.

ORE PETROGRAPHY

Ore petrography was conducted to locate suitable material for geochronology, and to determine the mineralogical relationships within veins that exist in each deposit. Standard and polished thin sections were prepared from the Buckskin National, Hollister, Midas, National, Sandman, and War Eagle Mountain deposits. Characteristic and other interesting features/textures in hand samples were also described and photographed so that textures on both the microscopic and macroscopic scale could be compared.

For this study, deposits that contain adularia as a common ore-host were of particular interest because these samples provide the most direct method for dating precious metal mineralization. In these deposits, electrum is the primary Au-mineral, and a number of Ag-selenides, Ag-sulfides, and Ag-sulfosalts including: naumannite (Ag_2Se), aguilarite (Ag_4SeS), acanthite (Ag_2S), pyrargyrite (Ag_3SbS_3), and proustite (Ag_3AsS_3) are common. Two distinct occurrences of adularia are present in the deposits evaluated for this study. The Jumbo, New Alma, Ten Mile and Sandman deposits contain thin (1- 20 mm) veins or fracture encrustations of adularia ± quartz, which host electrum and/or gold almost exclusively. This contrasts with the deposits found at Buckskin National, Hollister, Midas, National, and War Eagle Mountain, which consist of much thicker (up to 5 m) banded quartz ± adularia ± calcite veins that generally contain more Ag-selenides, sulfides and sulfosalts, along with rare high-fineness gold. Adularia has been

reported at most of the deposits in this study; however crystals large enough for dating were not found in the samples collected at the Buckskin National, Hollister, Midas, or National deposits.

Deposits with veins containing principally adularia or veins in which adularia served as the primary precious metal host, have been important historic producers but have not been mined recently on a large scale. In these deposits, adularia veins are typically narrow (1 - 20 mm), often form encrustations on open fractures, and precious metal minerals typically are located near the host rock/vein margins (Fig. 4 and 5).

FIG. 4. Photograph of crustiform adularia crystals from the Sandman deposit, forming a thin layer (3-4 mm) over the silicified tuffaceous host rock.
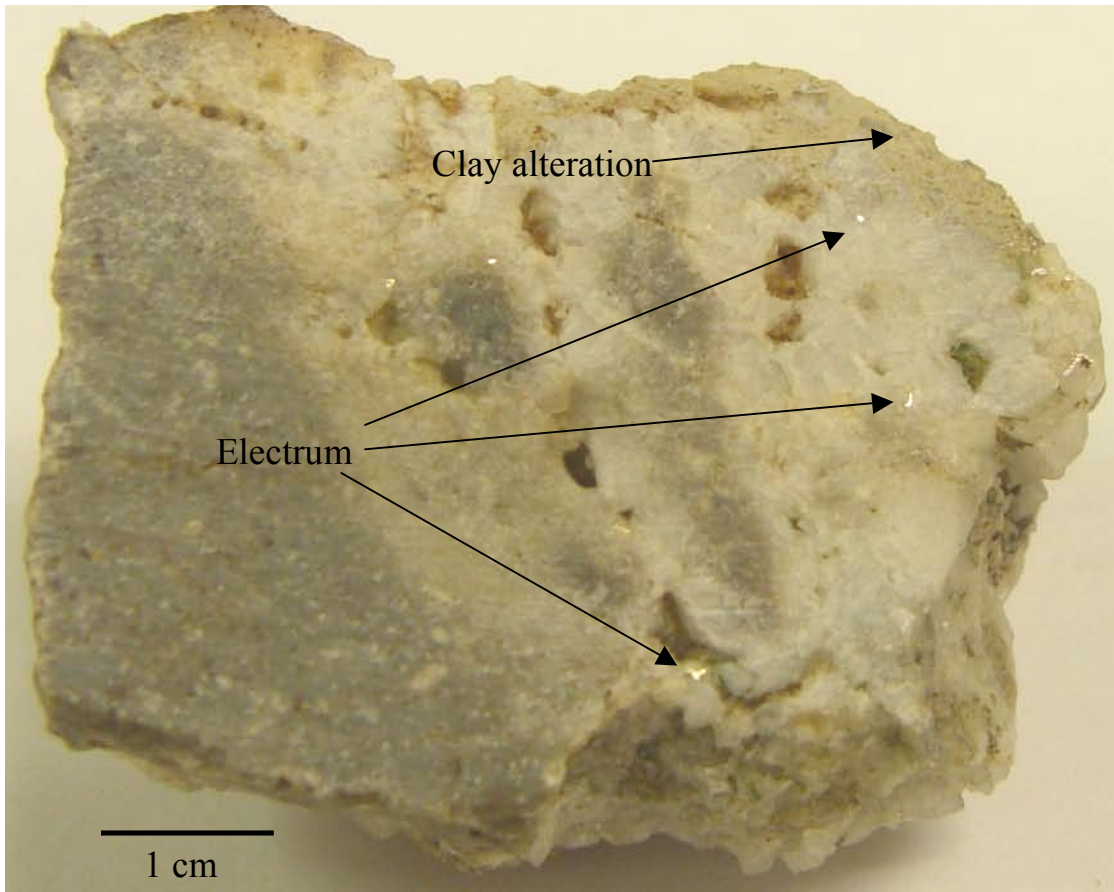
FIG. 5 Sample HCN-1, Sandman deposit. Photograph of gold bearing adularia vein and brecciated tuffaceous host rock. Note the surface layer of alteration to white clay.

Native gold and electrum are nearly the exclusive ore minerals present in the adularia veins. Geochemical data indicate relatively low levels of base metals, Se, and Te (discussed below). Some of the Jumbo and New Alma samples have thin bands of quartz that either precede or overgrew the adularia. Field observations indicate these quartz layers are nearly barren of precious metals and geochemical data for one such layer (NEWA2-1) support this conclusion.

The banded quartz ± adularia ± calcite veins collected for this study have considerably different features compared to the adularia-dominated veins. Unlike the adularia veins that often do not exceed a few centimeters in thickness, the banded veins

range from less than 1 m up to 5 m in width and can be laterally extensive for nearly 2 km with remarkable uniformity in mineral composition (Vikre, 1985; Goldstrandt and Schmidt 2000). Evidence for colloidal silica and deposition of ore minerals from colloids are also common.

Colloids serve an important role in epithermal systems by transporting components from deeper in the system to the shallow environment (Saunders, 1994). Evidence for deposition of silica and precious metals from colloids is present in ores from the National district and the Hollister deposit. Samples from the National deposit contain dendritic electrum "forests" along with pyrargyrite surrounded by "jig saw" quartz (Fig.6). Additionally, samples from the Buckskin National deposit contain dendritic naumannite, also called "sagenitic" by Vikre (1985), and numerous thin bands of jig saw quartz (Fig. 7). "Sluice box" textures in samples from Hollister (Fig. 8) indicate electrum and Ag-sulfide/selenide colloids were caught up and deposited on the leeward side of veins as they moved upward with the hydrothermal fluids. Similar textures have also been reported at Midas (Goldstrand and Schmidt, 2000). Electrum dendrites indicate rapid precipitation from a supersaturated solution and jig saw quartz forms when amorphous (colloidal) silica (re)crystallizes to form quartz (Saunders, 1994). These textures indicate both the silica and precious metals were deposited as colloids in a rapid manner from a supersaturated fluid (Saunders, 1994; Saunders et al., 1996).
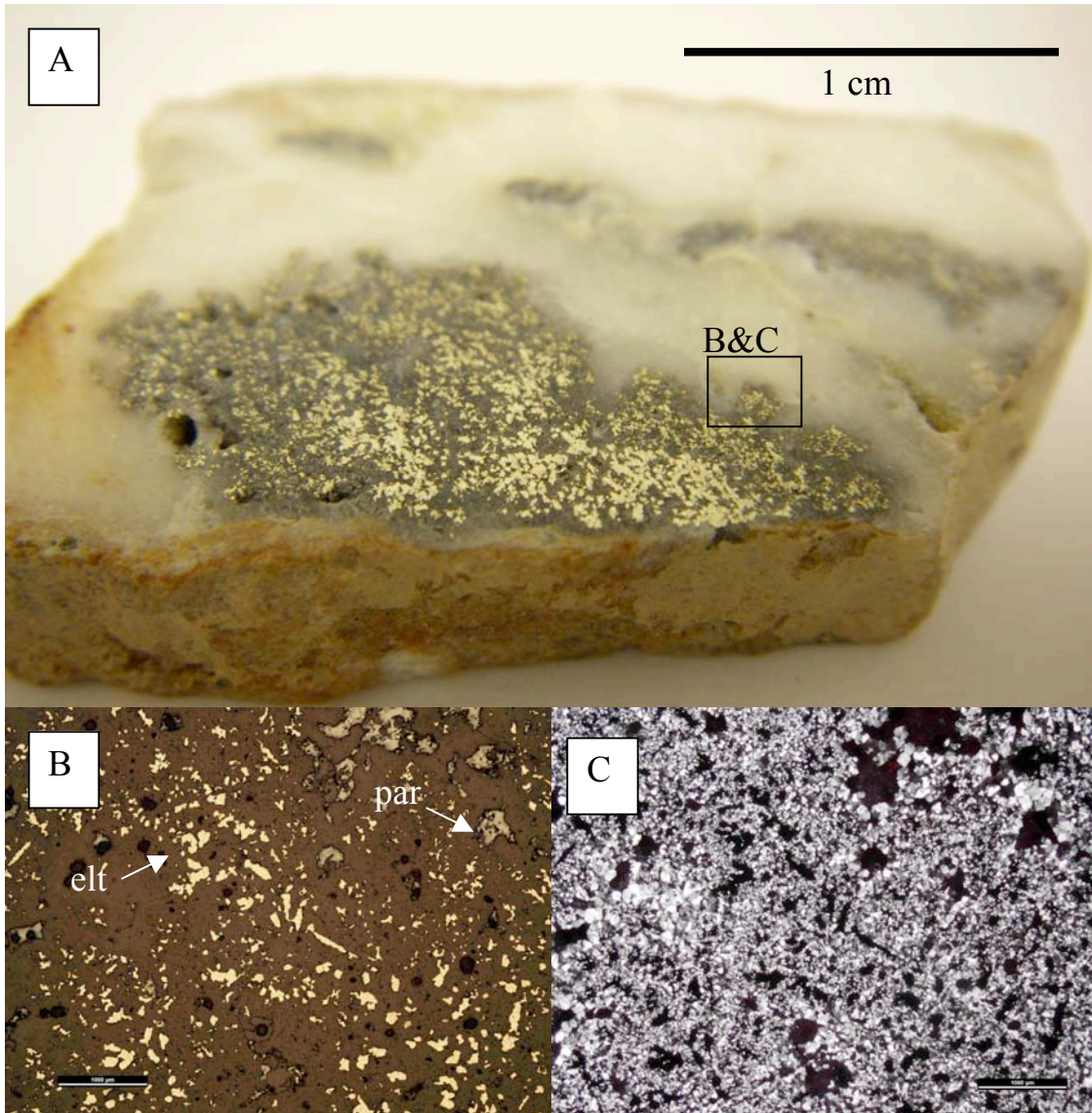
FIG. 6. Sample NMD-2, National deposit. A. Photograph of dendritic electrum. B. Photomicrograph (reflected light) of electrum (elt) and pyrargyrite (par). C. Photomicrograph (crossed polars) of jig saw quartz surrounding electrum and pyrargyrite. (Photomicrograph scale bar = 1 mm). Note: photo inserts indicate the area the photomicrograph was taken, not necessarily the field of view.
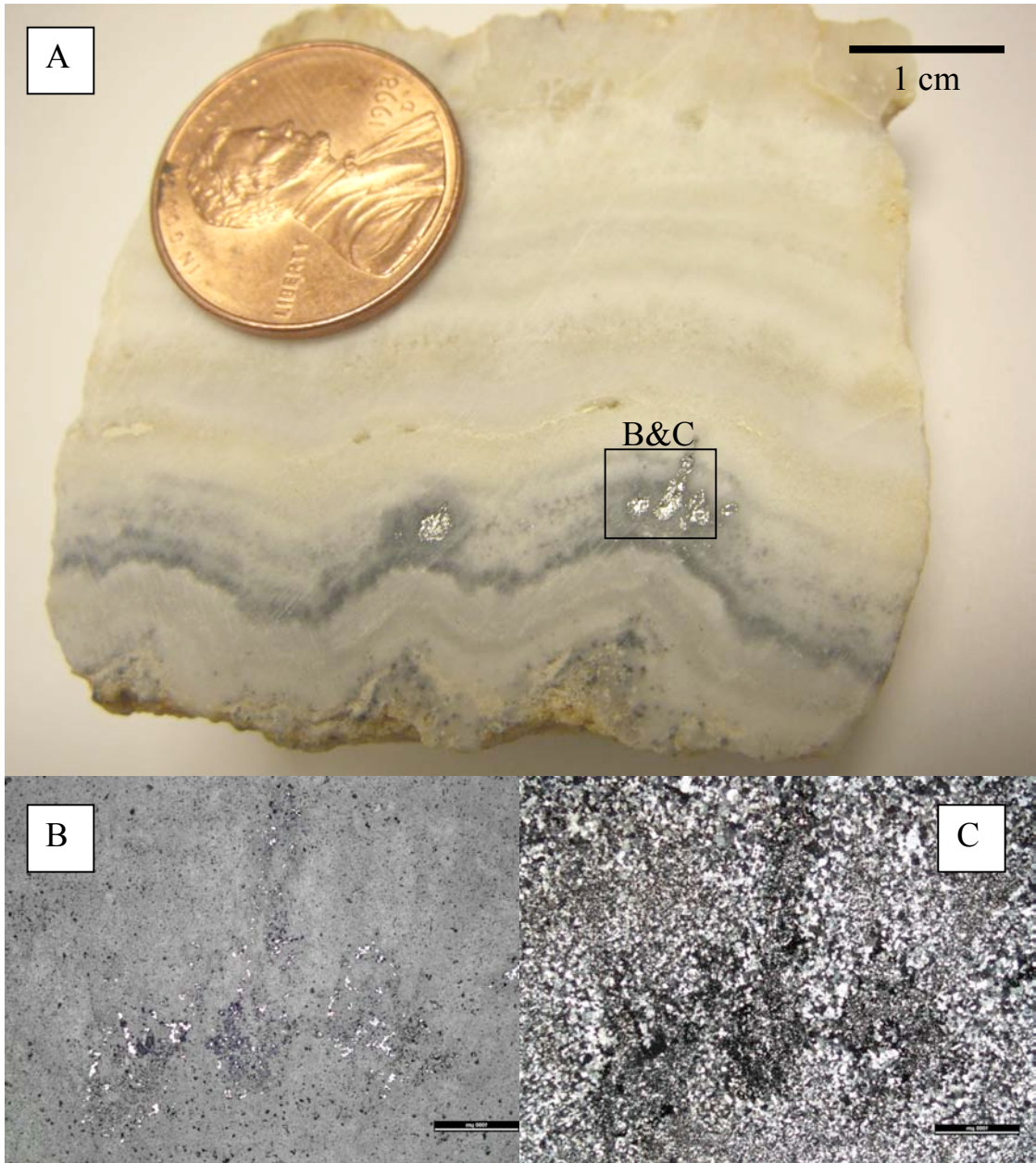
FIG. 7. Sample: BNM, Buckskin National deposit. **A**. Photograph of banded quartz vein with sagenitic naumannite. B. Photomicrograph (reflected light) of sagenitic naumannite. **C**. Photomicrograph (crossed polars) of jig saw quartz surrounding sagenitic naumannite. (Photomicrograph scale bar = 1 mm).
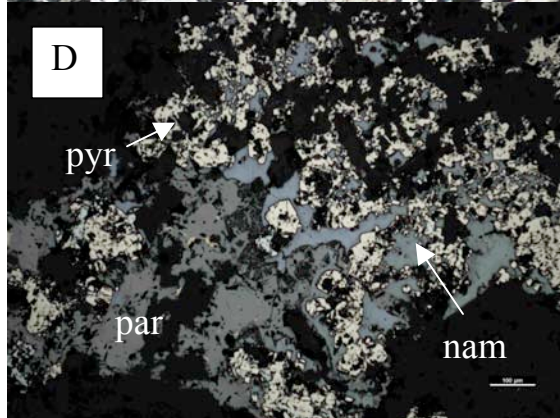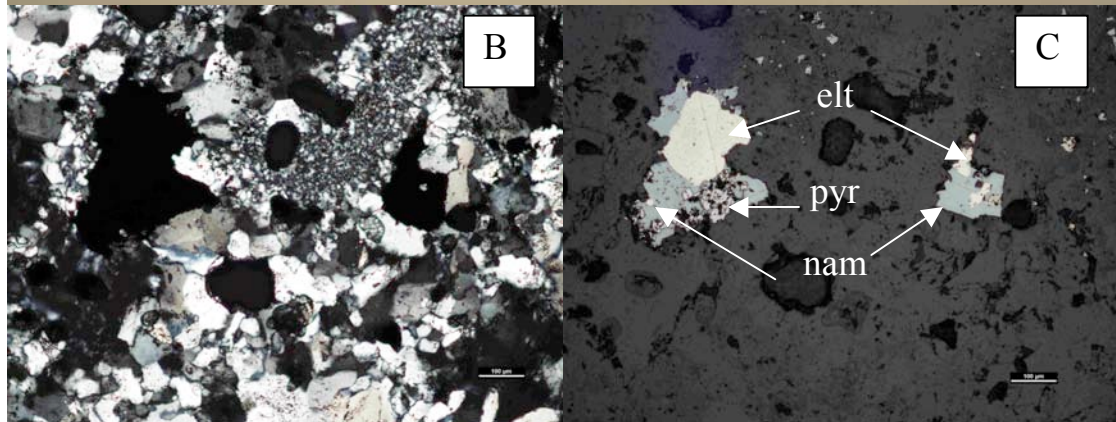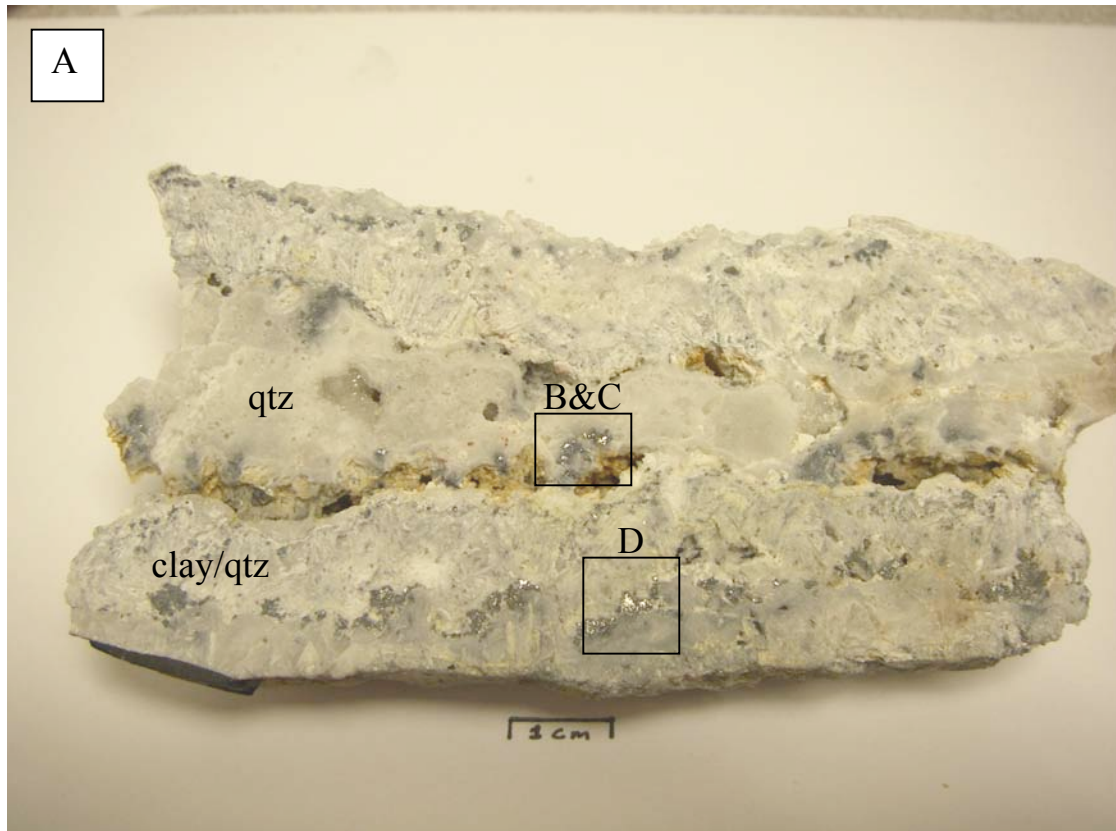
FIG. 8. Sample HSC-1, Hollister deposit. A. Photograph of banded vein with a central quartz band (qtz) surrounded by two clay-rich bands (clay/qtz), clay-rich bands contain quartz replacement of bladed calcite, also note the sluice box textures of the naumannite and electrum in these layers as the ore minerals are deposited primarily on the leeward (left) side. B. Photomicrograph (crossed polars) of quartz surrounding ore minerals. C.Photomicrograph (reflected light) of electrum (elt) rimmed by pyrite (pyr) and naumannite (nam). D. Photomicrograph (reflected light) of pyrite (pyr) replaced by naumannite (nam) and pyargyrite (par). (Photomicrograph scale bar = 0.1 mm).

29

There is evidence from ore textures on the microscopic scale that mineral deposition took place in stages at some deposits. Ores from the Hollister deposit show electrum rimmed by naumannite and pyrite in one band, and naumannite and pyrargyrite replacing pyrite in another (Fig. 8). Additionally, a sample collected at War Eagle mountain contains galena rimmed by naumannite and chalcopyrite (Fig. 9). Similar textures of early base metal sulfides followed by later precious metal minerals have been reported in the National district and Midas deposit (Vikre, 1985; Goldstrand and Schmidt 2000).
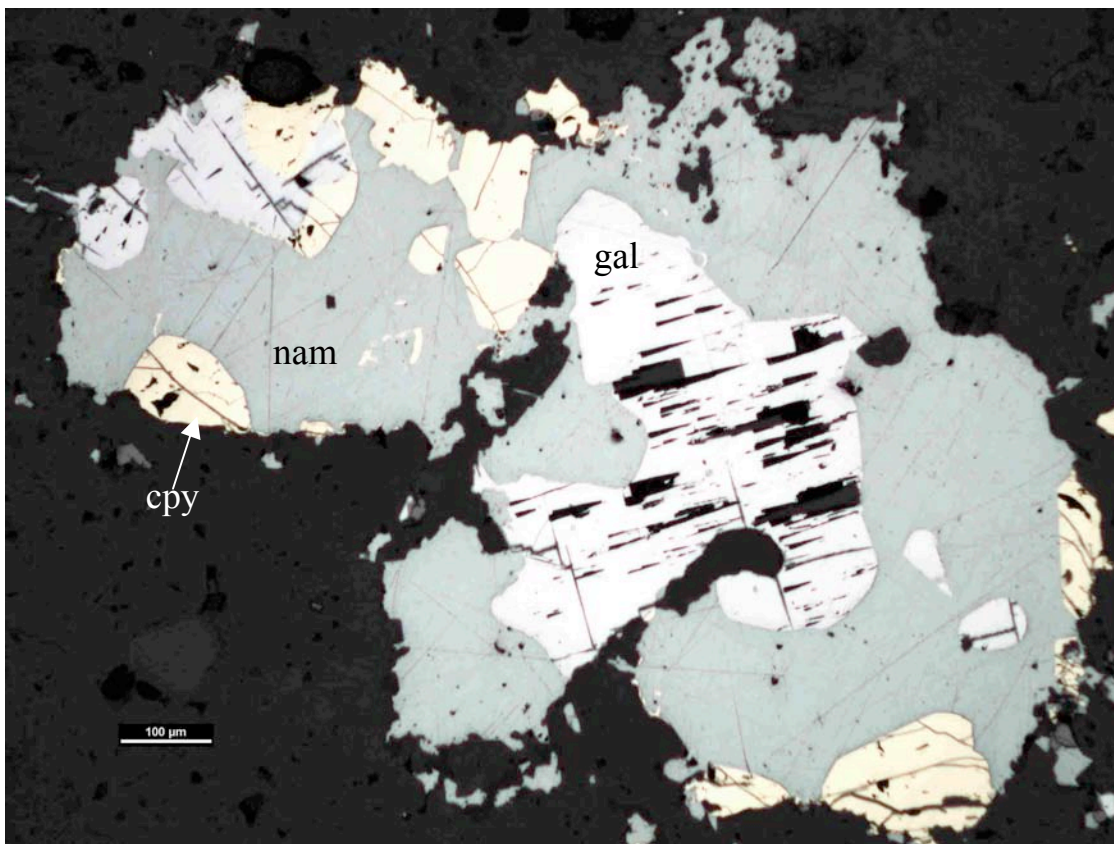
FIG. 9. Sample: WEMBU, Oro Fino vein, War Eagle Mountain. Photomicrograph (reflected light) of galena (gal) rimmed by naumannite (nam) and chalcopyrite (cpy). (Photomicrograph scale bar = 0.1mm).

Veins that contain multiple generations of banding indicate systems that were fairly long lived and received input of fluids with different chemistries. Sample BNM-2 from the Buckskin National deposit is ~3 cm long and contains at least eight bands of Ag-selenides/sulfides (some with visible electrum), along with multiple layers of quartz in between (Fig. 10).
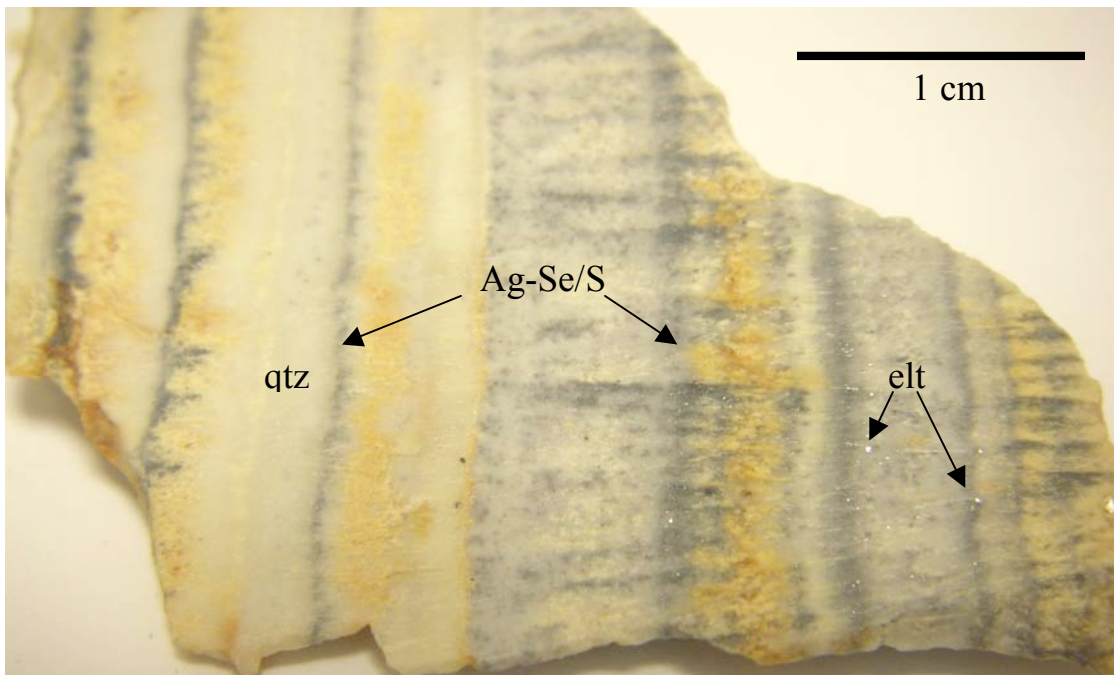
FIG. 10. Sample BNM-2, Buckskin National deposit. Photograph of banded ores with typical cyclic deposition of quartz (qtz), electrum (elt), and Ag-selenides/sulfides (Ag-Se/S) in discreet bands.

Some of these ores also contain evidence of brecciation, either tectonic or hydrothermal, during vein formation. Sample OF-1 from the Oro Fino vein, War Eagle Mountain contains altered basalt breccia, which was later over-grown by a layer of quartz, then a layer of naumannite-bearing adularia (Fig. 11). At the microscopic scale, naumannite is hosted by the adularia as small blebs and the quartz appears barren. A thin band of much finer-grained quartz occurs at the quartz/adularia margin.

31

Deposition of precious metals frequently occurred near transition boundaries of either quartz and adularia (Fig. 11) or euhedral quartz and microcrystalline quartz (Fig. 12). The banding in these veins likely indicates a change in equilibrium or fluid chemistry that resulted in Au/Ag-mineral precipitation.

Boiling is also considered an important deposition mechanism in epithermal systems. Bladed calcite (Fig. 13) and bladed quartz pseudomorphs (Fig. 14; Fig. 15), which indicate boiling (Simmons and Christenson, 1994), are present at or near some metal deposition margins.
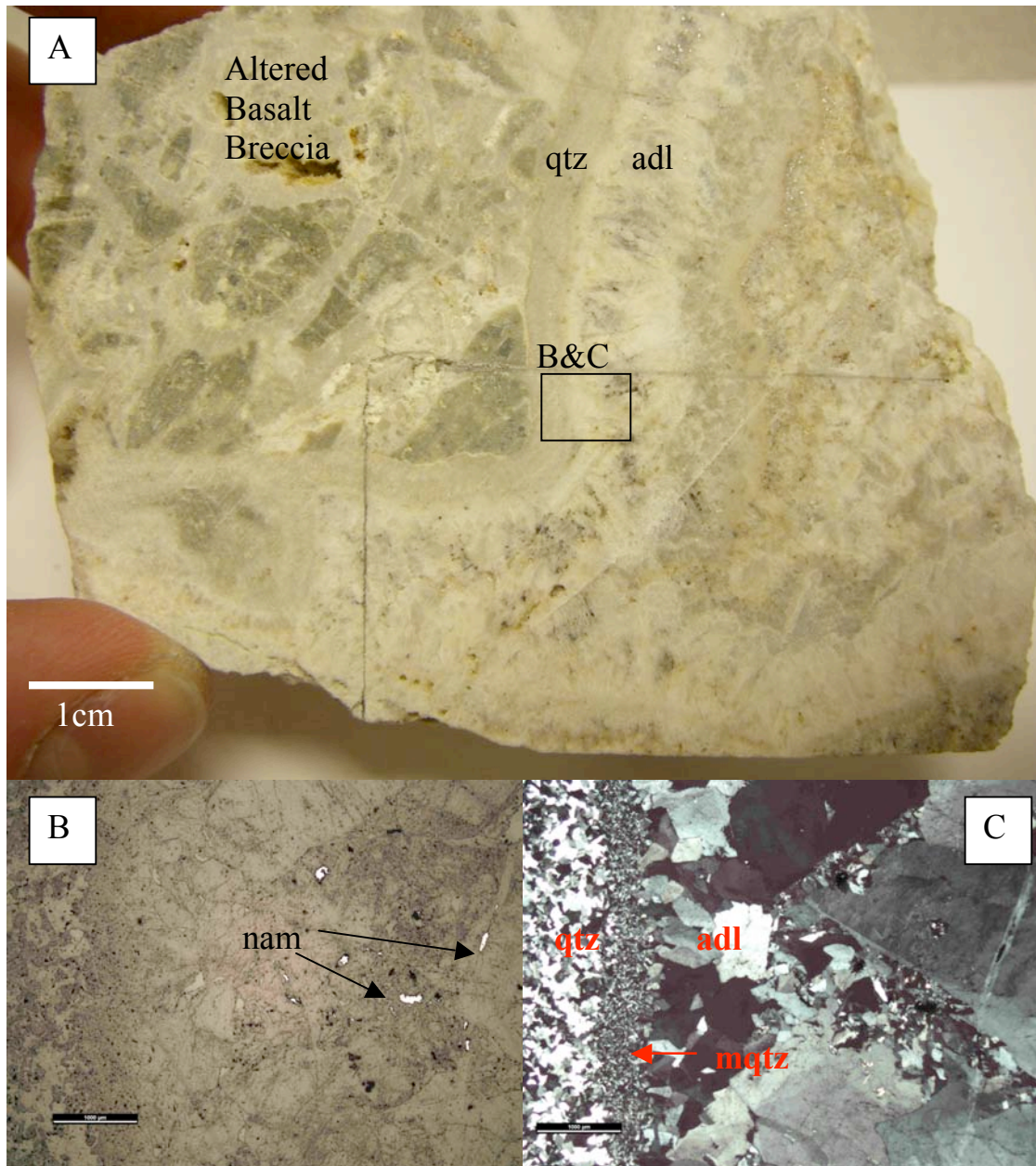
FIG. 11. Sample OF-1, War Eagle Mountain deposit. A. Photograph of Oro Fino vein. Sequence of events appears to be altered basalt breccia covered by a band of quartz (qtz) then a band of Au/Ag-bearing adularia (adl). B. Photomicrograph (reflected light) of the quartz/adularia boundary with naumannite (nam) bearing adularia. C. Photomicrograph (crossed polars) of the quartz/adularia boundary, note the microcrystalline quartz (mqtz) band at the boundary and the much coarser naumannite-bearing adularia. (Photomicrograph scale bar = 1 mm).
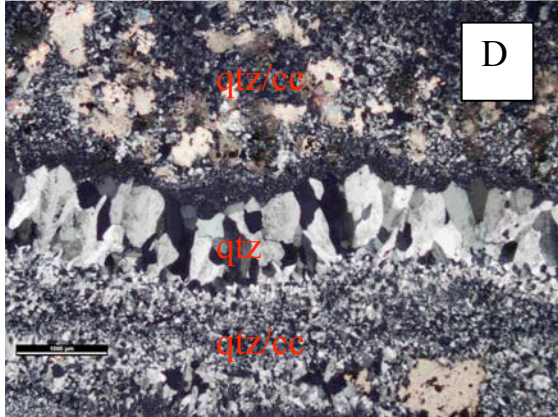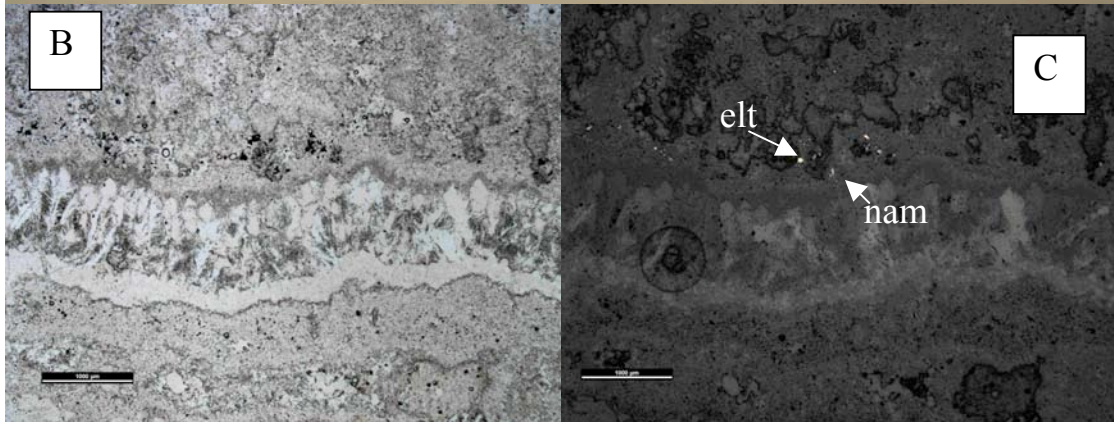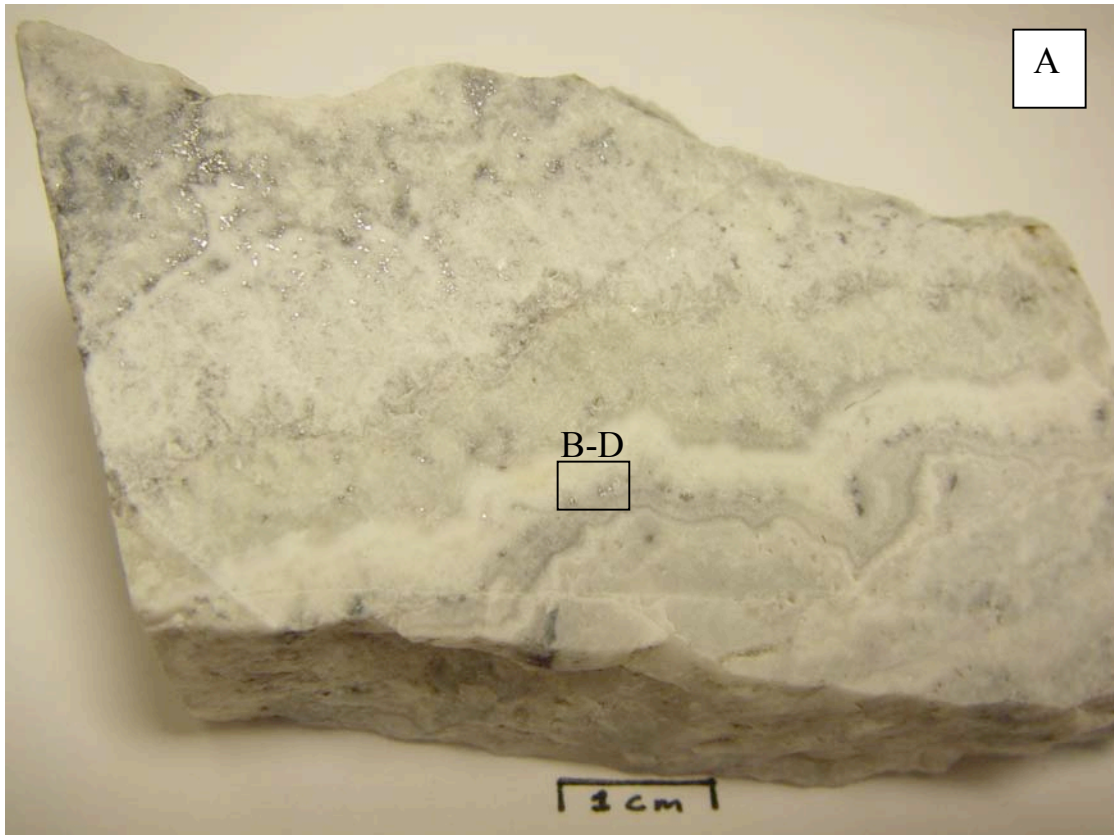
FIG. 12. Sample MGCV-2 banded ores from the Midas deposit. A. Photograph of banded vein showing at least six deposition events. B. Photomicrograph (plane polarized light) of the banded vein. C. Photomicrograph (reflected light) of electrum (elt) and naumannite (nam) in the jig saw quartz portion of the vein. D. Photomicrograph (crossed polars) of the banded vein, note the euhedral quartz (qtz) band bounded on both sides by ore bearing calcite/jig saw quartz (qtz/cc) bands. (Photomicrograph scale bar = 1 mm).
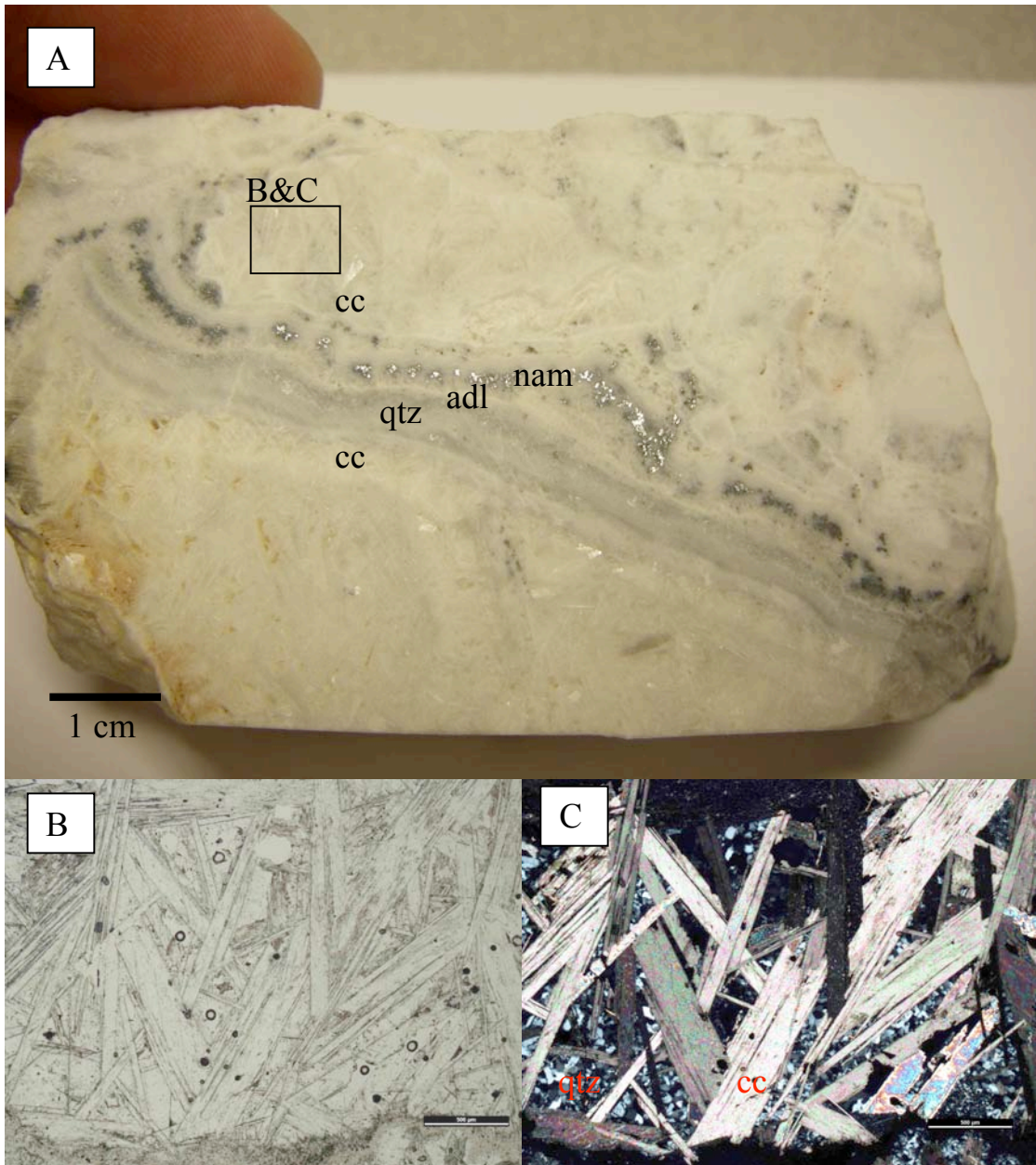
FIG. 13. Sample MGCV-1, Midas deposit. A. Photograph of banded ore with two stages of bladed calcite (cc) and bands of quartz (qtz), adularia, and naumannite (nam) in between. B. Photomicrograph (plane polarized light) of bladed calcite surrounded by quartz. C. Photomicrograph (crossed polars) of bladed calcite surrounded by quartz. (Photomicrograph scale bar = 0.5 mm).
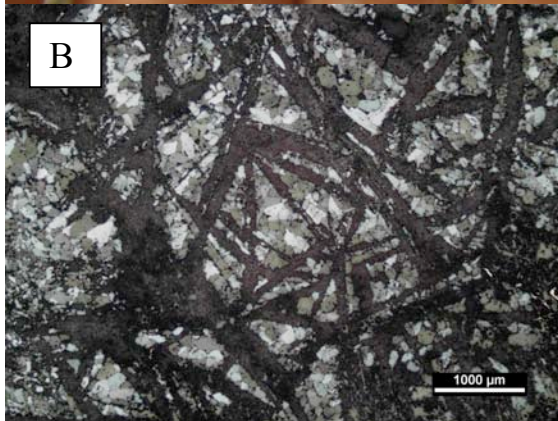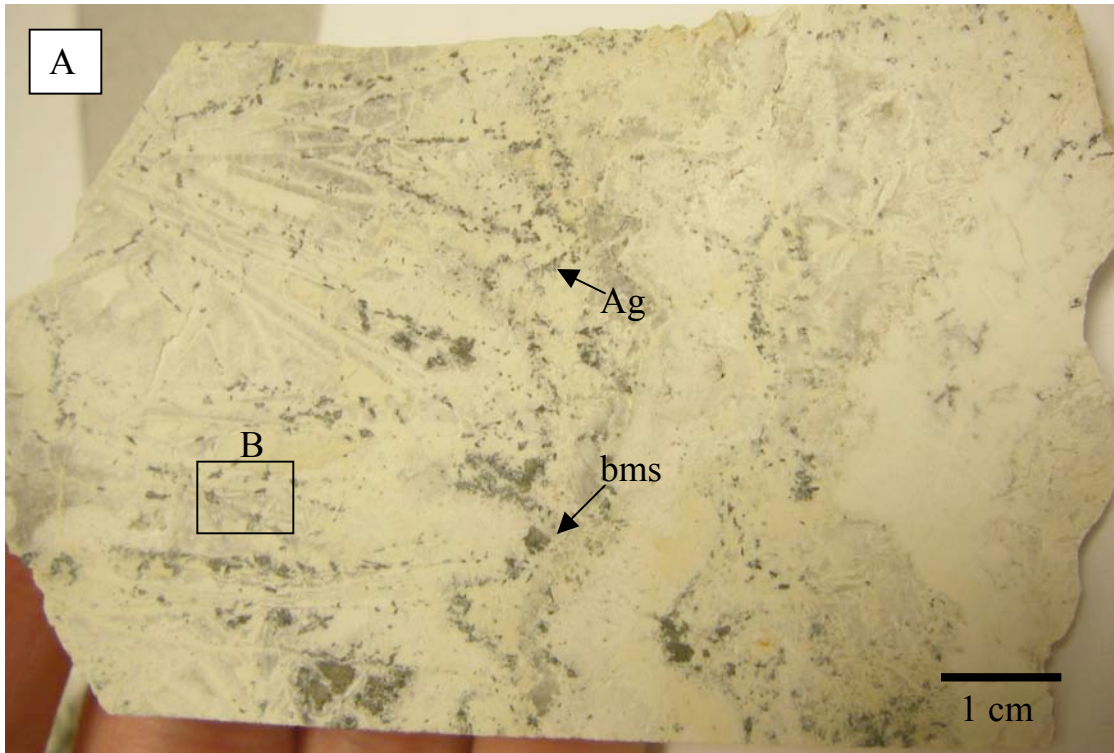
FIG. 14. Sample HGV-3, Hollister deposit. A. Photograph of quartz pseudomorphs after calcite in banded ore with abundant Ag-minerals (Ag) and base metal sulfides (bms) along the margins of calcite replacement. B. Photomicrograph (crossed polars) of microcrystalline quartz, which has replaced the bladed calcite. (Photomicrograph scale bar = 1 mm).
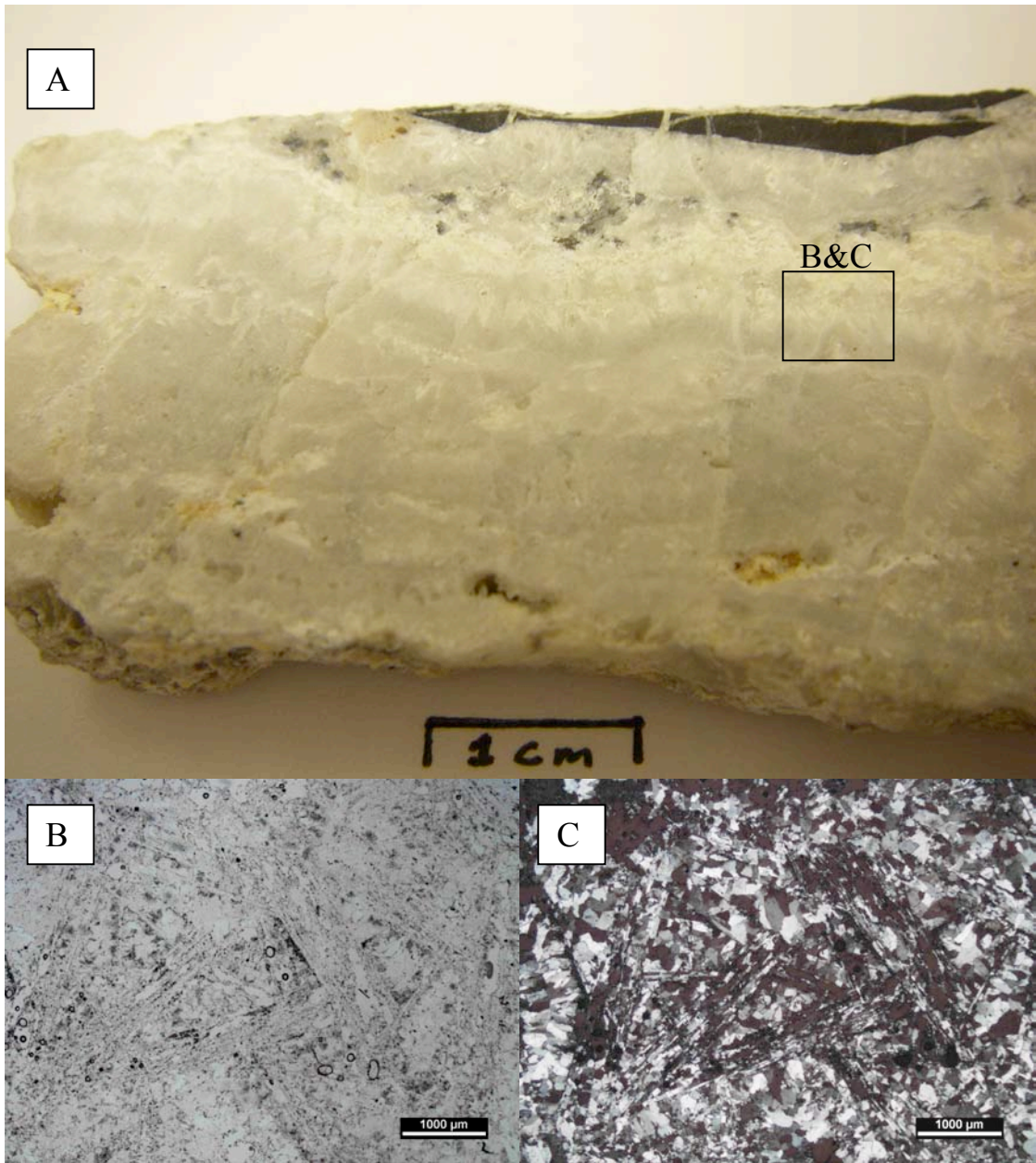
FIG. 15. Sample HSC-2, Hollister deposit. A. Photograph of bladed quartz after calcite below a band of ore-bearing quartz. B. Photomicrograph (plane polarized light) of quartz pseudomorphic after calcite. C. Photomicrograph (crossed polars) of quartz pseudomorphic after calcite. Note that the quartz grains are much coarser relative to those in Fig. 12. (Photomicrograph scale bar = 1 mm).

GEOCHEMISTRY

Typical elemental enrichments for low-sulfidation epithermal precious metal systems are well established; yet the actual concentrations of these elements vary considerably from deposit to deposit. The deposits of the northern Great Basin contain economic amounts of Au and Ag ± Hg, along with significant concentrations of As, Sb, Se, Mo, Tl, and W, which can be important pathfinders useful for exploration (John, 2001). Base metal contents are often low (Saunders, 1990; John, 2001) and selenium has been observed as an important component of ore minerals in some deposits (Vikre, 1984; Halsor et al., 1988; Goldstrand and Schmidt, 2000). A similar geochemical signature exists for the Japanese deposit examined in this study (Izawa et al., 1990). The deposits of Colorado have a geochemical signature similar to those of Nevada and Japan with the exception that Te, rather than Se, is abundant and an important constituent in ore minerals (Simmons et al., 2005).

Multi-element geochemical analysis was preformed on a number of samples from deposits within the northern Great Basin (Fig. 16) as well as other low-sulfidation epithermal deposits from Colorado and Japan for comparison. Selected elements deemed most relevant are listed in Table 2; a complete table of all the geochemical data can be found as an Excel file in the accompanying CD-ROM appendix.
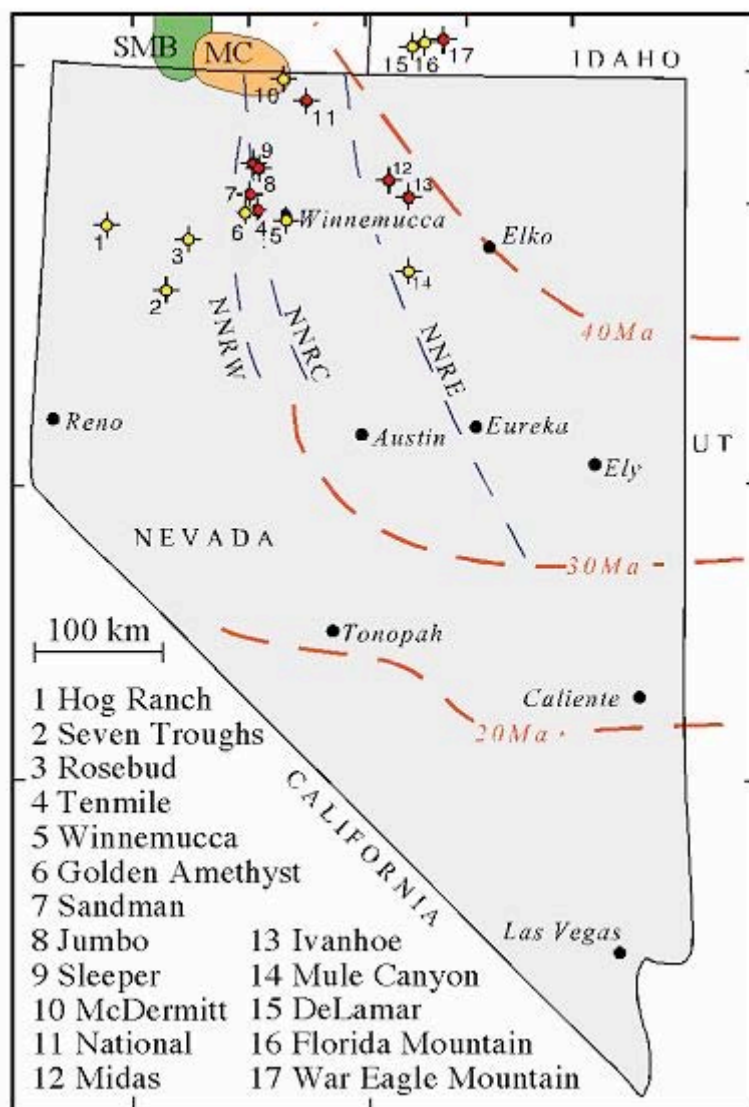
FIG. 16. Map Showing locations for many of the 17-14 Ma low-sulfidation epithermal deposits in the northern Great Basin (modified from Saunders et al. 1996), through-going structures as defined by geophysical data (Ponce and Glen, 2002) and the regional trend (dashed contours) of Cenozoic-subduction magmatism (McKee and Moring, 1996). Deposits sampled for this study are colored in red.

Table 2. Selected Geochemical Data for Epithermal Precious Metal Ores

Sample #	Location	Sample Type	Au	Mo	Cu	Pb	Zn	Ag	As	Sb	Cr	Ba	Hg	Se	Te
NOFS2-1	War Eagle Mtn.	Qtz Vein	28	1.4	8	1	<5	108	<5	1	5	6	<.05	6	<1
OF-1	War Eagle Mtn.	Qtz\Adl Vein	56	1.5	117	104	12	2469	6	8	12	16	<.05	229	2
OF-2	War Eagle Mtn.	Qtz\Adl Vein	1	0.9	71	5	<5	19	10	1	5	10	<.05	<2	<1
WEMS3-1	War Eagle Mtn.	Qtz\Adl Vein	7	<.5	179	36	<5	459	12	13	4	7	<.05	39	1
WEMS3-2	War Eagle Mtn.	Qtz\Adl Vein	2	<.5	24	5	5	145	<5	2	3	5	<.05	15	<1
WEMBU	War Eagle Mtn.	Adl Vein	149	1.9	1553	2313	1324	5725	<5	1	2	6	<.05	1689	18
BNM	Buckskin National	Qtz Vein	32	1.5	12	38	26	697	265	63	9	5	1.2	168	<1
BNM-2	Buckskin National	Qtz Vein	78	1.6	25	36	83	3354	71	174	14	12	13.8	651	<1
BNM-3	Buckskin National	Qtz Vein	782	2.2	200	1801	838	3300	44	648	12	<5	18.3	4952	<1
NMD	National	Qtz Vein	2	0.5	78	157	24	1335	586	1469	6	5	1.4	55	3
NMD-2	National	Qtz Vein	32940	5.8	2905	107	289	3834	924	8175	21	71	72.4	143	<1
NMD-3	National	Qtz Vein	170	2.4	125	51	45	210	5258	174	9	64	0.6	11	<1
NMD-4	National	Qtz Vein	2	1.0	2216	40354	22613	202	46996	368	10	7	0.2	401	1
HGV-1	Hollister	Qtz\Clay Vein	437	3.1	487	166	74	372	339	53	8	16	0.5	89	4
HGV-2	Hollister	Qtz\Clay Vein	3	1.1	607	22	169	107	408	70	8	12	0.3	161	2
HGV-3	Hollister	Qtz\Clay Vein	2	0.6	198	1	<5	161	295	49	2	29	<.05	62	3
HGV-4	Hollister	Qtz\Clay Vein	1	0.5	771	68	81	422	252	122	4	21	0.2	50	7
HSC-1	Hollister	Qtz\Clay Vein	418	1.1	1437	72	606	6082	392	1394	6	36	1.9	2604	3
HSC-2	Hollister	Qtz\Clay Vein	9	0.8	130	25	115	614	69	58	5	7	1.2	203	2
HSIN	Hollister	Siliceous Sinter	n/a	<.5	6	2	<5	2	<5	2	11	368	>200	3	<1
MGCV-1	Midas	Qtz\CC\Adl Vein	253	0.8	237	106	57	3002	<5	2	5	7	15.9	1013	<1
MGCV-2	Midas	Qtz\CC\Adl Vein	429	0.5	96	22	29	3742	<5	<.5	3	<5	1.7	1254	<1
MCGGC	Midas	Qtz\CC\Adl Vein	1511	0.7	4531	477	53	3276	<5	1	6	<5	4.1	3278	<1
MTGCG	Midas	Qtz\CC\Adl Vein	294	0.7	773	357	154	4974	<5	<.5	4	<5	15.6	2240	1
SMGK	Sandman	Adl Vein	1160	1.1	48	11	39	517	9	5	13	47	0.5	21	<1
SMGK-2	Sandman	Adl Vein	2556	1.0	34	14	28	1363	9	3	8	30	0.3	7	2
SMGK-3	Sandman	Host Rock	13	1.3	62	16	41	19	10	3	14	67	0.3	5	<1
SMPP	Sandman	Qtz Vein	35	1.3	76	12	37	79	29	2	7	62	0.3	5	<1
HCN-1	Sandman	Adl Vein	1540	0.9	17	4	16	708	<5	1	13	37	0.7	<2	<1

Table 2. *Cont.*

Sample #	Location	Sample Type	Au	Mo	Cu	Pb	Zn	Ag	As	Sb	Cr	Ba	Hg	Se	Te
JUM1-1	Jumbo	Adl Vein	906	0.5	37	5	35	591	10	16	5	27	0.7	<2	<1
JUM2-1	Jumbo	Adl Vein	13	3.2	54	20	38	12	223	10	16	97	0.9	5	<1
JUM2-2	Jumbo	Adl Vein	12	4.8	48	10	43	17	8	11	22	34	0.7	<2	<1
JUM2-3	Jumbo	Qtz\Adl Vein	771	2.1	87	12	25	813	207	19	6	64	0.4	7	1
JUM3-1	Jumbo	Adl Vein	9	3.4	72	26	233	6	364	52	9	53	0.5	47	<1
HCN-3OX	Jumbo	Adl Vein	415	1.1	11	1	15	299	<5	3	5	15	0.1	<2	<1
HCN-3RE	Jumbo	Adl Vein	597	0.8	6	2	<5	428	<5	2	4	14	0.3	<2	<1
JUM-1	Jumbo	Qtz\Adl Vein	3748	6.1	157	65	66	1742	493	67	10	173	25.2	9	67
NEWA1-1	New Alma	Qtz\Adl Vein	6	2.2	19	9	121	8	27	7	5	107	0.2	<2	<1
NEWA1-2	New Alma	Qtz\Adl Vein	6	1.8	27	10	46	3	45	4	11	17	0.2	3	<1
NEWA1-3	New Alma	Qtz\Adl Vein	0	0.8	10	6	32	1	32	2	7	21	0.1	<2	<1
NEWA2-1	New Alma	Qtz Vein	0	2.0	19	26	61	1	32	4	14	33	0.1	<2	4
HCN-2	New Alma	Adl Vein	175	<.5	4	4	<5	159	24	1	2	19	0.1	3	1
HCN-4	Ten Mile	Adl Vein	n/a	1.0	65	11	70	2	144	195	10	61	<.05	<2	<1
SLP-8	Sleeper	Qtz Vein	9788	4.3	277	82	62	5473	26	260	9	181	70.0	64	143
SLP-10	Sleeper	Qtz Vein	8599	1.8	272	51	96	3756	59	1692	6	25	47.0	27	18
KORYU-4	Koryu, Japan	Qtz\Adl Vein	2211	1.3	35269	8458	6894	4224	599	344	7	9	0.7	5906	19
BG-2	Bessie G, CO	Qtz Vein	2289	2.2	1191	99	223	1463	149	377	12	640	>200	3	5300
SSMCO	Silverton, CO	Qtz Vein	28767	8.0	15731	195700	7893	4797	23	148	18	173	3.2	7	137
CMCO	Cresson, CO	Qtz Vein	7816	693.1	8939	1152	1896	2820	610	5560	4	881	11.5	11	10549
NMNV-1	Golden Age, CO	Qtz Vein	1902	9.7	211	1712	110	229	198	40	13	200	1.6	<2	2296
VM-1	Vindicator, CO	Qtz Vein	25136	2.6	207	390	57	6123	4987	760	6	49	58.0	39	28
BRM-1	Black Rose, CO	Qtz Vein	3926	25.1	416	5016	157	2470	829	87	13	214	>200	3	6762

Notes: all deposits are located in the northern Great Basin unless otherwise indicated. All data is in ppm.

Abbreviations: Adl = adularia, CC = calcite, Qtz = quartz.

41

Since the goal of this study was to evaluate the relative abundances of different elements in the ores of these systems, samples for geochemical analysis were "high-graded" to contain the highest percentage of ore minerals possible and minimize the amount of gangue minerals and host rock. For this reason the concentration of each element is less important than the ratios and relative abundances compared to other elements. It should be noted that this practice of high-grading the samples could cause some elemental ratios to be inaccurate and further work is warranted to determine methods that will minimize this issue. It appears however, that the geochemistry of these ore samples was not grossly misrepresented. Geochemistry data amongst samples from the same deposit are generally quite consistent and; the results are consistent with the major ore minerals observed in hand samples and thin sections (described above).

As a whole, samples are typical high-grade ore common to this type of epithermal deposit. Au concentrations greater than 1 ppm are present in nearly all of the samples and Ag concentrations generally exceed 100 ppm. The northern Great Basin deposits typically have higher precious metal to base metal ratios, compared to the deposits of Colorado and Japan. In the higher grade deposits of the northern Great Basin, Au and Ag concentrations far exceed base metal concentrations. The relatively lower grade samples typically have equal amounts of Ag and base metals with considerably less Au. The most notable difference that exists between deposits of different regions is the amounts of Au, Ag, Se and Te present. Deposits located in the northern Carlin Trend (Midas and Hollister), National district (National and Buckskin National), War Eagle Mountain, ID, and Koryu, Japan, all contain very Se-rich ores that are nearly devoid of Te along with typical Ag/Au ratios of >10 to 1. Conversely, the deposits of Colorado contain low levels

of Se, abundant Te, and Au concentrations that are often at least twice that of Ag. The

deposits located in the Slumbering Hills (Jumbo, New Alma, Sandman, Sleeper, and Ten

Mile) have ore chemistries considerably different from any of the other deposits in this

study. The Au/Ag ratio is nearly 2 to 1 and all the deposits with the exception of Sleeper

contain nearly no Se or Te, as well as having considerably lower base metal

concentrations.

Statistical Analysis

A Pearson correlation matrix was calculated, using the limited geochemical data

gathered for this study, for the northern Great Basin precious metal epithermal deposits.

Although there are far too few data points to accurately characterize these deposits,

results indicate several moderate to strong correlations between different elements. Plots

were produced using both log normalized (Table 3) and "raw" (Table 4) concentration

data and show similar trends in elemental relationships.

Table 3. Correlation Matrix of Log Normalized Concentration Data

	Au	Mo	Cu	Pb	Zn	Ag	Ni	Co
Mo	0.336							
Cu	0.123	0.149						
Pb	0.099	0.176	**0.722**					
Zn	0.113	0.383	**0.632**	**0.793**				
Ag	**0.625**	-0.103	0.434	0.429	0.210			
Ni	-0.215	0.384	-0.069	-0.228	0.141	**-0.539**		
Co	-0.182	0.303	0.206	-0.091	0.289	-0.327	**0.836**	
Mn	0.209	0.238	0.028	0.210	0.380	-0.096	0.004	0.129
Fe	-0.091	**0.506**	0.147	0.128	0.393	-0.422	**0.672**	**0.606**
As	-0.190	0.332	0.342	0.369	0.481	-0.111	0.427	0.483
Sr	0.187	0.142	-0.132	-0.321	-0.199	-0.108	0.164	0.251
Sb	0.096	0.380	0.395	0.361	0.456	0.228	0.351	0.361
Cr	0.217	**0.687**	0.044	0.185	0.306	-0.134	0.242	0.113
Ba	0.239	**0.559**	-0.119	-0.294	-0.008	-0.283	**0.630**	**0.543**
Hg	**0.627**	0.418	0.332	0.380	0.425	0.496	-0.186	-0.079
Se	0.119	-0.063	**0.692**	**0.707**	**0.533**	**0.636**	-0.483	-0.201
Te	0.244	0.249	0.366	0.271	0.194	0.414	0.083	0.230

	Mn	Fe	As	Sr	Sb	Cr	Ba	Hg
Fe	0.149							
As	-0.126	**0.601**						
Sr	0.298	0.279	-0.113					
Sb	-0.267	0.250	**0.765**	-0.249				
Cr	0.188	0.422	0.328	-0.125	0.409			
Ba	0.165	**0.528**	0.297	0.415	0.251	0.424		
Hg	0.279	-0.004	0.178	0.161	0.460	0.394	0.132	
Se	-0.042	-0.224	0.134	-0.295	0.259	-0.082	**-0.514**	0.382
Te	-0.160	0.010	0.191	0.179	0.352	-0.121	0.267	0.256

	Se
Te	0.191

Notes: Plot is a Pearson correlation matrix of log normalized geochemical data for the northern Great Basin deposits in this study (excludes the Colorado and Japan data). Correlations >0.5 are in bold.

Table 4. Correlation Matrix of Concentration Data

	Au	Mo	Cu	Pb	Zn	Ag	Ni	Co
Mo	**0.551**							
Cu	0.409	0.094						
Pb	-0.051	-0.073	0.334					
Zn	-0.043	-0.066	0.335	**0.999**				
Ag	0.352	0.145	0.408	-0.077	-0.071			
Ni	-0.062	0.101	-0.085	0.020	0.026	-0.262		
Co	-0.071	-0.128	-0.007	0.065	0.066	-0.175	0.480	
Mn	-0.071	-0.034	0.029	0.223	0.224	0.047	**0.673**	0.093
Fe	-0.007	**0.505**	0.060	0.403	0.408	-0.204	0.123	0.028
As	-0.038	-0.054	0.315	**0.991**	**0.991**	-0.120	0.026	0.071
Sr	0.024	0.429	-0.122	-0.071	-0.072	0.050	0.002	0.012
Sb	**0.925**	0.428	0.442	0.001	0.012	0.316	-0.051	-0.049
Cr	0.432	**0.643**	0.095	0.063	0.067	-0.043	-0.067	-0.223
Ba	0.324	**0.694**	-0.106	-0.119	-0.113	0.060	0.303	0.032
Hg	**0.834**	**0.574**	0.254	-0.062	-0.058	**0.559**	-0.110	-0.095
Se	-0.066	-0.105	0.457	0.036	0.032	**0.606**	-0.166	-0.110
Te	0.258	0.470	-0.027	-0.037	-0.038	0.388	-0.057	-0.029

	Mn	Fe	As	Sr	Sb	Cr	Ba	Hg
Fe	0.035							
As	0.214	0.418						
Sr	-0.012	**0.640**	-0.065					
Sb	-0.069	-0.045	0.017	-0.086				
Cr	-0.109	0.192	0.080	-0.020	0.420			
Ba	0.144	0.465	-0.086	**0.513**	0.113	0.310		
Hg	-0.012	0.004	-0.062	0.139	**0.665**	0.316	0.479	
Se	0.080	-0.155	-0.022	-0.075	0.024	-0.063	-0.274	0.064
Te	-0.068	0.185	-0.043	0.349	-0.015	0.016	**0.710**	**0.629**

	Se
Te	-0.078

Notes: Plot is a Pearson correlation matrix of geochemical data for the northern Great Basin deposits in this study (excludes the Colorado and Japan data). Correlations >0.5 are in bold.

Gold shows a strong correlation (>0.8) with Hg and Sb along with moderate correlations (0.5 – 0.8) with Ag and Mo. The strong Hg correlation fits well with field observations and published data that indicates cinnabar commonly occurs in the upper zones of these ore deposits (Vikre, 2007). Tetrahedrite ($(Cu,Fe,Zn,Ag)_{12}Sb_4S_{13}$) is common in some ores, and may partially explain the strong Sb correlation. However, the weak correlation between Au and Cu suggests that Sb is contained in other minerals such as stibnite (Sb_2S_3), which is common in the upper zones of the veins in the National district (Lindgren, 1915; Vikre, 1984). The relationship with Ag is also to be expected as electrum is the most common Au-bearing ore mineral. The moderate correlation with Mo may indicate a connection to deeper porphyry systems, which are thought to act as sources of metal-bearing magmatic fluids (Hedenquist and Lowenstern, 1994).

The strongest correlation for Ag is with Se (0.6), which is well supported by field observations and published data (Vikre, 1984; Halsor et al., 1988; Goldstrand and Schmidt, 2000) that indicate the Ag-minerals naumannite (Ag_2Se) and aguilarite (Ag_4SeS) are present in many of these deposits. Silver has a moderate correlation with Hg (0.5-0.6), likely for the same reason that gold does.

Zinc shows a strong association with Pb. This is likely related to the base metal zones that commonly occur within these systems, generally below the precious metal zones. Field observations and petrography found abundant sphalerite and galena associated with some ore samples. Copper has moderate correlations with Pb, Zn and Se. Chalocopyrite is common in many of the polished thin sections that also contain other ore minerals. Copper has a weak correlation with Sb, As, and Ag, which is likely due to the

46

fact that tetrahedrite and tennantite ($(Cu,Fe)_{12}As_4S_{13}$) are common in some of the deposits in this study.

The relationship between As and Sb is weak to moderate as could be expected by examining the data (Table. 3). Whereas both elements are present in almost every sample, concentrations varied from sub-equal to inverse, thus no clear relationship is discernable here.

By looking at the data in Table 3 a strong negative correlation between Te and Se could be expected, and that is the case if both the Nevada and Colorado ores are considered. However, if only the Nevada ores are considered, which are generally quite low in Te and enriched in Se, no clear correlation exists.

Epithermal Trilinear Diagram

Numerous classification schemes exist for epithermal deposits, and these schemes have been well summarized by Sillitoe and Hedenquist, (2003) and Simmons et al. (2005). Previous classification schemes have focused on alteration and gangue mineral assemblages, which are good indicators of the ore-forming fluid chemistry. However, a geochemical classification scheme for low-sulfidation ores has not been attempted.

Trilinear diagrams are often used to characterize natural waters based on their major ionic species. In the classic Piper diagram, the cations Ca, Mg and Na + K are plotted onto one triangle and the anions Cl, SO_4, and $HCO_3 + CO_2$ are plotted onto the other. When the points plotted in the triangles are projected into the quadrilateral field, differences in water chemistries can be clearly seen. Waters with similar sources and chemistries fall into the same area of the quadrilateral field. Dominant ions and

47

hydrochemical facies can be determined using a trilinear plot of major ions (Fetter, 2001). Thus, trilinear plots of water chemistry are useful for determining the natural water's source and how the water chemistry has evolved.

For this study, a trilinear diagram was modified such that the molar ratios of Au, Ag, and Pb/10 were normalized to 100% and then plotted in the metals triangle. Similarly the molar ratios of Se, Te, and Sb/10 + As/10 were normalized and then plotted in the metalloid triangle. The elements Pb, As, and Sb are common in epithermal ores and thus have higher background levels than Au, Ag, Se, and Te. For this reason the concentrations of Pb, As and Sb were reduced by a factor of 10 to compensate for the much more abundant elements. It should be noted that the "raw data" with no factor 10 reductions were also plotted on a trilinear diagram with similar results, except that most of the trends observed were masked or subdued. By plotting all of the geochemical data from the epithermal ores (Nevada, Colorado, and Japan), on the new epithermal trilinear plot, it was determined that certain end-member compositions exist within the data as a whole. The two most prominent end members (Fig. 17) of these are the Au-telluride dominated ores of Colorado and the Ag-selenide dominated "ginguro" ores found at deposits such as Midas, Hollister, War Eagle Mountain, Koryu, and Hishikari. A third group of deposits (National and Hog Ranch), which contain high levels of Pb, As, and Sb plot just to the left or within the Au-telluride field.
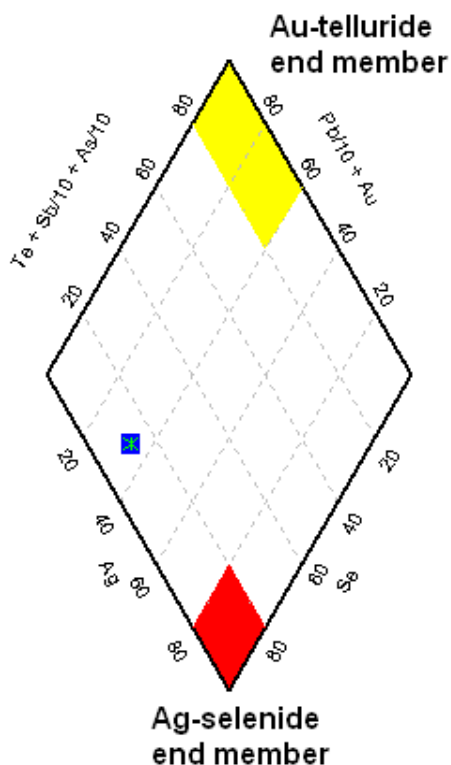
FIG. 17. Illustration of proposed fields for the modified trilinear diagram. Au-tellurides (yellow) and Ag-selenides (red). Chondritic meteorite data (Anders and Grevesse, 1989) are also plotted here (blue square) and are thought to mimic mantle chemistry (Winters, 2001), or at least early earth mantle.

Geochemical District Descriptions

  National District: The National and Buckskin-National deposits both lie in the National district. Samples were collected from dumps around the numerous historical workings. Gold levels vary greatly in the National deposit ores, including some of the highest values (32,940 ppm) recorded for any sample in this study, and all Au levels are well over what could be considered "ore grade." Silver levels are slightly less variable ranging from 200 to 3800 ppm. Notably high levels of Pb, Zn, As, and Sb also are present in the ores. Selenium levels reach a maximum of 401 ppm and Te is nearly undetectable. When these data are plotted on the epithermal trilinear diagram (Fig. 18) it can be seen that As and Sb are the dominate metalloids in the National ores, and the amounts of Pb,

Au and Ag have a much higher degree of variability. The high degree of scatter, and range of minerals observed in the different samples collected, suggests more samples are needed to adequately characterize the National ores.

The Buckskin-National ores share a similar geochemical signature to the National samples expect for a few notable dissimilarities. Gold concentrations are elevated in all samples (32 to 782 ppm) and Ag levels are exceptionally high (up to 3350 ppm). Significant levels of Pb, Zn, As and Sb are present but generally are an order of magnitude lower than those detected at National. Selenium levels are generally higher and there is no detectable Te in any of the samples. It is interesting to note that when the Buckskin National data are plotted on the epithermal trilinear diagram (Fig. 18) the data all plot neatly within the Ag-selenide field, unlike the National ores.

War Eagle Mountain: The northern-most samples gathered during field work are from War Eagle Mountain, Silver City district, Idaho. Samples were collected from the numerous dumps surrounding historic workings, as well as from the outcropping Oro Fino vein. All the samples collected contained high levels of Au (up to 149 ppm) and Ag (up to 5700 ppm), as well as very high levels of Se (nearly 1700 ppm). Tellurium was generally below detection limits (<1 ppm) with a maximum of 18 ppm and Hg was not detected in any of the samples. The ores of War Eagle Mountian also plot on the epithermal trilinear diagram (Fig. 18) within the Ag-selenide field along with the ores from Buckskin National.
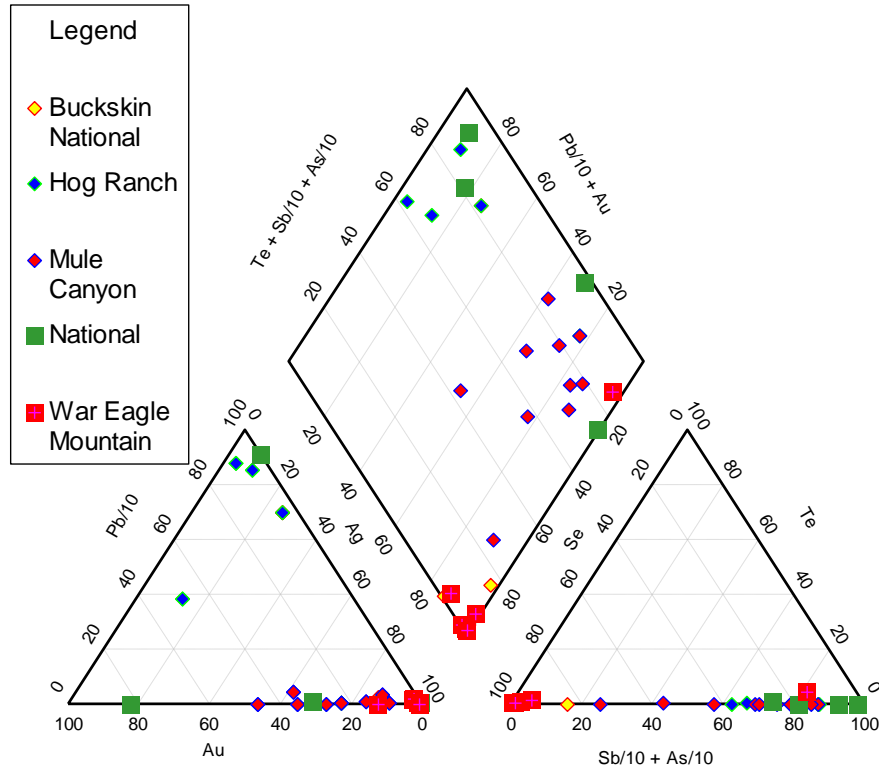
FIG. 18. Epithermal trilinear diagram of several northern Great Basin deposits showing the broad spectrum of ore chemistries. Hog Ranch (Bussey, 1996) and Mule Canyon (John et al., 2003) data are plotted for comparison. Note some of the Buckskin National data points are obscured by the overlapping War Eagle Mountain points.

Northern Carlin Trend: The Midas deposit contains ores that closely resemble the "ginguro" (silver-black) ores of many Japanese epithermal deposits such as Hishikari (Izawa et al., 1990). Abundant precious and base metal selenides have been reported at the Midas deposit as well as replacement textures of naumannite after base-metal sulfides (Golstrand and Schmidt, 2000). Samples were collected at the underground workings of the Ken Snyder mine, operated by Newmont Gold. Silver concentrations are remarkably consistent in all the samples analyzed for this study, ranging from approximately 3000-5000 ppm. Gold values were more variable with a high of 1500 ppm and low of 250 ppm

and showed a positive correlation to the values of Se in each sample. Curiously low are As, Sb and Te which were all near or below detection limits.

Samples from the Ivanhoe district were collected at the new underground workings in the Hollister Development Block, owned by Great Basin Gold. The samples collected show remarkable geochemical similarities to the ores at the nearby Midas mine. Extremely high Au (>400 ppm) and Ag (>6000 ppm) values were detected as well as high levels of Se (>2600 ppm) and low levels of Te (< 10 ppm). Abundant tetrahedrite and tennantite are present in hand samples, thus concentrations of As, Sb and Cu are high. Ores from the Midas and Hollister deposits plotted (Fig. 19) in or near the Ag-selenide field as expected.
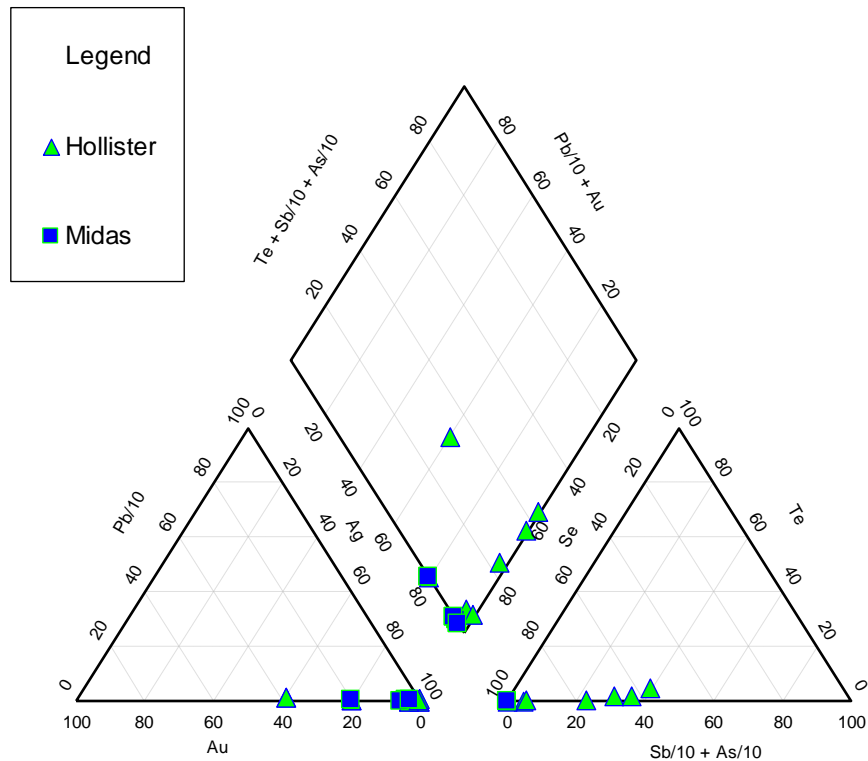
FIG. 19. Epithermal trilinear diagram of the Hollister and Midas deposits both of which plot within the Ag-selenide field.

Slumbering Hills: Within the Slumbering Hills and surrounding pediment are the Sleeper, Jumbo, New Alma, Sandman, and Ten Mile deposits. All have similar geochemical signatures and are known to have formed at around the same time (see below).

The most recently exploited deposit in the area is Sleeper, which was mined from the mid-1980's to mid-1990's. Samples analyzed for this study have extremely high levels of Au and Ag with a ratio of nearly 2 to 1. Concentrations of Cu, Sb and Mn all range from 150 to 300 ppm. Sample SLP-10 also contained some of the highest levels of U recorded (18 ppm), possibly due to leaching from the rhyolite host rock. The Sleeper deposit was the only deposit in the Slumbering Hills to contain noteworthy levels of Se (27 - 64 ppm) and Te (18 - 143 ppm). Nearly all the samples from Jumbo, New Alma, Sandman, and Ten Mile contain very low or undetectable levels of Se and Te, and it appears they do not form any important ore minerals.

The Jumbo and New Alma deposits lie just to the east of Sleeper in the northern Slumbering Hills. The general geochemical signature for both deposits is similar to that of Sleeper and their close proximity and similar ages suggest all three deposits are genetically linked. The Jumbo deposit has a Au/Ag ratio of approximately 2 to 1 with one sample having nearly 4000 ppm Au and several others having Au levels in the hundreds of ppm. Levels of Cu, Zn, Mn, As, and Sb all register in the tens to hundreds of ppm. The high manganese concentrations are likely due to the black oxide coating, which occurred on several of the samples from Jumbo and New Alma.

New Alma samples generally have much lower overall Au and Ag numbers, most being less than 10 ppm, one high-grade sample did contain higher Au (175 ppm) and Ag

53

(159 ppm) levels, and generally samples had approximately equal amounts of Au and Ag. Relatively high levels of Cu, Zn, Mn and As were also present in similar ratios to the Jumbo samples. Manganese was especially high in these samples, which all had a black oxide coating on them.

The Sandman deposit lies in the southern pediment of the Slumbering Hills. Recently it has been the subject of much exploration activity and is currently being drilled by Fronteer Development Group (Fronteer Development Group press releases 2007), which recently aquired it from New West Gold. Vein sets are predominately adularia and the only significant precious metal bearing mineral is electrum. The adularia veins contain high concentrations of Au (up to 2500 ppm) and Ag (up to 1300 ppm) and a similar Au/Ag ratio as the other Slumbering Hills deposits. Samples of host rock and quartz veins contain levels of Au and Ag ranging from 10 to 80 ppm. Base metals all occur in low levels (<100 ppm) and Mn (130 to 260 ppm) likely is present as a weathering product. The levels of As and Sb were also quite low, generally not exceeding 10 ppm.

The Ten Mile district has been well described by Bowell et al. (2000). A sample split from the geochronology samples was submitted for geochemical analysis and yielded relatively low Ag levels (1.5 ppm). Levels of Cu (64 ppm), Zn (70) ppm, As (144 ppm) and Sb (195 ppm) were high considering the very low precious metal contents. This could be due to the very weathered nature of the sample. It was also noted by Bowell et al. (2000) that supergene processes played an important role in ore modification in this district. Gold concentrations were below detection limits, thus the Ten Mile data could not be plotted on the epithermal trilinear diagram.

If the geochemical data for the Slumbering Hills are considered as a whole, deposits throughout the region overlap somewhat in chemistry, but a distinct wide change can be observed between the northern deposits (Sleeper, Jumbo, New Alma) and the Sandman deposit, which sits in the southern pediment of the Slumbering Hills. The metals data are very tightly clustered in a field that indicates the ores are high in Au and Ag and generally very low in Pb. The large degree of scatter for these deposits, when projected into the quadrilateral section of the trilinear diagram (Fig. 20), is caused by a large variation in the metalloid content of the ores.
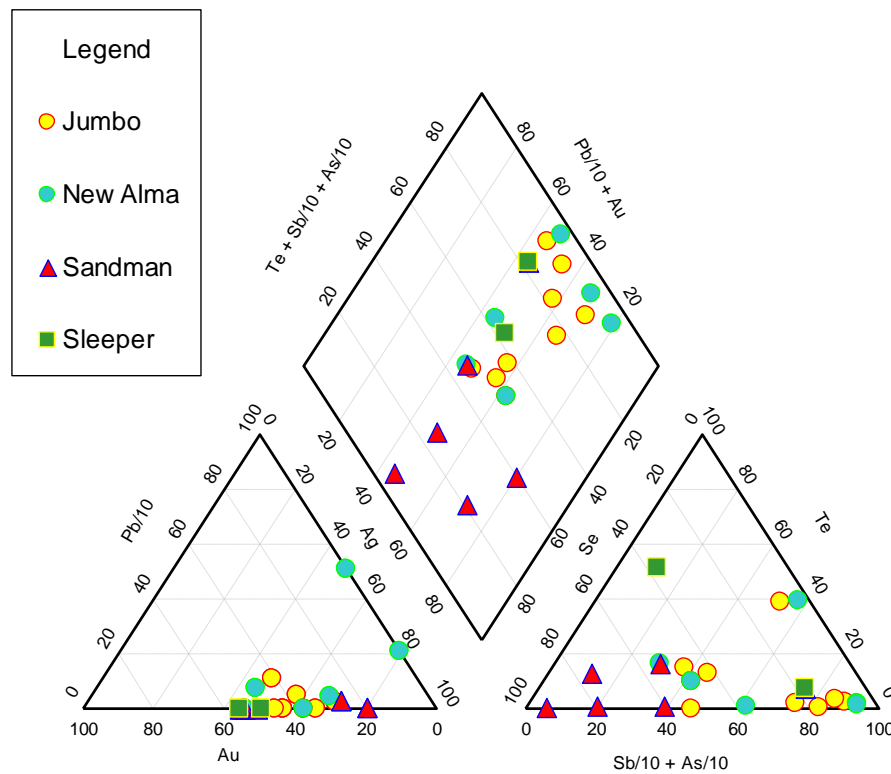
FIG. 20. Epithermal trilinear diagram of Slumbering Hills area deposits shows a gradual change in deposit geochemistry from north to south.

Japanese Epithermal Deposits: The Japanese epithermal precious metal deposits are considerably younger ($\sim$ 1 Ma) than the other deposits in this study (Sanematsu et al., 2006) and formed in a subduction related volcanic island arc tectonic setting (Izawa et al.,

1990) that may be related to back-arc rifting (Garwin et al., 2005). However, texturally and chemically they have a number of similarities to the epithermal ores of the northern Great Basin, including banded quartz/adularia ± calcite veins, as well as abundant electrum and naumannite (Izawa et al., 1990). The sample from the Koryu deposit, Japan, is a classic example of ginguro ore consisting of quartz/adularia veins. For the present study the sample was high-graded to contain abundant naumannite and electrum. The geochemical composition of this sample is very similar to the other selenium dominated precious metal systems (Midas, Hollister, and War Eagle Mountain) in this study. As with the other deposits, this sample contains extremely high levels of Au (2200 ppm) and Ag (4200 ppm), along with abundant base metals, and high levels of As and Sb. Selenium is also very abundant (5900 ppm) and plays an important role in the formation of ore minerals.

When data from this study and previously reported data from the Hishikari deposit (Izawa et al., 1990) were plotted, two clusters of data were created (Fig. 21). This distribution in some ways resembles that seen in the Slumbering Hills deposits. The metals data cluster close together and indicate roughly equal Au/Ag concentrations with very low levels of Pb. The metalloid data have a much larger spread that ranges from very Se-rich to very Sb and As-rich along with ubiquitous low Te levels.
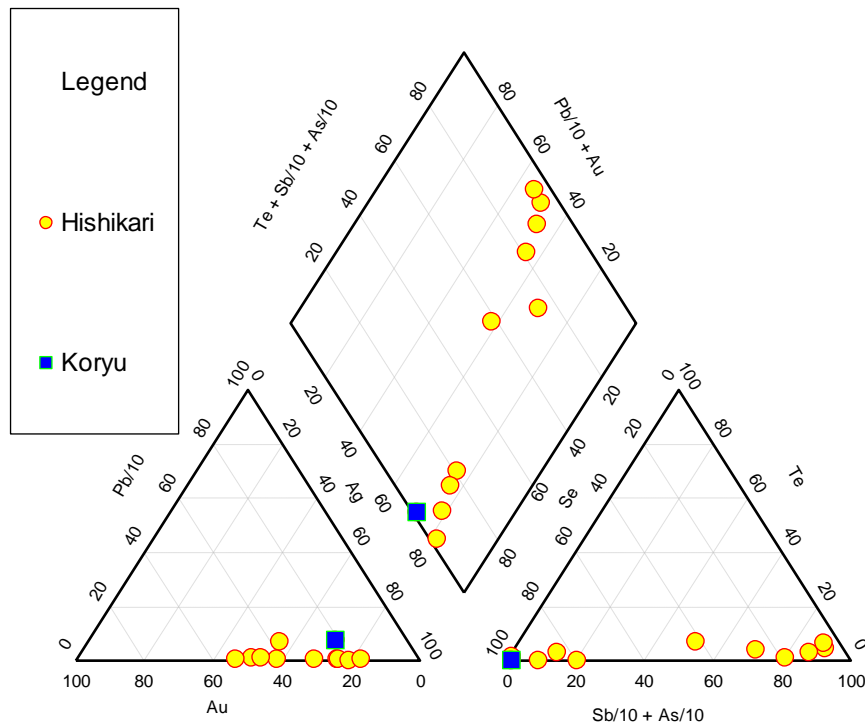
FIG. 21. Epithermal trilinear diagram of Koryu and Hishikari, Japan (Izawa et al. 1990).

Colorado Telluride Deposits: The Colorado ores included in this study represent the opposite end member in geochemical classification of low-sulfidation epithermal precious metal deposits. All samples were provided by James Saunders and Robert Cook (Golden Age) and consisted of quartz veins that had been sampled specifically to contain abundant Au/Ag-telluride minerals. A number of interesting similarities and differences can be observed between the selenide-dominated and telluride-dominated deposits. In the Colorado ores, Te levels can exceed 10,000 ppm while Se levels generally do not exceed 10 ppm. An interesting exception is the Vindicator mine sample, which had slightly more Se (39 ppm) than Te (28 ppm), along with some of the highest Au (25,000 ppm) and Ag (6000 ppm) levels of any sample. High levels of base metals along with Sb and As are

also present. The Cresson mine had notably abundant Mo (693 ppm), nearly two orders

of magnitude greater than levels detected any other deposit in this study.

As expected, all the Colorado telluride ores plot within the Au-telluride field (Fig.

22). Since only a few samples were used for this study, with the goal being that they

serve as a basis for comparison, it is only possible to make general observations and

inferences about what this data may mean for the classification system as a whole. It has

been suggested that these Au-Te deposits represent a subclass of low-sulfidation

epithermal deposits (Sillitoe and Hedenquist, 2003).
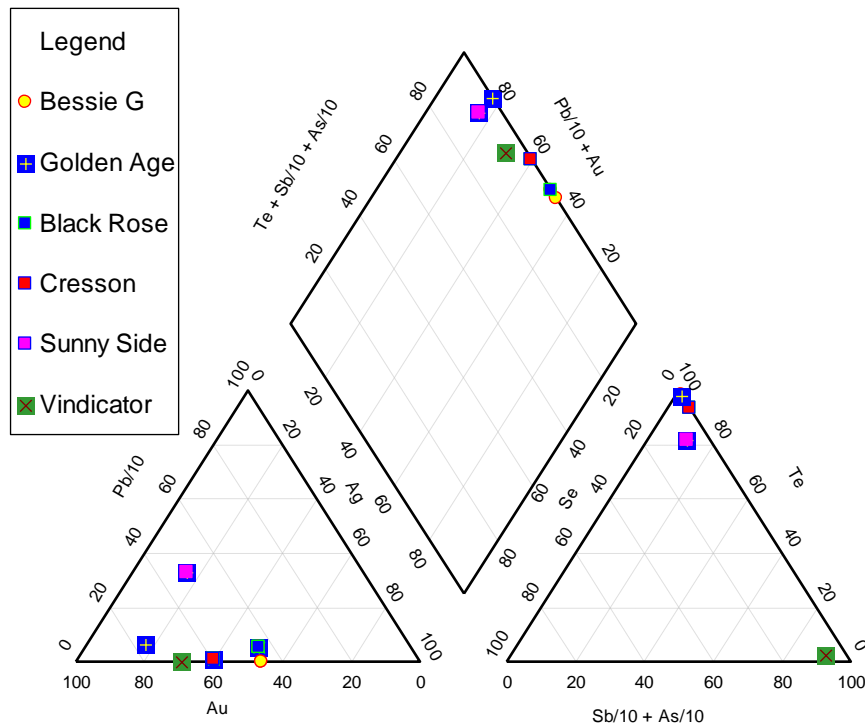
FIG. 22. Epithermal trilinear diagram of Colorado Au-telluride deposits which
defines the telluride field.

GEOCHRONOLOGY

One of the goals of this study was to provide new geochronology data for low-sulfidation precious metal epithermal deposits in the northern Great Basin that had either been significant historic producers or, as is the case of the Sandman deposit, may see future development. Through field work, adularia with inter-grown Au/Ag-minerals was obtained from four sites in and around the Slumbering Hills, Nevada (Jumbo, New Alma, Sandman, and Ten Mile) as well as two sites on War Eagle Mountain, Idaho. Since the overall aim of this study was to examine possible links between these mid-Miocene epithermal deposits and the initiation of the Yellowstone hotspot, the combination of closely clustered deposits in two broadly separated areas makes it possible to examine the timing of deposit formation on a local and regional scale. The geochronology results from this study augment previous studies for similar deposits in the region and thus provide more evidence that mineralization was coincident in time and space with the initiation of the Yellowstone hotspot.

Geochronology Technique and Results

The samples for this study were found to be highly radiogenic and contain a significant amount of extraneous ^{40}Ar in surface defects and fluid inclusions (Appendix 2). Single crystal incremental heating was determined to be the most effective

59

method of analysis (see Methodology) for these samples as it allows for removal of extraneous ^{40}Ar and evaluation of potential loss of accumulated radiogenic argon.

Data reduction was preformed using the Excell add-on Isoplot (Ludwig, 2003) to create model-age spectrum and isotope correlation diagrams. The model-age spectrum and isotope correlation diagrams yield plateau and isochron ages respectively that are the same within uncertainty. However, the uncertainty of the isochron age is considerably higher (Appendix 2). The higher uncertainty of the isochron age reflects the fact that all analyses are highly radiogenic with little spread to define the regression, thus the plateau age is preferred. For this reason, only the release spectra (Table 5) for each deposit will be discussed in this thesis.

When the ages determined in this study are compared to those from previous studies (Table 6) it is clear that these new data fall well within the expected time frame for mineralization within the area. A broad range of ages is present both for the entire region and within individual districts. This suggests that mineralization occurred throughout the region from approximately 16.5 Ma to 15.1 Ma with no discernable trend that would suggest mineralization started in one area and spread in any particular direction (Fig. 16).

Table 5. Summary of Geochronology Results

Sample ID	Deposit	Irradiation Filename	Location Latitude	Longitude	Plateau Age (Ma)
HCN-1	Sandman	au5.1a.adl.ih1	41º 03.959'N	118º 01.222'W	16.17 ± 0.03
		au5.1a.adl.ih2			15.99 ± 0.04
		au5.1a.adl.ih3			16.19 ± 0.04
		au5.1a.adl.ih4			16.07 ± 0.04
		au5.1a.adl.ih5			16.16 ± 0.04
				Preferred Age	**16.17 ± 0.04**
HCN-2	New Alma	au5.1c.adl.ih.1	41º 17.857'N	118º 00.362'W	15.86 ± 0.04
		au5.1c.adl.ih.2			16.04 ± 0.02
		au5.1c.adl.ih.3			16.05 ± 0.03
		au5.1c.adl.ih.4			no plateau
		au5.1c.adl.ih.5			15.99 ± 0.03
				Preferred Age	**16.03 ± 0.07**
HCN-3RE	Jumbo	au5.1f.adl.ih1	41º 18.475'N	118º 01.228'W	16.54 ± 0.04
		au5.1f.adl.ih2			no plateau
		au5.1f.adl.ih3			16.53 ± 0.03
		au5.1f.adl.ih4			16.54 ± 0.05
		au5.1f.adl.ih5			no plateau
				Preferred Age	**16.53 ± 0.04**
HCN-4	Ten Mile	au5.1h.adl.ih1	40º 58.577'N	117º 54.510'W	16.50 ± 0.03
		au5.1h.adl.ih2			16.42 ± 0.03
		au5.1h.adl.ih3			no plateau
		au5.1h.adl.ih4			16.53 ± 0.03
		au5.1h.adl.ih5			no plateau
				Preferred Age	**16.52 ± 0.04**
OF-1	War Eagle Mtn.	au3.3d.adl.31	43º 00.669'N	116º 41.857'W	16.32 ± 0.03
		au3.3d.adl.32			16.31 ± 0.03
		au3.3d.adl.33			16.21 ± 0.04
		au3.3d.adl.34			16.09 ± 0.04
		au3.3d.adl.35			16.08 ± 0.04
				Preferred Age	**16.31 ± 0.04**
WEMS3-1	War Eagle Mtn.	au8.2c.adl.41	43º 00.339'N	116º 41.926'W	15.55 ± 0.04
		au8.2c.adl.42			15.66 ± 0.03
		au8.2c.adl.43			15.55 ± 0.04
		au8.2c.adl.44			15.67 ± 0.04
		au8.2c.adl.45			15.78 ± 0.05
				Preferred Age	**15.61 ± 0.10**

Notes: Uncertainties are one standard deviation. The preferred age was calculated using a weighted average. Irradiation filenames correspond to an analysis of a single crystal. See Appendix 2 for full analytical data and Appendix 3 for J-values.

Table 6. Revised Geochronology of mid-Miocene Au-Ag Deposits in the Northern Great Basin

Deposit	Age ± 1σ (Ma)	Dating Method	Predominant Host Rocks	Reference
Jumbo	17.3 ± 0.5	K/Ar	metasediments	Conrad et al., 1993
War Eagle Mtn.	16.6-15.2	K/Ar	granite	Halsor et al., 1988
Jumbo	**16.53 ± 0.04**	**Ar/Ar**	**metasediments**	**this study**
Ten Mile	**16.52 ± 0.04**	**Ar/Ar**	**metasediments**	**this study**
War Eagle Mtn. 1	**16.31 ± 0.04**	**Ar/Ar**	**granite**	**this study**
Sandman	**16.17 ± 0.04**	**Ar/Ar**	**granite**	**this study**
Sleeper	16.1-14.3 ± 0.07	Ar/Ar	rhyolite	Conrad and McKee, 1996
New Alma	**16.03 ± 0.03**	**Ar/Ar**	**metasediments**	**this study**
Buckskin National	15.8-15.4 ± 0.2	K/Ar	rhyolite	Vikre, 1985
DeLamar, ID	15.7 ± 0.5	K/Ar	rhyolite	Halsor et al., 1988
War Eagle Mtn. 3	**15.61 ± 0.1**	**Ar/Ar**	**granite**	**this study**
Mule Canyon	15.6 ± 0.04	Ar/Ar	rhyolite	John et al., 2003
McDermitt (Hg)	15.6 ± 0.4	K/Ar	rhyolite	Noble et al., 1988
Midas	15.4-15.3 ± 0.08	Ar/Ar	rhyolite	Leavitt et al., 2004
Hog Ranch	15.2-14.8 ± 0.4	K/Ar	rhyolite	Bussey, 1996
Hollister	15.19 ± 0.05	Ar/Ar	rhyolite	Peppard, 2002
Seven Troughs	13.82 ± 0.02	Ar/Ar	rhyolite	Hudson et al., 2006

Notes: War Eagle Mtn. 1 refers to the Oro Fino vein, War Eagle Mtn. 3 refers to sample site 3 in this study. McDermitt is an epithermal mercury deposit.

Slumbering Hills Deposits

The deposits located in and around the Slumbering Hills that were dated for this study (Fig. 23) are the Sandman, New Alma, Jumbo, and Ten Mile deposits.
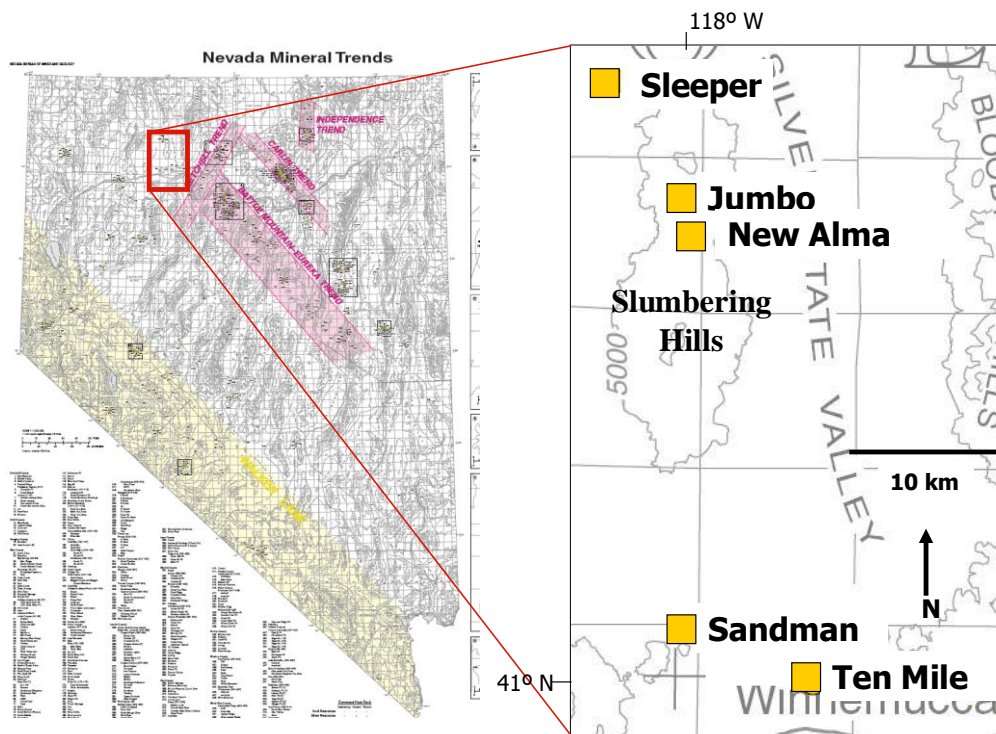
FIG. 23. Map of Slumbering Hills area deposits. Modified from Wendt (2003).

Sandman: The Sandman deposit defines an area that sits in the southern pediment of the Slumbering Hills. The area has been the subject of a number of exploration projects and is currently being explored for epithermal precious metal mineralization. Samples collected for this study consist of silicified tuff with thin (up to 4 mm) adularia veins and fracture encrustations that contained abundant visible gold.

Five crystals from geochemistry sample HCN-1 were analyzed by incremental heating and produced plateau ages (Fig. 24) with a range of 16.19 ± 0.04 to 15.99 ± 0.04 Ma. A preferred age of 16.17 ± 0.04 Ma was determined by calculating the weighted average of the three oldest crystals. At the 95% confidence level, there is 85% chance that the spread of those three plateau ages are consistent with a normal distribution of

63

errors in precision. As with the other Slumbering Hills deposits, the veins at Sandman are generally not more than a few centimeters wide; therefore, it is unlikely that a significant amount of time elapsed between the depositions of different crystals. The significantly younger ages of the two crystals excluded from the preferred age calculation likely reflect alteration or a higher diffusivity of ^{40}Ar. In either case the loss of Ar would cause the crystals to yield erroneously young ages. Field observations support this conclusion as many samples from Sandman have a thin coating of clay over the euhedral adularia crystals (Fig.5).
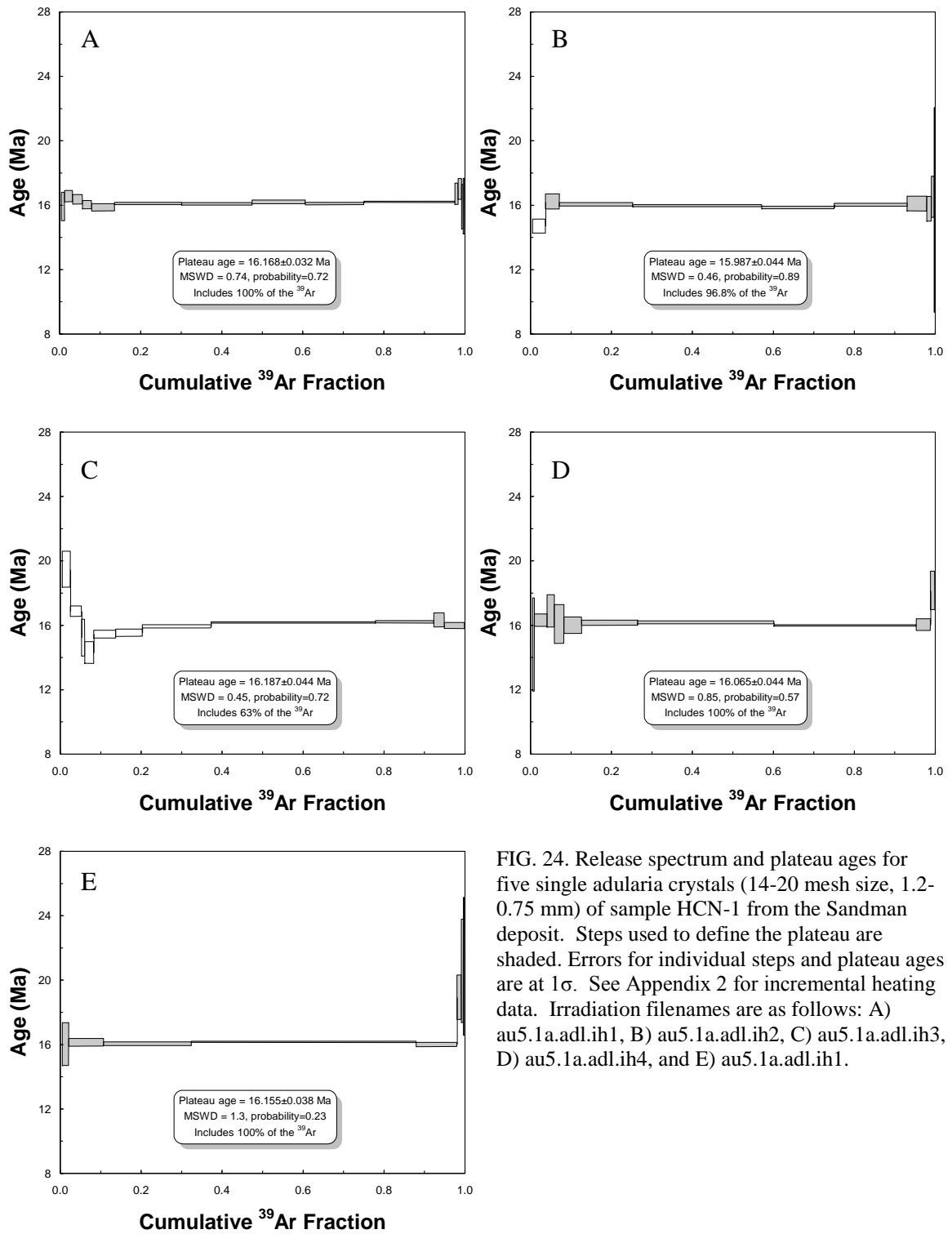
FIG. 24. Release spectrum and plateau ages for five single adularia crystals (14-20 mesh size, 1.2-0.75 mm) of sample HCN-1 from the Sandman deposit. Steps used to define the plateau are shaded. Errors for individual steps and plateau ages are at 1σ. See Appendix 2 for incremental heating data. Irradiation filenames are as follows: A) au5.1a.adl.ih1, B) au5.1a.adl.ih2, C) au5.1a.adl.ih3, D) au5.1a.adl.ih4, and E) au5.1a.adl.ih1.

65

New Alma: The New Alma deposit sits just south of the old Jumbo mine workings in the Slumbering Hills. Four of the five adularia crystals analyzed produced plateau ages that range from 16.05 ± 0.03 to 15.86 ± 0.04 Ma (Fig. 25). The one crystal that did not produce a plateau age (au5.1c.adl.ih4) still yields individual heating increment ages that are consistent within uncertainty of the other samples (Appendix 2). The preferred age, calculated using a weighted average of the oldest three plateau ages, is 16.03 ± 0.07 Ma.

The significantly younger age of one crystal, 15.86 ± 0.04 Ma, excluded from the preferred age calculation likely reflects loss of Ar due to alteration. At the 95% confidence level, there is 26% probability that the spread of plateau ages of the three oldest crystals are consistent with a normal distribution of errors in precision. However, if all four crystals are averaged, this probability drops to 0.1%. This indicates that statistically it is highly unlikely the difference in ages is due to errors in precision alone. Thus, the crystals are either of different ages or some have been subject to Ar loss. The very thin nature of the adularia veins makes more than one generation of crystals unlikely in these samples. Field observations suggest that the samples taken from New Alma have undergone intense surface oxidation and are coated in a Fe-oxide and/or Mn-oxide coating. Thus it seems likely that late oxidation caused loss of Ar in some of the crystals.

A

Plateau age = 15.864±0.042 Ma
MSWD = 0.96, probability=0.46
Includes 94.9% of the ^{39}Ar

B

Plateau age = 16.037±0.022 Ma
MSWD = 1.4, probability=0.19
Includes 92% of the ^{39}Ar

C

Plateau age = 16.054±0.027 Ma
MSWD = 1.09, probability=0.37
Includes 92% of the ^{39}Ar

D

E

Plateau age = 15.994±0.027 Ma
MSWD = 1.2, probability=0.28
Includes 81.1% of the ^{39}Ar
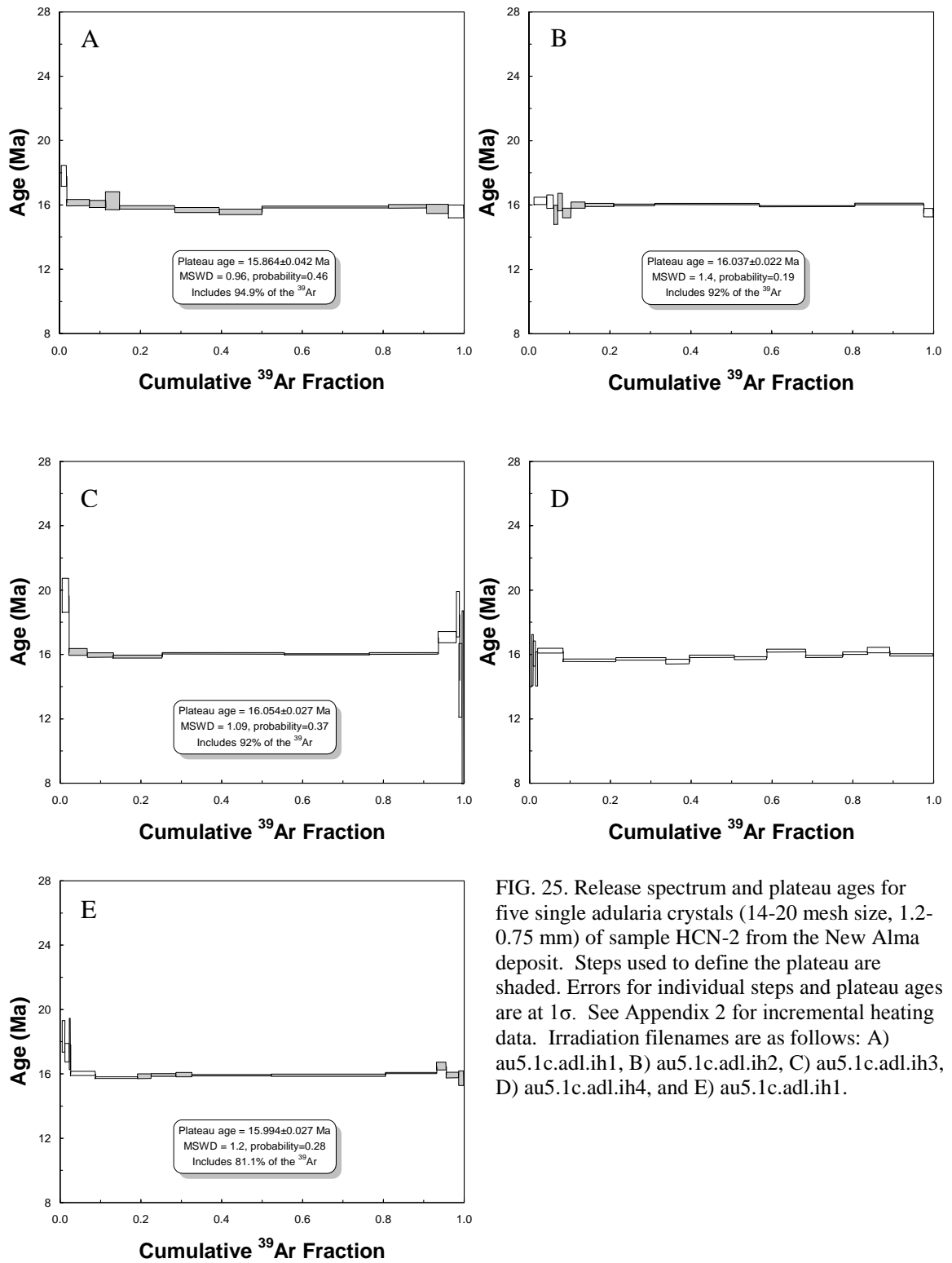
FIG. 25. Release spectrum and plateau ages for five single adularia crystals (14-20 mesh size, 1.2-0.75 mm) of sample HCN-2 from the New Alma deposit. Steps used to define the plateau are shaded. Errors for individual steps and plateau ages are at 1σ. See Appendix 2 for incremental heating data. Irradiation filenames are as follows: A) au5.1c.adl.ih1, B) au5.1c.adl.ih2, C) au5.1c.adl.ih3, D) au5.1c.adl.ih4, and E) au5.1c.adl.ih1.

Jumbo: The Jumbo deposit sits in the northern Slumbering Hills just to the east of the Sleeper mine. The Jumbo deposit is the only deposit examined in the Slumbering Hills that has previously been dated. A study by Conrad et al. (1993), using K/Ar methods, determined that adularia in veins had an age of 17.3 Ma. However, the bulk-sample total-fusion techniques used in that study are inherently limited because of their inability to resolve potential contributions from various sources of extraneous argon (inherited 'excess' ^{40}Ar, or other non-atmospheric argon). Thus, it was decided a reexamination of the Jumbo deposit using improved techniques was warranted.

Of the five adularia crystals analyzed in this study, three yield plateau ages (Fig. 26). Plateau ages for these three crystals overlap within uncertainties and yield a preferred age of 16.53 ± 0.04 Ma. The majority of the heating increments for the other two crystals fall within 2σ of this age (Appendix 2). The new data suggest that the earlier result for Jumbo appears anomalously old due to an unresolved component of extraneous ^{40}Ar. Evidence for this can be observed in Appendix 2 and Figure 26, by noting that the initial or final steps of each incremental heating schedule contain generally high levels of ^{40}Ar, low radiogenic yields, and older calculated ages than expected. This is likely due to extraneous ^{40}Ar trapped on the surface or in fluid inclusions.
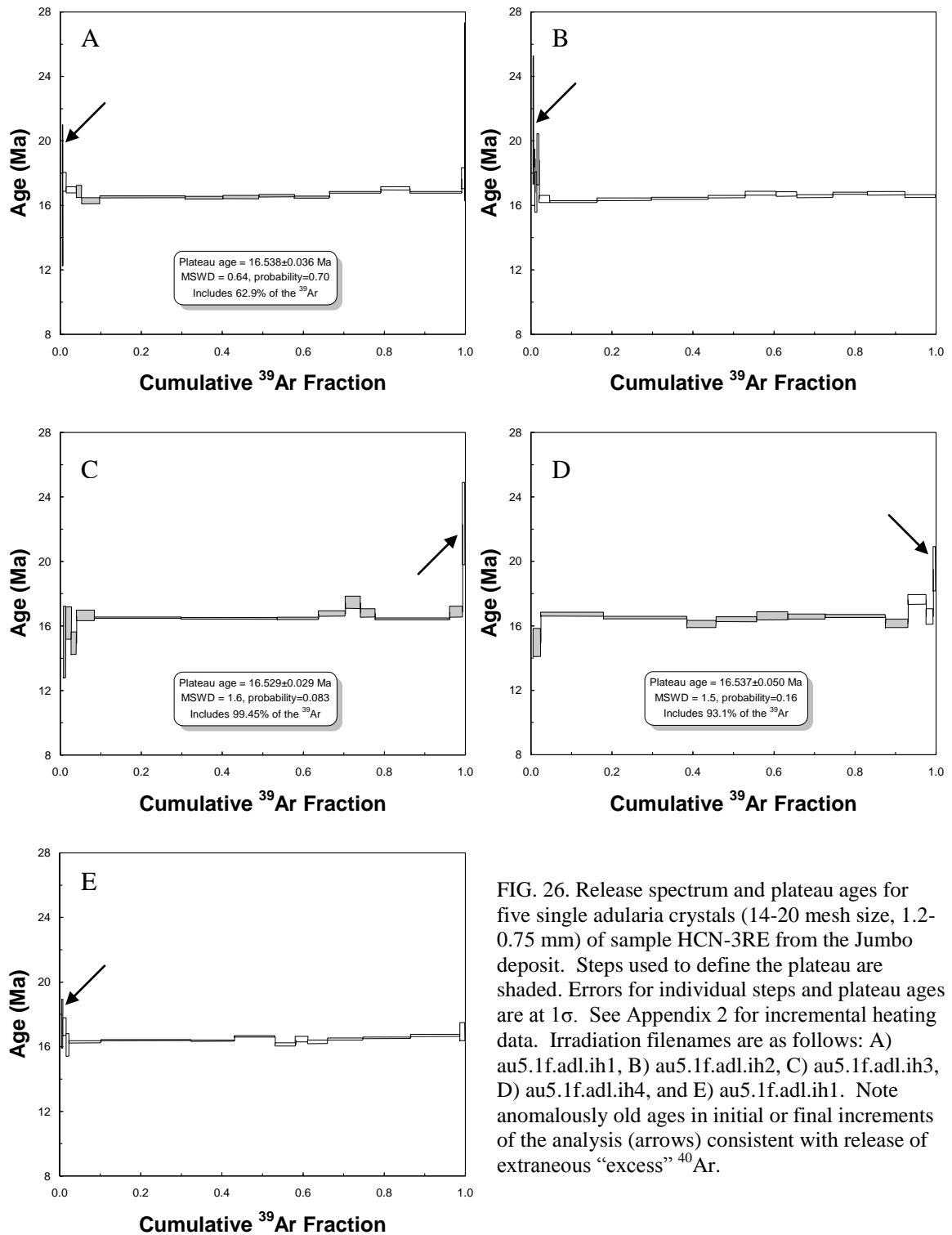
FIG. 26. Release spectrum and plateau ages for five single adularia crystals (14-20 mesh size, 1.2-0.75 mm) of sample HCN-3RE from the Jumbo deposit. Steps used to define the plateau are shaded. Errors for individual steps and plateau ages are at 1σ. See Appendix 2 for incremental heating data. Irradiation filenames are as follows: A) au5.1f.adl.ih1, B) au5.1f.adl.ih2, C) au5.1f.adl.ih3, D) au5.1f.adl.ih4, and E) au5.1f.adl.ih1. Note anomalously old ages in initial or final increments of the analysis (arrows) consistent with release of extraneous "excess" ^{40}Ar.

Plot A:
Plateau age = 16.538±0.036 Ma
MSWD = 0.64, probability=0.70
Includes 62.9% of the ^{39}Ar

Plot C:
Plateau age = 16.529±0.029 Ma
MSWD = 1.6, probability=0.083
Includes 99.45% of the ^{39}Ar

Plot D:
Plateau age = 16.537±0.050 Ma
MSWD = 1.5, probability=0.16
Includes 93.1% of the ^{39}Ar

69

Ten Mile: The Ten Mile district sits to the south east of the Slumbering Hills and just to the north of the town of Winnemucca, Nevada. Plateau ages from three samples (Fig. 27) range from 16.53 ± 0.03 to 16.42 ± 0.03 Ma. The two crystals that did not generate a plateau age still had incremental heating steps that yielded ages within this range (Appendix 2). A weighted average of the two oldest crystals yields a preferred age of 16.52 ± 0.04 Ma.

All samples collect at the Ten Mile deposit are highly oxidized making material suitable for dating difficult to obtain. This is likely the reason for the younger age of the excluded plateau age and the reason why the other two crystals did not generate plateau ages. There also is a significant component of excess ^{40}Ar in some the samples. In these samples the first and last few heating increments have very low radiogenic yields and extremely old calculated ages (Appendix 2). Consequently, the samples from Ten Mile are not ideal for geochronology work. However, careful examination of the data allows for a reasonable and reliable age to be interpreted from these less than desirable samples.
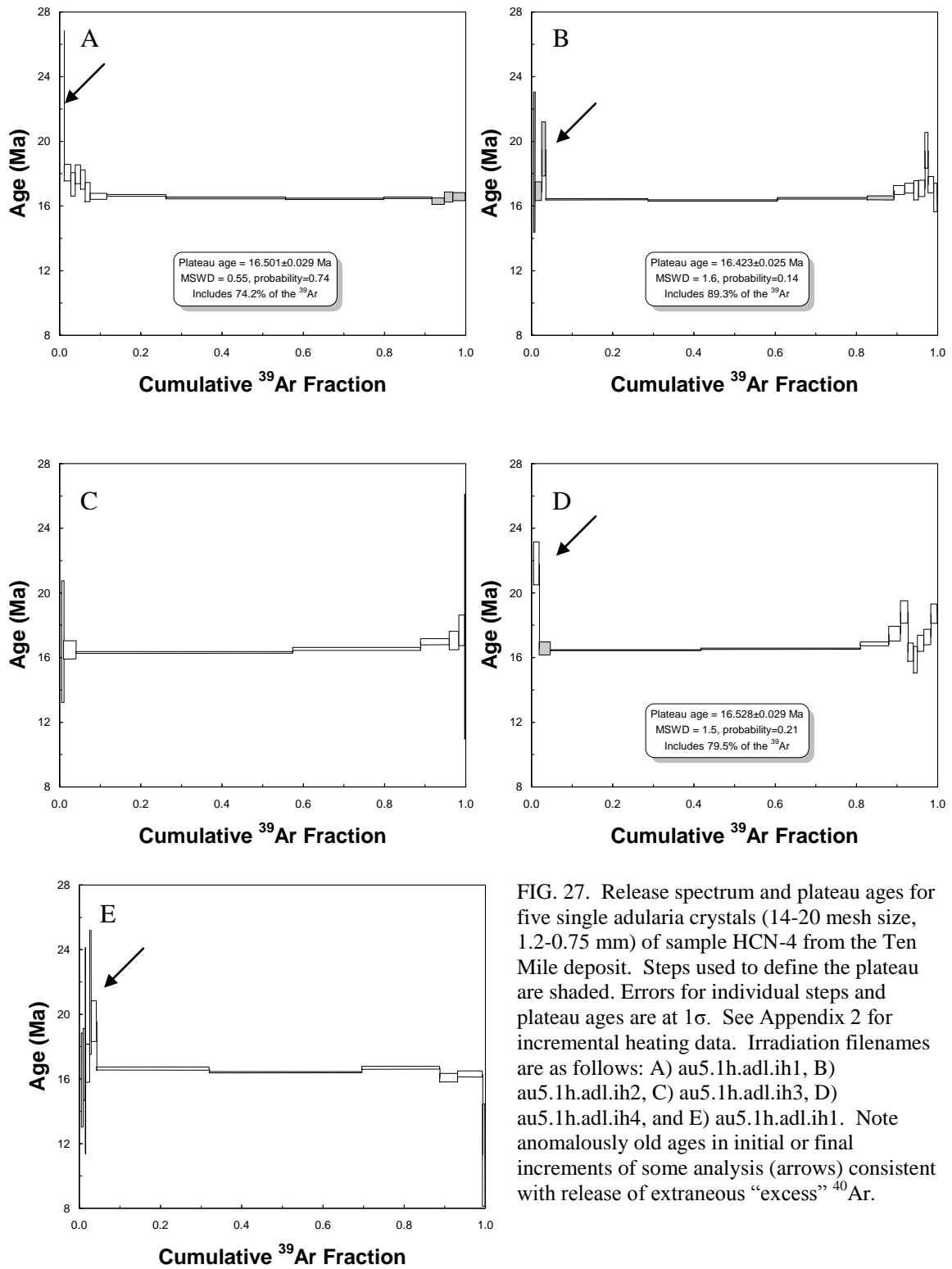
FIG. 27. Release spectrum and plateau ages for five single adularia crystals (14-20 mesh size, 1.2-0.75 mm) of sample HCN-4 from the Ten Mile deposit. Steps used to define the plateau are shaded. Errors for individual steps and plateau ages are at 1σ. See Appendix 2 for incremental heating data. Irradiation filenames are as follows: A) au5.1h.adl.ih1, B) au5.1h.adl.ih2, C) au5.1h.adl.ih3, D) au5.1h.adl.ih4, and E) au5.1h.adl.ih1. Note anomalously old ages in initial or final increments of some analysis (arrows) consistent with release of extraneous "excess" ^{40}Ar.

Plateau age = 16.501±0.029 Ma
MSWD = 0.55, probability=0.74
Includes 74.2% of the ^{39}Ar

Plateau age = 16.423±0.025 Ma
MSWD = 1.6, probability=0.14
Includes 89.3% of the ^{39}Ar

Plateau age = 16.528±0.029 Ma
MSWD = 1.5, probability=0.21
Includes 79.5% of the ^{39}Ar

War Eagle Mountain Deposit

War Eagle Mountain sits in the Silver City district of southwestern Idaho. The area has been the site of precious metal mining for well over a hundred years and numerous historic workings cover War Eagle Mountain (Fig. 28). Samples suitable for dating were collected from a vein outcrop directly beneath the Oro Fino mine (OF-1) and another unnamed adit located ~0.5 km southwest (WEMS3-1). Previous work by Halsor et al. (1988) using K-Ar methods, determined that adularia from veins on War Eagle Mountain range in age from 16.6 to 15.2 Ma.
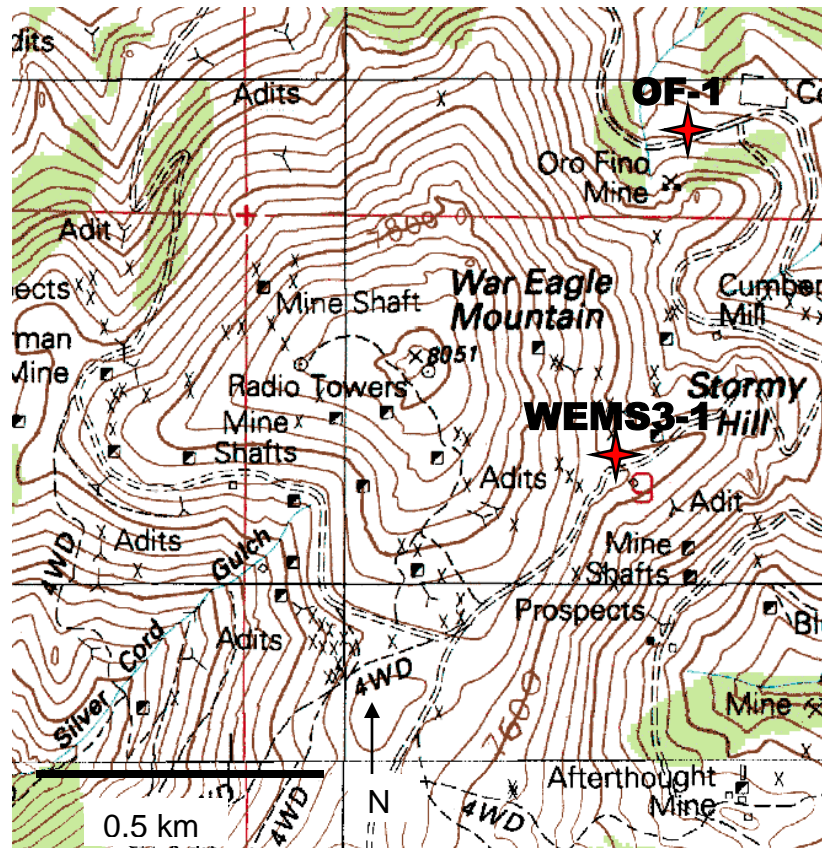
FIG. 28. Map of sample locations of OF-1 and WEMS3-1 taken from historic workings on War Eagle Mountain. Contour lines are labeled in feet. Modified from USGS DeLamar Quadrangle Topography Map.

Plateau ages were determined for all ten crystals analyzed from War Eagle Mountain. Sample OF-1 from the Oro Fino vein generated plateau ages that range from 16.32 ± 0.03 to 16.08 ± 0.04 Ma (Fig. 29). A weighted average of the oldest two plateau ages yields a preferred age of 16.31 ± 0.04 Ma. Plateau ages from sample WEMS3-1 range from 15.78 ± 0.05 to 15.55 ± 0.04 Ma (Fig. 30). A preferred age of 15.63 ± 0.11 Ma was calculated using the youngest four plateau ages because they overlap at 2σ. The oldest plateau age appears to contain some component of excess ^{40}Ar (Fig. 30 E) that may have caused it to appear anomalously old.

The characteristics of the War Eagle Mountain deposit are different from those of the Slumbering Hills. The wide range of ages for samples from War Eagle Mountain implies the system was long lived. The veins that host precious metals are much thicker (1-2 m) and show evidence of many deposition and brecciation events. The data generated by this study and previous work suggest the hydrothermal system on War Eagle Mountain was active for at least 600,000 years.
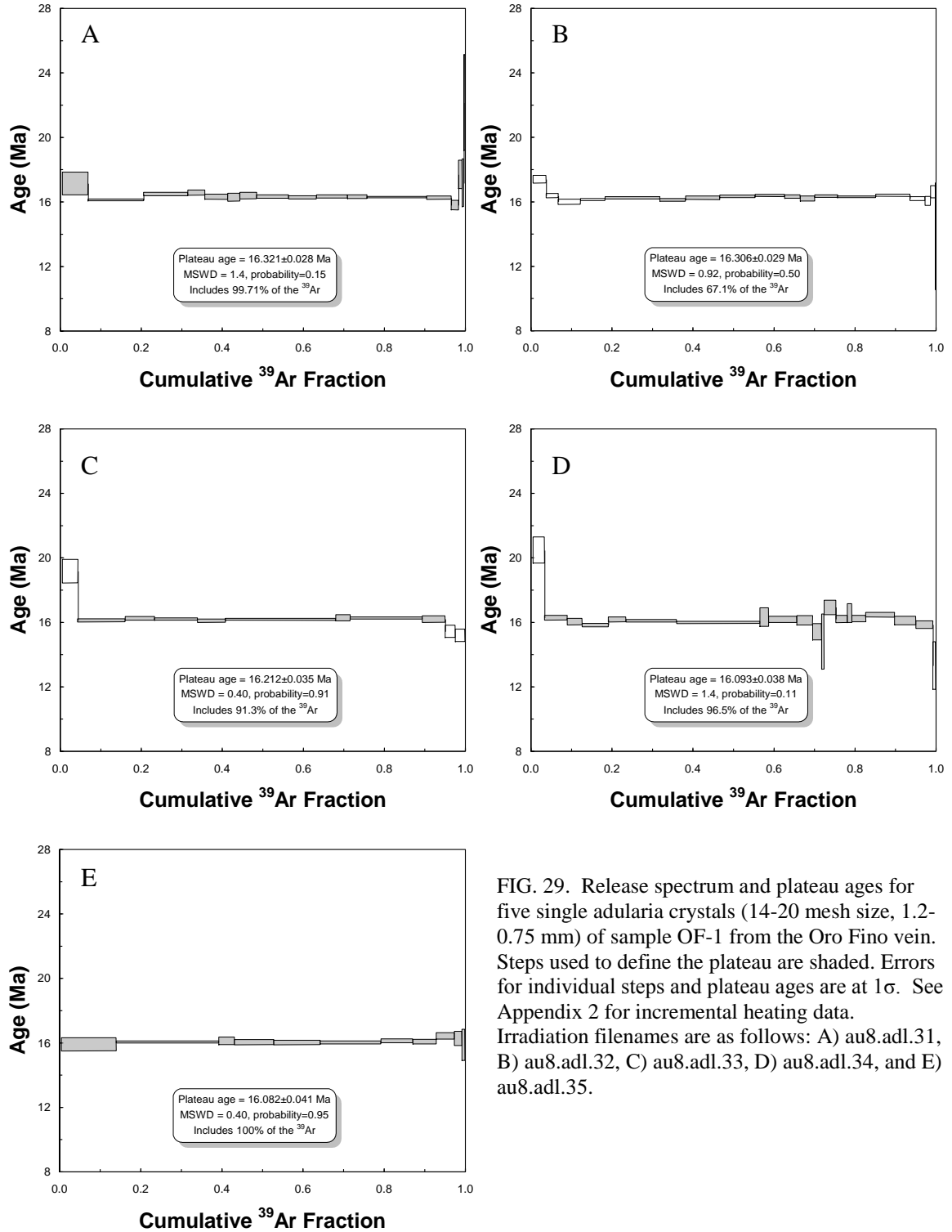
FIG. 29. Release spectrum and plateau ages for five single adularia crystals (14-20 mesh size, 1.2-0.75 mm) of sample OF-1 from the Oro Fino vein. Steps used to define the plateau are shaded. Errors for individual steps and plateau ages are at 1σ. See Appendix 2 for incremental heating data. Irradiation filenames are as follows: A) au8.adl.31, B) au8.adl.32, C) au8.adl.33, D) au8.adl.34, and E) au8.adl.35.
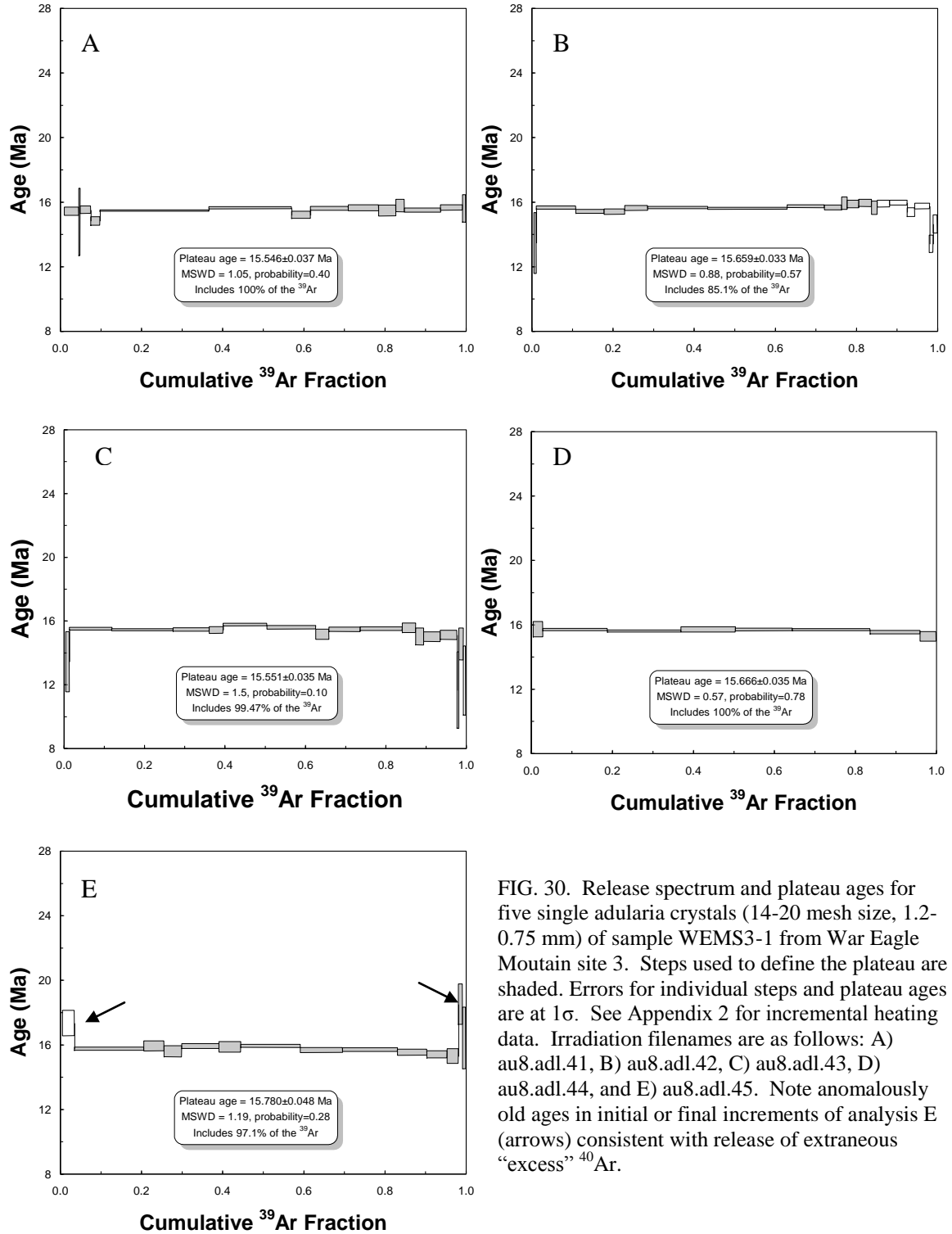
FIG. 30. Release spectrum and plateau ages for five single adularia crystals (14-20 mesh size, 1.2-0.75 mm) of sample WEMS3-1 from War Eagle Moutain site 3. Steps used to define the plateau are shaded. Errors for individual steps and plateau ages are at 1σ. See Appendix 2 for incremental heating data. Irradiation filenames are as follows: A) au8.adl.41, B) au8.adl.42, C) au8.adl.43, D) au8.adl.44, and E) au8.adl.45. Note anomalously old ages in initial or final increments of analysis E (arrows) consistent with release of extraneous "excess" [40]Ar.

DISCUSSION

Ore Petrography

A number of different interpretations have been made about the ore textures present in low-sulfidation epithermal deposits. Recent evidence indicates Au is transported from a deeper porphyry environment into the epithermal environment (Heinrich et al., 2004; Heinrich, 2005; Simmons and Brown, 2006). Banding of ore minerals could represent pulses of precious metal bearing magmatic fluids that mixed with heated meteoric water and rapidly changed the equilibrium causing precipitation of ore minerals. The presence of dendritic ore minerals and/or jig saw quartz in many of the samples indicates that rapid precipitation from a supersaturated solution is a common occurrence in these epithermal systems. Rather than periods of boiling caused by sealing and reopening of fluid conduits by precipitation of quartz, followed by pressure release due to a critical increase in pressure or seismic activity (Guilbert and Park, 1985), it is likely these systems are essentially always boiling and pseudomorphic quartz textures could simply indicate equilibrium changes that occurred in the boiling zone.

The presence of adularia as the dominant or even exclusive vein material in some deposits is somewhat of a geochemical conundrum. It has been suggested that adularia forms at the expense of quartz due to the higher solubility of quartz under alkaline conditions (Sillitoe, 2002). Fluids in low-sulfidation epithermal systems are widely considered to be near-neutral pH, low-salinity chloride-dominated solutions, which

76

would likely not easily transport the required aluminum to form adularia. Field observations in this study indicate that all of the "adularia-only" deposits are hosted or underlain by argillaceous-metasedimentary or granitic rocks. These rocks could serve as an abundant source of aluminum and potassium and thus allow for supersaturation of aluminum and potassium at depth, causing adularia rather than quartz to form as the primary vein material. This scenario likely would require lower pH fluids and steam-heated groundwater to leach the required aluminum and potassium. The adularia-only deposits also contain electrum almost exclusively as the precious metal mineral with very little selenide or sulfide minerals, suggesting different geochemical conditions from the selenide/sulfide-rich deposits. Adularia is present in both electrum-dominated and selenide/sulfide-dominated deposits. This may indicate that different factors control precious metal mineralogy (magmas?) and adularia precipitation (host rocks?). Further work investigating how host rocks affect vein mineralogy and styles of mineralization in low-sulfidation ores is warranted.

Geochemistry

The deposits in this study within the same district or sub-region have generally similar but not necessarily the same geochemistries. The Slumbering Hills area deposits (Jumbo, New Alma, Sandman, Sleeper and Ten Mile) all have high Au to Ag ratios, electrum as the primary precious metal mineral, low base metal contents, and relatively low to undetectable amounts of Se or Te. The Midas and Hollister deposits, which are both located on the northern part of the Carlin trend, also have very similar geochemical signatures including: high Ag to Au ratios, relatively high base metal contents, high

levels of Se and very low Te, along with Ag-selenides, sulfides and sulfosalts as the dominate precious metal minerals. These geochemical similarities coupled with the fact that all of the above spatially related deposits formed within a time span of ~0.5 Ma, suggests that similar geologic processes were operating throughout the region on a district-wide or even larger scale. Additionally, there are important exploration implications as both areas likely host similar undiscovered "blind" deposits. Other spatially related deposits such as National and Buckskin National have a larger degree of geochemical variation between them. A wider suite of samples is needed to fully quantify their geochemical differences. However, a number of processes could explain the variability present between these two deposits (see below). On a broader regional scale the deposits of the northern Great Basin fall within or near the Ag-selenide end member of the epithermal trilinear diagram, whereas the Colorado deposits plot at or near the Au-telluride end member. This suggests that both regional and local-scale geologic processes described in detail in the literature clearly also have a profound impact on ore chemistry.

In addition to the geochemical consistency amongst spatially related deposits, geochemical correlations further support the theory that the majority of the precious metals and some base metals in epithermal systems have a common source. A statistical analysis of just the northern Great Basin deposits indicates that Au has a strong to moderate statistical correlation with Hg, Sb, Ag, and Mo. A strong correlation also exists between Ag and Se. Experimental heating of chondritic meteorites, which are thought to approximate the composition of the mantle (Winters, 2001), found that As, Hg, S, Sb, Se, Te, and locally Cd were preferentially released at atmospheric pressures and temperatures of 200-900º C (Lauretta et al., 2002). Another study found that Au had similar volatility

78

to Hg (Lauretta et al., 2001). This suggests that these elements could be released together during a process such as mantle distillation or magma degassing.

A study by Saunders and Romberger (1985) suggested that Te can play an important role in Au transport in Au-telluride epithermal deposits and that fluids in these deposits have a significant magmatic signature. A more recent study found that a substantial amount of Au can be transported by a sulfur-dominated vapor under experimental conditions similar to those in the upper mantle (Peregoedova et al., 2006). These data coupled with the recent evidence that Au is transported from the deeper porphyry environment to the epithermal environment (Heinrich et al., 2004; Heinrich, 2005; Simmons and Brown, 2006) suggests that many of the "epithermal suite" elements in these systems may have a magmatic source.

Geochronology

There is mounting evidence that low-sulfidation epithermal deposits form relatively quickly. Data from this study and others (see Mining District Geology) indicates low-sulfidation epithermal systems in the northern Great Basin were active on a district wide scale for 0.3 to 0.6 Ma. A recent study of the Hosen-1 vein at the Hishikari deposit, Japan, found that the time interval from the margin to the center of the 2 m wide vein was about 260,000 years, and that vein formation occurred episodically with intervals of 30,000 to 110,000 years separating individual mineralizing events (Sanematsu et al., 2006). Another study that examined gold in magmatic hydrothermal solutions at the Ladolam hydrothermal system, Papua New Guinea, estimated that the huge gold deposit there could have formed within 55,000 years (Simmons and Brown,

2006). In the northern Great Basin, spatially related deposits such as those in the Slumbering Hills, northern Carlin Trend, or War Eagle Mountain have a maximum variation in age of around 600,000 years. In this study, uncertainty in age measurements range from 20,000 to 50,000 years, and variations between individual crystals for each deposit range from 0.1 to 1 Ma. These data indicate that future geochronology work should be conducted with the understanding that the difference in time between individual mineralizing events may approach the margin of uncertainty of current geochronology methods.

Within sample groups some plateau ages do not overlap, this may be explained by the analysis of crystals individually, rather than a group of crystals as a bulk sample. If a bulk sample had been analyzed the imperfections in individual crystals, such as excess Ar or loss of Ar due to weathering, would likely have been masked. Thus, a more "average" gas composition would have been analyzed. This average gas composition would not likely give the correct age for a deposit but rather an age that was slightly older or younger, and the effects of Ar gain or loss would be masked such that it may not be detectable. By using a smaller amount of material (single crystals) with an instrument designed to analyze the smaller sample, less error is introduced into the measurement and a more accurate age can be determined. The single crystals ages for each sample can be viewed as a group and a weighted averaged used to calculate a preferred age. Using this method, crystals that yield statistically anomalous ages or show signs of Ar gain or loss can be ignored. If these same crystals had been part of a bulk sample, they may have adversely affected the accuracy of the analysis, yet this effect may not have been obvious.

For the purposes of understanding the formation of these deposits, precision may be less important than the geologic "accuracy." If the loss of ^{40}Ar has been heterogeneous in a given population of crystals, then the precise average for a group (bulk sample) may have less meaning than an accurate range of ages. Examination of sample petrography including alteration effects, or evidences for multiple vein forming events, can give geologic context to the range of ages and make them more meaningful.

CONCLUSIONS

A number of lines of evidence suggest that mid-Miocene low-sulfidation epithermal precious metal mineralization in the northern Great Basin is related to the initial development of the Yellowstone hotspot. The mineralogy and geochemistry for the northern Great Basin deposits examined in this study show remarkable similarities, and may indicate a common source for the major metal and metalloid ore components. The earliest volcanism associated with the Yellowstone hotspot occurs in the nearby Steens Mountain basalts at 16.59 ± 0.10 Ma (Brueseke et al, 2007). The redefined age for the Jumbo deposit of 16.53 ± 0.04 Ma makes it the oldest known low-sulfidation deposit in the northern Great Basin, and clearly indicates mineralization began shortly after the first volcanism related to the Yellowstone hotspot. The data generated by this study and others indicates that mineralization continued at a reasonably steady rate until at least 15.1 Ma.

Ore petrography compliments other studies and indicates that the deposits in this study contain precious metals as electrum or Ag-selenides, sulfides, and sulfosalts hosted in adularia ± quartz ± calcite veins. The intimate association of adularia with these precious metal minerals allows for unambiguous geochronology of the mineralization events. Adularia hosts a variety of precious metal minerals and occurs in these deposits as either thin adularia-only fracture encrustations with electrum as the almost exclusive

precious metal mineral or as much wider banded veins that contain multiple generations of adularia + quartz ± calcite along with much higher Se content. The presence of Se has a strong impact on the mineralogy of Ag. In Se-poor deposits Ag is mostly found in the mineral electrum, whereas in Se-rich deposits the Ag-selenide naumannite is the primary Ag-mineral.

Multi-element geochemical analysis of samples from the northern Great Basin, and for comparison Colorado and Japan, indicates that nearly all samples contain variable but significant levels of Au, Ag, Pb, As, Sb, Se and Te. The most notable difference that exists between deposits of different regions is the amounts of Au, Ag, Se and Te present. Deposits located in the northern Carlin Trend (Midas and Hollister), National district (National and Buckskin National), War Eagle Mountain, ID, and Koryu, Japan all contain Se-rich ores that are nearly devoid of Te, along with typical Ag/Au ratios of 10 to 1. The deposits of Colorado contain very low amounts of Se, abundant Te, and Au concentrations that are often at least twice that of Ag. The deposits located in the Slumbering Hills (Jumbo, New Alma, Sandman, Sleeper, and Ten Mile) have ore chemistries that are considerably different from any of the other deposits in this study. The Au/Ag ratio is nearly 2 to 1 and all the deposits with the exception of Sleeper contain nearly no Se or Te, as well as having considerably lower levels of base metals.

A statistical analysis of just the northern Great Basin deposits indicates that Au shows a strong to moderate statistical correlation with Hg, Sb, Ag, and Mo. A strong correlation also exists between Ag and Se. This may indicate a common source for all the elements. A new system was devised to classify low-sulfidation ores base on elemental ratios. An epithermal trilinear diagram using the metals Au, Ag, and Pb and metalloids

As, Sb, Se, and Te indicate that end members in composition exist amongst the low-sulfidation deposits. One end member is represented by the Au-Te ores of the Colorado epithermal deposits and the other end member is represented by the Ag-Se rich "ginguro-type ores" as seen at Hishikari, Japan and Midas, Nevada. Multiple samples collected at a single deposit generally cluster well together, whereas the assortment in compositions amongst deposits ranges between both end members. If just the deposits of the northern Great Basin are considered, samples plot consistently in the Ag/Au-rich areas of the field and there is considerably more variability in the metalloids field especially related to the Sb+As versus Se levels.

The geochronology data generated by this study and others indicate low-sulfidation epithermal mineralization in the northern Great Basin began around 16.5 Ma and continued until at least 15.1 Ma. This study found that in the Slumbering Hills, Nevada area, the earliest mineralization occurred in the Awakening district at Jumbo at 16.53 ± 0.04 Ma and continued within the district until at least 16.03 ± 0.07 Ma at New Alma. To the south of the Slumbering Hills, mineralization occurred at the Ten Mile and Sandman deposits at 16.52 ± 0.04 Ma and 16.17 ± 0.04 Ma respectively. On War Eagle Mountain, Idaho the Oro Fino vein dated at 16.31 ± 0.04 Ma and the area to the southwest (site 3 in this study) was found to be 15.61 ± 0.10 Ma.

Jumbo is only slightly younger than the oldest magmatism thought to be associated with the Yellowstone hotspot (16.59 ± 0.10 Ma, Steens Mountain basalt, Brueseke et al., 2007). However, for the region as a whole, no discernable trend presents itself that would suggest deposits get generally younger to the east in line with the track of the Yellowstone hotspot.

The data in this study indicate that low-sulfidation epithermal deposits in the northern Great Basin share similar mineralogy, geochemistry, and formed just after early Yellowstone hotspot volcanism. This suggests that the two events are related and that the deposits all share a common source for the majority of ore-mineral constituents. On a broader scale if the deposits of Colorado and Japan are considered, deposits occur in a variety of tectonic settings but share a consistent mineralogy and geochemistry that varies between Se-rich and Te-rich end members.

SPECULATIONS AND IMPLICATIONS FOR EXPLORATION

A growing body of research suggests that previous genetic models for epithermal precious metal systems, which suggest metals are sourced from host rock leaching or even ambiguous sources, are in need of revision. A compromise of genetic models seems reasonable based on indications that Au and possibly other elements have magmatic sources and that these systems form relatively rapidly. Rather than a strictly crustal or magmatic source for the components in epithermal systems; it appears the epithermal suite elements have a magmatic source, and more common elements that comprise the gangue minerals likely are leached from the local host rocks. This could explain why the mid-Miocene epithermal deposits of the northern Great Basin are relatively similar geochemically, yet have a variety of vein and gangue minerals associated with them.

A number of other characteristics of low-sulfidation epithermal deposits can also be proposed. The fact that adularia is present in Se-poor and Se-rich deposits likely indicates that they have separate origins, such as Se is sourced from the mantle, whereas adularia forms when the surrounding host rocks contain enough K and Al to allow it.

For the epithermal trilinear diagram, the elements Au, Ag, Se and Te were chosen because they may have a mantle source. The elements As and Sb may have both crustal and mantle sources, and Pb may be mostly leached from local host rocks. By using these

elements to evaluate epithermal ores, it may be possible to determine how crustal and mantle contributions influence ore geochemistry. Gold shows a strong to moderate statistical correlation with Hg, Sb, Ag, and Mo, and Ag correlates strongly with Se. This likely indicates the elements all have the same (magmatic?) source.

Many of the spatially related deposits discussed above have remarkably consistent geochemistries. Other spatially related deposits such as the National and Buckskin National deposits have a larger degree of geochemical variation between them, thus a wider suite of samples is needed to fully quantify their geochemical differences. However, given that both of these deposits are situated within the National district and are in close proximity, several possibilities could explain their geochemical differences; 1) different pluses of magma carrying different ratios of ore forming elements (i.e. more Pb in the National ores, more Ag in the Buckskin National ores), 2) some type of fractionation occurs on a district-wide scale that results in chemically similar but still unique ores being formed in different deposits, or 3) interaction with local host rocks contribute varying amounts of different elements (i.e. more Sb and As at National, more Se at Buckskin National).

One important question with exploration implications is; does epithermal precious metal mineralization associated with the Yellowstone hotspot continue to this day or were the events that created the deposits in the northern Great Basin a unique occurrence? If the Yellowstone hotspot continues to be an ore-forming system then other deposits would be expected along the hotspot's track. On the other hand, the mantle may have been depleted early on and thus the Yellowstone hotspot did not remain an ore-forming system.

87

The importance of geochronology for exploration cannot be overlooked as well. This type of deposits appears to have only formed in a narrow window of time (ca 16.5-15 Ma), thus volcanism of this age is has the potential to be a part of an ore-forming system that may not be exposed. Additionally, there is strong geochemical and geochronology evidence that the geologic processes that drove these precious metal epithermal systems were active over relatively large areas and durations of 0.5 Ma or more. This suggests locations such as the Slumbering Hills and the northern Carlin trend remain highly prospective for further exploration.

REFERENCES

Anders, E., and Grevesse, N., 1989, Abundances of the elements: meteoritic and solar: Geochimica et Cosmochimica Acta, v. 53, p. 197-214.

Armstrong, R.L., Taubeneck,W.P., Hales, P.O., 1977, Rb–Sr and K–Ar geochronology of Mesozoic granitic rocks and their Sr isotopic compositions, Oregon, Washington, and Idaho: Geologic Society of America Bulletin, v. 88, p. 397–411.

Asher, R.R., 1968, Geology and mineral resources of a portion of the Silver City region, Owhyee County, Idaho: Idaho Bureau of Mines Geology Pamphlet 138, 106 p.

Bartlett, M.W., Enders, M.S., and Hruska, D.C., 1991, Geology of the Hollister gold deposit, Ivanhoe district, Elko County, Nevada, *in* Raines, G.L., Lisle, R.E., Schafer, R.W., and Wilkinson, W.H., eds., Geology and ore deposits of the Great Basin: Geological Society of Nevada Symposium, Reno, 1990, Proceedings, p. 957-978.

Bowell, R.J., Hunerlach, M.P., Parshley, J., and Sears, S., 2000, The Ten Mile district, Winnemucca, Nevada: Geology, mineralogy and supergene gold enrichment: Geological Society of Nevada, Geology and Ore Deposits 2000: The Great Basin and Beyond Symposium, May 15-18, 2000, Reno-Sparks, Nevada, Proceedings, p. 349-363.

Brueseke, M.E., and Hart, W.K., 2004, The physical and petrologic evolution of a multi-vent volcanic field associated with Yellowstone-Newbery volcanism: Eos, Transactions of AGU, v. 87(47), p. V53A-0605.

Brueseke, M.E., Heizler, M.T., Hart, W.K., and Mertzman, S.K., 2007, Distribution of Oregon Plateau (U.S.A.) flood basalt volcanism: The Steens Basalts revisited: Journal of Volcanology, v. 161, p. 187-214.

Brueseke, M.E., Hart, W.K., Heizler, M.T., 2007, Chemical and physical diversity of mid-Miocene silicic volcanism in northern Nevada: Bulletin of Volcanology, in press.

Brueseke, M.E., Heizler, M.T., Hart, W.K., and Mertzman, S.A., 2007, Distribution and geochronology of Oregon Plateau (U.S.A.) flood basalt volcanism: The Steens Basalt revisited: Journal of Volcanology and Geothermal Research, v. 161, p. 187-214.

Bussey, S.D., 1996, Gold mineralization and associated rhyolitic volcanism at the Hog
  Ranch district, northwest Nevada: Geological Society of Nevada, Geology and Ore
deposits of the American Cordillera Symposium, Reno-Sparks, Nevada, April 1995,
  Proceedings, p. 181-207

Camp, V.E., and Ross, M.E., 2004, Mantle dynamics and genesis of mafic magmatism in
  the intermontane Pacific Northwest: Journal of Geophysical Research, v. 109, B08204,
  14p.

Cline, J.S., Hofstra, A.H., Muntean, J.L., Tosdal, R.M., and Hikey, K.A., 2005, Carlin-
  type gold deposits in Nevada: critical geologic characteristics and viable models:
  Economic Geology 100th Anniversary Volume, p. 451-484.

Connors, K.A., Noble, D.C., Bussey, S.D., and Weiss, S.I., 1993, Initial gold contents of
  silicic volcanic rocks: Bearing on the behavior of gold in magmatic systems: Geology,
  v. 21, p. 937-940.

Conrad, J.E., and McKee, E.H., 1996, High-precision $^{40}Ar/^{39}Ar$ ages of rhyolitic host
  rock and mineralized veins at the Sleeper deposit, Humboldt County, Nevada:
  Geological Society of Nevada, Geology and Ore Deposits of the American Cordillera
  Symposium, Reno-Sparks, Nevada, April 1995, Proceedings, p. 257-262

Conrad, J.E. McKee, E.H., Rytuba, J.J., Nash, J.T., and Utterback, W.C., 1993,
  Geochronology of the Sleeper deposit, Humboldt County, Nevada: Epithermal gold-
  silver mineralization following emplacement of a silicic flow-dome complex:
  Economic Geology, v. 88, p. 81-91

Crafford, E.E.J., and Grauch, V.J.S., 2002, Geologic and geophysical evidence for the
  influence of deep crustal structures on Paleozoic tectonics and the alignment of world-
  class gold deposits, north-central Nevada, USA: Ore Geology Review, v. 21, p. 157–
  184.

Cummings, M.L., Evans, J.G., Ferns, M.L., Lees, K.R., 2000. Stratigraphic and structural
  evolution of the middle Miocene synvolcanic Oregon–Idaho graben: Geology Society
  of America Bulletin: v. 112, p. 668–682.

Dalrymple, G.B., Alexander, E.C., Lanphere, M.A., and Kraker, G.P., 1981, Irradiation
  of samples for $^{40}Ar/^{39}Ar$ dating using the Geological Survey TRIGA Reactor: USGS
  Professional Paper 1176, 55 p.

Ekren, E.B., McIntyre, D.H., Bennett, E. H., and Malde, H.E., 1981, Geologic map of
  Owyhee County, Idaho, west of longitude 116º W, W.S. Geologic Survey Map 1-1256.

Fetter, C.W., 2001, Applied Hydrogeology: Prentice-Hall, New Jersey, 374p.

Garwin, S., Hall, R., and Watanabe, Y., 2005, Tectonic setting, geology, and gold and copper mineralization in Cenozoic magmatic arcs of southeast Asia and the west Pacific: Economic Geology 100th Anniversary Volume, p. 891-930.

Glen, J.M.G., and Ponce, D.A., 2002, Large-scale fractures related to inception of the Yellowstone hotspot: Geology, v. 30, p. 647-650.

Goldstrand, P.M., and Schmidt, K.W., 2000, Geology, mineralization, and ore controls at the Ken Snyder gold-silver mine, Elko County, Nevada: Geological Society of Nevada, Geology and Ore Deposits 2000: The Great Basin and Beyond Symposium, May 15-18, 2000, Reno-Sparks, Nevada, Proceedings, p. 265-287

Guilbert, J.M., and Park, C.F., 1985, The geology of ore deposits: W. H. Freeman and Company, New York, 535 p.

Halsor, S.P., Bornhorst, T.J., Beebe, M., Richardson, K., and Strowd, W., 1988, Geology of the DeLamar silver mine, Idaho—a volcanic dome complex and genetically associated hydrothermal system: Economic Geology, v. 83, p. 1159-1169.

Hart, W.K., and Carlson, R.W., 1985, Distribution and geochronology of Steens Mountain-type basalts from the northwestern Great Basin: Isochron-West, v. 43, p. 5-10.

Hedenquist, J.W., and Lowenstern, J.B., 1994, The role of magmas in the formation of hydrothermal ore deposits: Nature, v. 370, p. 519-527

Heinrich, C.A., 2005, The physical and chemical evolution of low-salinity magmatic fluids at the porphry to epithermal transition; a thermodynamic study: Mineralium Deposita, v. 39, p. 864-889.

Heinrich, C.A., 2006, How fast does gold trickle out of volcanoes?: Science, v. 314, p. 263-264.

Heinrich, C.A., Driesner, T., Stefansson, A., Seward, T.M., 2004, Magmatic vapor contraction and the transport of gold from the porphyry environment to epithermal ore deposits: Geology, v. 32, p. 761-764.

Hollister, V., Hruska, D., and Morre, R., 1992, A mine-exposed host spring deposit and related epithermal gold resource: Economic Geology, v. 87, p. 421-424.

Hooper, P.R., 1997, The Columbia River flood basalt provinces; current status, *in* Mahoney, J.J., and Coffin, M., eds., Large igneous provinces: continental, oceanic, and planetary flood volcanism: Geophysical Monograph, v.100, p.1-27.

Hudson, D.M., John, D.A., and Fleck, R.J., 2006, Geologic setting, geochemistry, and geochronology of epithermal gold-silver deposits in the Seven Troughs District, northwest Nevada: Abstracts with Programs - Geological Society of America, v. 37, no. 7, p. 380.

Izawa E, Urashima Y, Ibaraki K, Suzuki, R, Yokohama T, Kawasaki K, Koga A, and Taguchi S, 1990, The Hishikari gold deposit: high-grade epithermal veins in Quaternary volcanics of southern Kyushu, Japan: Journal of Geochemical Exploration, v. 36, p. 1-56.

John, D.A., Garside, L.J., and Wallace, A.R., 1999, Magmatic and tectonic setting of late Cenozoic epithermal gold-silver deposits in northern Nevada, with an empasis on the Pah Rah and Virginia Ranges and the northern Nevada rift: Geological Society of Nevada Special Publication 29, p. 65-158.

John, D.A., Wallace, A.R., Ponce, D.A., Fleck, R., and Conrad, J.E., 2000, New perspectives on the geology and origins of the northern Nevada rift: Geological Society of Nevada, Geology and Ore Deposits 2000: The Great Basin and Beyond Symposium, May 15-18, 2000, Reno-Sparks, Nevada, Proceedings, p. 127-154.

John, D.A., 2001, Miocene and early Pliocene epithermal gold-silver deposits in the northern Great Basin, western USA: Characteristics, distribution and relationship to magmatism: Economic Geology, v. 96, p. 1827-1853.

John, D.A., Hofstra, A.H., Fleck, R.J., Brummer, J.E., and Saderholm, E.C., 2003, Geologic setting and genesis of the Mule Canyon low-sulfidation epithermal gold-silver deposit, north-central Nevada: Economic Geology, v. 98, p. 425-464.

Jordan, B.T., Grunder, A.L., Duncan, R.A., and Deino, A.L., 2004, Geochronology of age-progressive volcanism of the Oregon High Lava Plains: implications for the plume interpretation of Yellowstone: Journal of Geophysical Research, v. 109, B10202., 19 p.

Kamenov, G.D., Perfit, M.R., Jonasson, I.R., and Mueller, P.A., 2005, High-precision Pb isotope measurements reveal magma recharge as a mechanism for ore deposit formation: Examples from Lihir Island and Conical seamount, Papau New Guinea: Chemical Geology, v. 219, p. 131-148.

Kamenov, G.D., Saunders, J.A., Hames, W.E., and Unger, D.L., Mafic magmas as sources for gold in middle-Miocene epithermal deposits of northern Great Basin, USA: Evidence from Pb isotopic compositions of native gold: Economic Geology, in press.

Kistler, R.W., and Peterman, Z.E., 1978, Reconstruction of crustal California on the basis of initial strontium isotopic compositions of Mesozoic granitic rocks: U. S. Geological Survey Professional Paper, v. 107, p. 1-17.

Laurettea, D.S., Klaue, B., Blum, J.D., and Buseck, P.R., 2001, Thermal analysis of labile trace elements in CM and CV carbonaceous chondrites using ICP-MS: Lunar and Planetary Science XXXII, n. 1356.

Laurettea, D.S., Klaue, B., and Blum, J.D., 2002, Thermal analysis of volatile trace elements of carbonaceous and ordinary chondrites: Lunar and Planetary Science XXXIII, n. 16002.

Leavitt, E.D., Spell, T.L., Goldstrand, P.M., and Arehart, G.G., 2004, Geochronology of the Midas low-sulfidation gold-silver deposit, Elko County Nevada: Economic Geology, v. 99, p. 1665-1986.

Leeman, W.P., Oldow, J.S., and Hart, W.K., 1992, Lithosphere-scale thrusting in the western U.S. Cordillera as constrained by Sr and Nd isotoic transitions in Neogene volcanic rocks: Geology, v. 20, p. 63-66.

Lindgren, W., 1898, Orthoclase as gangue mineral in a fissure vein: American Journal of Science, v. 5, p. 418-420.

Lindgren, W., 1900, The gold and silver veins of Silver City, DeLamar, and other mining districts in Idaho: U. S. Geol. Survey 20th Ann. Rept., pt. IIIc, p. 77 - 189.

Lindgren, W., 1915, Geology and mineral deposits of the National mining district, Nevada: U. S. Geological Survey Bulletin 601, 58 p.

Ludwig, K.R., 2003, User's manual for Isoplot, v. 3.0, a geochronological tool kit for Microsoft Excel: Berkeley Geochronological Center, Special Publication no. 4.

McKee, E.H., and Moring, B.C., 1996, Cenozoic mineral deposits and related rocks: Nevada Bureau of Mines and Geology Open-File Report 96-2, p. 6-1 to 6-8

Muntean, J., Tarnocai, C., Coward, M., Rouby, D., and Jackson, A., 2001, Styles and restorations of Tertiary extension in north-central Nevada: Reno, Geological Society of Nevada Special Publication 33, p. 55-69.

Muntean, J.L., Cline, J., Johnston, M.K., Ressel, M.W., Seedorff, E., and Barton, M.D., 2004, Controversies on the origin of world-class gold deposits, part I: Carlin-type gold deposits in Nevada: SEG Newsletter, n. 59, p. 1-17.

Nash, J.T., 1972, Fluid inclusion studies of some gold deposits in Nevada: U.S. Geological Survey Professional Paper 800-C, p. C15-C19.

Nash, J.T., Utterback, W.C., and Trudel, W.C., 1995, Geology and geochemistry of Tertiary volcanic host rocks, Sleeper gold-silver deposit, Humboldt County, Nevada: U.S. Geological Survey Bulletin 2090, 63 p.

Neill, W. M., 1975, Geology of the southeastern Owyhee Mountains and environs, Owyhee County, Idaho: Unpublished M.S. thesis, Stanford University, 111p.

Noble, D.C., McCormack, J.K., McKee, E.H., Silberman, M.L., and Wallace, A.B., 1988, Time of mineralization of the evolution of the McDermitt caldera complex, Nevada-Oregon, and the relation of middle Miocene mineralization in the northern Great Basin to coeval regional basaltic magmatic activity: Economic Geology, v. 83, p. 859-863.

Pansze, A.J., 1975, Geology and ore deposits of the Silver City-DeLamar-Flint region, Owyhee County, Idaho: Idaho Bureau of Mines Geology Pamphlet 161, 79 p.

Peppard, B., 2002, Geology and geochemistry of the Ivanhoe vein system, Elko, Nevada: Unpublished M.S. thesis, Ann Arbor, University of Michigan, 49 p.

Peregoedova, A., Barnes,S.J., and Baker, D.R., 2006, An experimental study of mass transfer of platinum-group elements, gold, nickel and copper in sulfur-dominated vapor at magmatic temperature: Chemical Geology, v. 235, p. 59-75.

Pierce, K.L., Morgan, L.A., and Saltus, R.W., 2000, The Yellowstone plume head: Postulated tectonic relations to the Vancouver slab, continental boundaries, and climate: U.S. Geological Survey Open-File Report 00-498, 39 p.

Ponce, D.A., and Glen, J.M.G., 2002, Relationship of epithermal gold deposits to large-scale fractures in northern Nevada: Economic Geology, v. 97, p. 3-9.

Renne, P.R ., Swisher, C.C., Deino, A.L., Karner, D. B., Owens, T. L., and DePaolo, D.J., 1998, Intercalibration of standards, absolute ages, and uncertainties in ^{40}Ar/^{39}Ar dating: Chemical Geology, v. 145, p. 117-152.

Roberts, R.J., 1940, Quicksilver deposit at Buckskin Peak National mining district, Humboldt County, Nevada: U.S. Geological Survey Bulletin 922-E, p. 111-133.

Rytuba, J.J., and McKee, E. H., 1984, Peralkaline ash-flow tuffs of the McDermitt volcanic field, southeast Oregon and north Entral Nevada: Journal of Geophysical. Research, v. 89, p. 8616-8628.

Rytuba, J.J., 1989, Geology of volcanic-hosted Sleeper deposit, Humboldt County, Nevada: Geological Society of America Abstracts with Programs, v. 21, n. 5 p. 138.

Sanematsu, K., Watanabe, K., Duncan, R A., and Izawa, E., 2006, The history of vein formation determined by super ^{40}Ar/super ^{39}Ar dating of adularia in the Hosen-1 vein at the Hishikari epithermal gold deposit, Japan: Economic Geology, v. 101, p. 685-698.

Saunders, J.A., and Romberger, S.B., 1985, Ore petrology and geochemistry of Tertiary gold telluride deposits of the Colorado mineral belt: Geological Society of America Abstracts and Programs, v. 17, no. 7, p. 707.

Saunders, J.A., 1990, Colloidal transport of gold and silica in epithermal precious metal systems: Evidence from the Sleeper deposit, Nevada: Geology, v. 18, p. 757-760.

Saunders, J.A., 1994, Silica and gold textures in bonanza ores of the Sleeper Deposit, Humboldt County, Nevada; evidence for colloids and implications for epithermal ore-forming processes: Economic Geology, v. 89, p. 628-638.

Saunders, J.A., and Schoenly, P.A., 1995, Boiling, colloid nucleation and aggregation, and the genesis of bonanza Au-Ag ores of the Sleeper deposit, Nevada: Mineralium Deposita, v. 30, p. 199-210.

Saunders, J.A., Cook, R.B., and Schoenly, P.A., 1996, Electrum disequilibrium crystallization textures in volcanic-hosted bonanza epithermal gold deposits in northern Nevada: Geological Society of Nevada, Geology and Ore Deposits of the American Cordillera Symposium, Reno-Sparks, Nevada, April 1995, Proceedings, p. 173-179.

Sillitoe, R.H., 1989, Gold deposits in western Pacific island arcs; the magmatic connection: Economic Geology Monographs, v. 6, p. 274-291.

Sillitoe, R.H., 2002, Some metallogenic featues of gold and copper deposits related to alkaline rocks and consequences for exploration: Mineralium Deposita, v. 37, p. 4-13.

Sillitoe, R.H., and Hedenquist, J.W., 2003, Linkages between volcanotectonic settings, ore fluid compositions, and epithermal precious metal deposits: Society of Economic Geologists Special Publication 10, p. 315-343.

Simmons, S. F., and Brown, K.L., 2000, Hydrothermal minerals and precious metals in the Broadlands Ohaaki geothermal system: Implicatoins for understanding low-sulfidation epithermal environments: Economic Geology, v. 95, p. 971-999.

Simmons, S. F., and Brown, K.L., 2006, Gold in magmatic hydrothermal solutions and the rapid formation of a giant ore deposit: Science, v. 314, no.5797, p. 288-291.

Simmons, S.F., and Christenson, B.W., 1994, Origins of calcite in a boiling geothermal system: American Journal of Science, v. 294, p. 361-400.

Simmons, S.F., White, N.C., and John, D.A., 2005, Geological characteristics of epithermal precious and base metal deposits: Economic Geology 100th Anniversary Volume, p. 485-522.

Teal, L., and Jackson, M., 1997, Geologic Overview of the Carlin Trend gold deposits and descriptions of recent deep discoveries, Vikre, P., Thompson, T.B., Bettles, K., Christensen, O., and Parratt, R., eds., *in* Carlin-Type Gold Deposits Field Conference: Society of Economic Geologists Guidebook Series, v. 28, p. 3-38.

Tewalt, N, A., 1998, Subtle surface expression of high grade veins at the Ivanhoe project: Fall 1998 Field Trip Guidebook, Geological Society of Nevada Special Publication 28, p. 149-161.

Thomason, R. E., 1983, Volcanic stratigraphy and epithermal mineralization of the DeLamar silver mine, Owyhee County, Idaho: Unpublished M.S. thesis, Oregon State University, 70 p.

Vikre, P.G., 1985, Precious metal vein systems in the National district, Humboldt County, Nevada: Economic Geology, v. 80, p. 360-393.

Vikre, P.G., 1987, Paleohydrology of Buckskin Mountain, National district, Humboldt County, Nevada: Economic Geology, v. 82, p. 934-950.

Vikre, P.G., 2007, Sinter-vein correlations at Buckskin Mountain, National district, Humboldt County, Nevada: Economic Geology, v. 102, p. 193-224.

Wallace, A.R., 2003, Geology of the Ivanhoe Hg-Au district, northern Nevada: Influence of Miocene volcanism, lakes, and active faulting on epithermal mineralization: Economic Geology, v. 98, p. 409-424.

Wendt, C.J., 2003, Nevada Mineral Trends: Nevada Bureau of Mines, Open-file report 03-2.

Willden, R., 1964, Geology and mineral deposits of Humboldt County, Nevada: Nevada Bureau of Mines and Geology Bulletin 59, 154 p.

Winchell, A, N., 1912, Geology of the National district: Mining Scientific Press, Nov. 23. p. 655-658.

Winters, J.D., 2001, An introduction to igneous and metamorphic petrology: Prentice Hall, New Jersey, 699 p.

Zhang, Z., Mao, J., Fusheng, W., and Pirajno, F., 2006, Native gold and native copper grains enclosed by olivine phenocrysts in a picrite lava of the Emeishan large igneous province, SW China: American Mineralogist, v. 91, p. 1178-1183.

Zoback, M.L., and Thompson, G.A., 1978, Basin and Range rifting in northern Nevada: Clues from a mid-Miocene rift and its subsequent offsets: Geology, v. 6, p. 111-116.

Zoback, M.L., McKee, E.H., Blakely, R.J., and Thompson, G.A., 1994, The northern
  Nevada rift: Regional tectono-magmatic relations and middle Miocene stress direction:
  Geological Society of America Bulletin, v. 106, p. 371-382.

APPENDICES

APPENDIX 1
Analytical Facility Description

The Auburn Noble Isotope Mass Analysis Laboratory (ANIMAL) was utilized for age determinations in this study:

a. This facility is equipped with an ultra-high vacuum, 90-degree sector, 10 cm radius spectrometer optimized for $^{40}Ar/^{39}Ar$ research (single-crystal and multigrain sample incremental heating). The spectrometer employs second-order focusing (Cross, 1951), and is fitted with a high sensitivity electron-impact source and a single ETP electron multiplier (with signal amplification through a standard pre-amplifier). Analyses of this study were made using a filament current of 2.250 A, and potentials for the source and multiplier of 2000 V and 1250 V, espectively. The total volume of the spectrometer is 400 cc. Resolution in the instrument (with fixed slits for the source and detector) is constrained to ~150, and the high sensitivity and low blank of the instrument permits measurement of 10^{-14} mole samples to within 0.2% precision. Analyses comprised 10 cycles of measurement over the range of masses and half-masses from m/e=40 to m/e=35.5, and baseline corrected values were extrapolated to the time of inlet, or averaged, depending upon signal evolution.

b. The extraction line for this system utilizes a combination of Varian 'mini' and Nupro pneumatic valves, and Varian turbomolecular and ion pumps. Analysis of samples and blanks is fully automated and can be controlled via computer. Pumping of residual and sample reactive gases is accomplished through use of SAES AP-10 non-evaporable getters. Pressures in the spectrometer and extraction line, as measured with an ionization gauge, are routinely below ~$5x10^{-9}$ torr. A pipette delivers standard aliquots of air for use in measuring sensitivity and mass fractionation. Mass discrimination was typically 1.0026±0.0014 per amu (95% confidence level) in November of 2006.

c. The extraction line is fitted with a 50W Synrad CO2 IR laser for heating and fusing silicate minerals and glasses. The sample chamber uses a Cu planchet, KBr cover slips, and low-blank UHV ZnS window (manufactured at Auburn University and based on the design of Cox et al., 2003). In the present configuration, this laser system is suitable for incremental heating and fusion analysis of single crystals and multigrain samples. The laser beam delivery system utilizes movable optical mounts and a fixed sample chamber to further minimize volume and improve conductance of the extraction line. (The time required to inlet, or equilibrate, a 'half-split' of a sample is less than 7 s, and the inlet time for a full sample is ca. 20 s.) Typical blanks for the entire system (4 minute gettering time) in November of 2006 are as follows (in moles): ^{40}Ar, $5.7x10^{-17}$; ^{39}Ar, $1.3x10^{-17}$; ^{38}Ar, $2.8x10^{-18}$; ^{37}Ar, $2.0x10^{-18}$; ^{36}Ar, $1.2x10^{-18}$.

d. Computer control of the laser, laser optics, extraction line, mass spectrometer, and data recording is enabled with National Instruments hardware and the Labview programming environment. Initial data reduction is accomplished through an in-house Excel spreadsheet, with final reduction using Isoplot (Ludwig, 2003).

APPENDIX 2

Incremental heating data for the Sandman, New Alma, Jumbo, Ten Mile, and War Eagle Moutain deposits.

Sandman deposit step heating increments for 5 single adularia crystals (14-20, 1.2-0.75 mm) of sample: HCN-1
Irradiation filename: au5.1a.adl.ih1

%P	40Ar(*±atm)	39Ar(K)	38Ar(Cl±atm)	37Ar(Ca)	36Ar(Atm)	%Rad	R	Age (Ma)
3.0	3.64E-15 ± 3.38E-18	1.14E-17 ± 4.38E-19	2.5E-18 ± 2.7E-19	-1.5E-18 ± 5.9E-19	1.24E-17 ± 1.48E-19	0%	-1.2771	-6.45 ± -90
3.3	1.10E-15 ± 6.15E-18	1.61E-16 ± 1.18E-18	7.5E-19 ± 6.5E-20	5.6E-19 ± 3.9E-19	2.01E-18 ± 8.83E-20	46%	3.1759	15.93 ± 0.88
3.6	1.81E-15 ± 4.98E-18	4.08E-16 ± 9.36E-19	1.1E-18 ± 6.9E-20	-3.0E-19 ± 5.0E-19	1.55E-18 ± 9.60E-20	75%	3.3040	16.57 ± 0.36
4.0	1.65E-15 ± 5.31E-18	4.78E-16 ± 1.45E-18	1.3E-18 ± 5.3E-20	-1.3E-19 ± 4.7E-19	2.91E-19 ± 9.23E-20	95%	3.2630	16.37 ± 0.30
4.3	1.58E-15 ± 4.98E-18	4.64E-16 ± 1.49E-18	1.4E-18 ± 3.8E-20	5.7E-20 ± 5.6E-19	3.35E-19 ± 8.15E-20	94%	3.1987	16.05 ± 0.27
4.5	3.97E-15 ± 4.84E-18	1.17E-15 ± 3.14E-18	2.7E-18 ± 4.7E-20	3.5E-19 ± 4.4E-19	9.35E-19 ± 1.72E-19	93%	3.1654	15.88 ± 0.22
4.8	1.23E-14 ± 1.29E-17	3.39E-15 ± 6.30E-18	8.6E-18 ± 1.4E-19	-3.0E-20 ± 4.6E-19	4.78E-18 ± 1.77E-19	89%	3.2123	16.11 ± 0.09
5.0	1.31E-14 ± 1.07E-17	3.56E-15 ± 5.70E-18	8.9E-18 ± 1.0E-19	-8.9E-19 ± 5.0E-19	5.54E-18 ± 1.80E-19	87%	3.2071	16.09 ± 0.08
5.3	9.43E-15 ± 1.11E-17	2.69E-15 ± 8.12E-18	6.2E-18 ± 7.2E-20	1.3E-19 ± 4.7E-19	2.42E-18 ± 1.64E-19	92%	3.2343	16.22 ± 0.11
5.5	1.02E-14 ± 1.35E-17	2.95E-15 ± 8.41E-18	6.1E-18 ± 7.8E-20	9.7E-20 ± 4.4E-19	2.59E-18 ± 9.99E-20	93%	3.2121	16.11 ± 0.07
5.8	1.56E-14 ± 1.50E-17	4.61E-15 ± 9.84E-18	1.0E-17 ± 7.5E-20	-1.1E-18 ± 5.8E-19	2.19E-18 ± 1.00E-19	96%	3.2352	16.23 ± 0.05
6.0	5.39E-16 ± 2.84E-18	1.58E-16 ± 1.03E-18	2.9E-19 ± 3.4E-20	-7.5E-19 ± 4.0E-19	4.43E-20 ± 6.96E-20	98%	3.3345	16.72 ± 0.67
6.5	6.30E-16 ± 3.20E-18	1.82E-16 ± 1.10E-18	4.4E-19 ± 4.3E-20	-6.5E-19 ± 3.6E-19	3.70E-20 ± 7.92E-20	98%	3.3938	17.02 ± 0.66
7.0	2.76E-16 ± 3.07E-18	7.99E-17 ± 7.49E-19	1.7E-19 ± 4.0E-20	2.5E-20 ± 4.2E-19	7.48E-20 ± 7.36E-20	92%	3.1721	15.91 ± 1.39
8.0	1.89E-16 ± 3.02E-18	5.58E-17 ± 7.17E-19	-5.2E-20 ± -2.4E-20	-1.1E-18 ± 4.3E-19	3.96E-20 ± 6.37E-20	94%	3.1826	15.97 ± 1.73
9.0	1.90E-16 ± 3.18E-18	5.48E-17 ± 5.27E-19	-3.5E-19 ± -4.0E-19	-4.6E-19 ± 3.7E-19	4.70E-20 ± 6.96E-20	93%	3.2073	16.09 ± 1.91
10.0	3.37E-17 ± 2.03E-18	8.76E-18 ± 3.62E-19	-5.3E-19 ± -2.2E-19	-5.5E-20 ± 3.3E-19	2.64E-20 ± 8.13E-20	77%	2.9501	14.80 ± 13
11.0	1.13E-17 ± 2.12E-18	2.88E-18 ± 3.86E-19	-3.6E-19 ± -2.1E-19	9.5E-20 ± 4.6E-19	-2.35E-19 ± -1.17E-19	715%	28.0900	136.26 ± 60
12.0	1.27E-17 ± 2.25E-18	2.37E-18 ± 3.75E-19	-4.9E-19 ± -1.9E-19	-3.5E-19 ± 4.2E-19	-1.43E-19 ± -1.33E-19	432%	23.0992	112.79 ± 82
14.0	1.83E-16 ± 2.34E-18	1.57E-18 ± 3.48E-19	-2.1E-19 ± -2.0E-19	5.7E-19 ± 4.1E-19	5.35E-19 ± 8.63E-20	13%	15.6469	77.17 ± 186

Note: %P = percentage of total laser output (60 w).

Irradiation filename: au5.1a.adl.ih2

%P	40Ar(*±atm)	39Ar(K)	38Ar(Cl±atm)	37Ar(Ca)	36Ar(Atm)	%Rad	R	Age (Ma)
3.0	1.07E-15 ± 3.91E-18	4.63E-18 ± 4.01E-19	7.6E-19 ± 1.6E-19	2.5E-19 ± 3.4E-19	3.85E-18 ± 1.21E-19	-7%	-14.9832	-77.12 ± -154
3.3	1.12E-15 ± 3.86E-18	1.23E-16 ± 8.68E-19	8.8E-19 ± 8.6E-20	1.0E-19 ± 5.3E-19	2.84E-18 ± 1.25E-19	25%	2.2698	11.40 ± 1.57
3.6	1.44E-15 ± 3.49E-18	4.08E-16 ± 1.50E-18	1.2E-18 ± 5.0E-20	9.0E-19 ± 5.2E-19	8.11E-19 ± 1.19E-19	83%	2.9324	14.72 ± 0.44
4.0	1.50E-15 ± 6.75E-18	4.49E-16 ± 1.58E-18	1.4E-18 ± 5.0E-20	2.5E-19 ± 3.1E-19	1.46E-19 ± 1.40E-19	97%	3.2366	16.24 ± 0.47
4.3	8.09E-15 ± 6.48E-18	2.34E-15 ± 3.28E-18	6.6E-18 ± 1.1E-19	7.3E-19 ± 4.0E-19	2.01E-18 ± 1.62E-19	93%	3.2042	16.07 ± 0.11
4.5	1.50E-14 ± 1.63E-17	4.11E-15 ± 6.46E-18	1.0E-17 ± 1.1E-19	-1.7E-19 ± 4.4E-19	6.47E-18 ± 1.81E-19	87%	3.1853	15.98 ± 0.07
4.8	7.89E-15 ± 5.62E-18	2.30E-15 ± 4.91E-18	5.8E-18 ± 9.1E-20	1.0E-19 ± 4.2E-19	2.03E-18 ± 1.33E-19	92%	3.1603	15.85 ± 0.09
5.0	8.07E-15 ± 9.30E-18	2.33E-15 ± 3.52E-18	5.6E-18 ± 1.3E-19	1.4E-19 ± 4.4E-19	2.08E-18 ± 1.32E-19	92%	3.1983	16.04 ± 0.09
5.3	2.14E-15 ± 5.15E-18	6.17E-16 ± 1.50E-18	1.9E-18 ± 5.3E-20	2.7E-19 ± 3.7E-19	5.26E-19 ± 1.87E-19	93%	3.2121	16.11 ± 0.45
5.5	4.94E-16 ± 4.67E-18	1.43E-16 ± 7.53E-19	4.4E-20 ± 6.9E-21	3.0E-19 ± 3.9E-19	1.53E-19 ± 7.16E-20	91%	3.1469	15.79 ± 0.77
5.8	3.35E-16 ± 3.89E-18	9.69E-17 ± 1.19E-18	2.0E-19 ± 3.1E-20	1.9E-19 ± 4.4E-19	5.16E-20 ± 8.12E-20	95%	3.2972	16.54 ± 1.28
6.0	6.76E-17 ± 2.53E-18	1.78E-17 ± 4.14E-19	1.1E-19 ± 6.9E-20	-2.0E-19 ± 4.7E-19	3.92E-20 ± 7.57E-20	83%	3.1358	15.73 ± 6.35
6.5	2.09E-17 ± 2.73E-18	2.08E-18 ± 3.00E-19	-1.0E-21 ± -8.7E-21	-2.5E-19 ± 3.7E-19	-2.77E-19 ± -1.48E-19	492%	49.3967	233.17 ± 103.3
7.0	3.28E-17 ± 2.92E-18	3.61E-18 ± 2.53E-19	-7.4E-20 ± -3.8E-19	1.7E-19 ± 4.4E-19	2.54E-20 ± 7.50E-20	77%	7.0108	34.99 ± 31.09
8.0	2.12E-17 ± 2.36E-18	2.50E-18 ± 3.38E-19	2.4E-19 ± 1.3E-19	-1.6E-19 ± 4.1E-19	3.80E-20 ± 7.46E-20	47%	3.9613	19.85 ± 44.85
9.0	7.15E-19 ± 1.51E-18	1.07E-19 ± 2.99E-19	-2.0E-19 ± -2.2E-19	7.9E-19 ± 4.4E-19	5.00E-20 ± 6.86E-20	-1966%	-131.7752	-827.99 ± -2712.
10.0	2.17E-18 ± 2.24E-18	6.34E-19 ± 3.35E-19	-1.7E-19 ± -1.9E-19	-7.8E-20 ± 5.0E-19	-7.15E-20 ± -7.36E-20	1074%	36.7539	176.30 ± 185.9
11.0	1.15E-19 ± 1.94E-18	-9.15E-19 ± -4.02E-19	-2.9E-19 ± -1.9E-19	2.3E-19 ± 3.5E-19	-2.91E-19 ± -1.25E-19	74925%	-94.2096	-550.87 ± -337
12.0	1.33E-17 ± 1.83E-18	6.26E-19 ± 3.16E-19	-2.6E-19 ± -1.9E-19	5.8E-19 ± 4.9E-19	-8.17E-20 ± -6.85E-20	282%	59.8454	278.85 ± 183
14.0	2.98E-16 ± 2.65E-18	5.29E-19 ± 3.19E-19	-1.7E-19 ± -1.9E-19	2.9E-19 ± 4.7E-19	8.64E-19 ± 8.17E-20	14%	79.8724	363.30 ± 2041

Irradiation filename: au5.1a.adl.ih3

%P	40Ar(*±atm)	39Ar(K)	38Ar(Cl±atm)	37Ar(Ca)	36Ar(Atm)	%Rad	R	Age (Ma)
3.0	1.58E-15 ± 4.96E-18	2.17E-18 ± 4.14E-19	7.6E-19 ± 2.3E-19	2.4E-19 ± 4.4E-19	5.26E-18 ± 1.30E-19	2%	11.2053	55.60 ± 9
3.3	9.66E-16 ± 4.29E-18	1.66E-17 ± 4.22E-19	7.3E-19 ± 1.5E-19	-5.0E-21 ± 4.3E-19	3.04E-18 ± 8.48E-20	7%	4.0022	20.05 ± 12
3.6	1.93E-15 ± 6.71E-18	2.86E-16 ± 1.23E-18	1.2E-18 ± 6.5E-20	2.6E-19 ± 5.5E-19	2.79E-18 ± 2.13E-19	57%	3.8886	19.49 ± 1.12
4.0	1.98E-15 ± 5.23E-18	3.92E-16 ± 1.97E-18	1.3E-18 ± 5.5E-20	1.5E-19 ± 4.6E-19	2.24E-18 ± 7.73E-20	67%	3.3681	16.89 ± 0.33
4.3	4.89E-16 ± 4.32E-18	1.14E-16 ± 5.03E-19	2.5E-19 ± 3.8E-20	8.7E-19 ± 4.8E-19	4.78E-19 ± 8.72E-20	71%	3.0387	15.25 ± 1.15
4.5	1.31E-15 ± 5.09E-18	3.04E-16 ± 8.22E-19	1.1E-18 ± 5.4E-20	7.5E-19 ± 4.4E-19	1.48E-18 ± 1.37E-19	67%	2.8536	14.32 ± 0.68
4.8	2.89E-15 ± 3.96E-18	7.88E-16 ± 2.74E-18	2.3E-18 ± 5.5E-20	-3.6E-19 ± 4.1E-19	1.54E-18 ± 1.25E-19	84%	3.0817	15.46 ± 0.24
5.0	3.25E-15 ± 2.81E-18	9.26E-16 ± 2.21E-18	2.1E-18 ± 7.3E-20	-7.3E-20 ± 4.7E-19	1.27E-18 ± 1.32E-19	88%	3.0999	15.55 ± 0.22
5.3	8.95E-15 ± 1.02E-17	2.42E-15 ± 7.17E-18	6.7E-18 ± 5.1E-20	-2.4E-19 ± 5.1E-19	4.29E-18 ± 1.51E-19	86%	3.1760	15.93 ± 0.11
5.5	2.15E-14 ± 1.58E-17	5.77E-15 ± 9.92E-18	1.7E-17 ± 1.6E-19	-4.2E-19 ± 5.2E-19	9.70E-18 ± 1.74E-19	87%	3.2252	16.18 ± 0.06
5.8	7.20E-15 ± 5.77E-18	2.07E-15 ± 4.60E-18	5.3E-18 ± 1.0E-19	7.1E-20 ± 4.9E-19	1.66E-18 ± 8.88E-20	93%	3.2346	16.23 ± 0.08
6.0	1.25E-15 ± 4.30E-18	3.56E-16 ± 1.84E-18	1.4E-18 ± 6.0E-20	-2.7E-19 ± 4.4E-19	3.12E-19 ± 1.01E-19	93%	3.2592	16.35 ± 0.43
6.5	2.49E-15 ± 8.55E-18	7.13E-16 ± 2.49E-18	1.6E-18 ± 5.1E-20	1.2E-19 ± 5.9E-19	7.41E-19 ± 8.49E-20	91%	3.1892	16.00 ± 0.20
7.0	4.35E-17 ± 1.66E-18	1.17E-17 ± 3.59E-19	1.4E-19 ± 1.1E-19	-4.0E-19 ± 5.1E-19	8.78E-20 ± 9.20E-20	40%	1.4982	7.53 ± 11
8.0	2.01E-17 ± 1.79E-18	9.40E-18 ± 3.27E-19	-2.5E-19 ± -3.4E-19	-1.6E-19 ± 5.1E-19	-6.71E-20 ± -7.99E-20	199%	4.2490	21.28 ± 12
9.0	5.99E-18 ± 2.05E-18	1.48E-18 ± 2.91E-19	1.4E-19 ± 2.0E-19	4.8E-20 ± 4.9E-19	8.40E-20 ± 7.76E-20	-314%	-12.7128	-65.22 ± -81
10.0	2.98E-18 ± 1.55E-18	1.16E-18 ± 3.70E-19	-6.8E-20 ± -2.3E-19	4.0E-19 ± 4.7E-19	1.11E-19 ± 8.86E-20	-998%	-25.6109	-133.90 ± -127

Irradiation filename: au5.1a.adl.ih4

%P	40Ar(*±atm)	39Ar(K)	38Ar(Cl±atm)	37Ar(Ca)	36Ar(Atm)	%Rad	R	Age (Ma)
3.0	6.66E-16 ± 4.41E-18	7.80E-19 ± 3.32E-19	1.4E-19 ± 1.7E-19	2.5E-19 ± 4.7E-19	2.06E-18 ± 2.05E-19	9%	74.4690	340.90 ± 2285
3.3	2.50E-16 ± 3.00E-18	1.25E-17 ± 4.56E-19	-7.6E-20 ± -3.3E-19	1.0E-19 ± 5.4E-19	1.01E-18 ± 8.37E-20	-19%	-3.7349	-18.92 ± -12
3.6	2.48E-16 ± 1.93E-18	4.51E-17 ± 5.07E-19	-2.5E-19 ± -2.5E-19	-2.9E-21 ± 4.7E-19	3.88E-19 ± 8.69E-20	54%	2.9538	14.82 ± 2.89
4.0	1.08E-15 ± 2.21E-18	3.17E-16 ± 1.18E-18	4.3E-19 ± 2.4E-20	9.1E-20 ± 3.6E-19	1.42E-19 ± 7.85E-20	96%	3.2550	16.33 ± 0.37
4.3	5.75E-16 ± 3.67E-18	1.76E-16 ± 1.57E-18	9.0E-19 ± 8.5E-20	-2.6E-20 ± 4.6E-19	-5.81E-20 ± -1.17E-19	103%	3.3699	16.90 ± 1.00
4.5	7.77E-16 ± 3.78E-18	2.38E-16 ± 1.49E-18	3.9E-19 ± 2.6E-20	-5.0E-19 ± 6.1E-19	4.98E-20 ± 1.92E-19	98%	3.2070	16.09 ± 1.20
4.8	1.43E-15 ± 4.25E-18	4.30E-16 ± 1.01E-18	8.3E-19 ± 5.5E-20	-4.5E-19 ± 4.4E-19	1.71E-19 ± 1.46E-19	96%	3.1946	16.03 ± 0.51
5.0	4.64E-15 ± 6.10E-18	1.39E-15 ± 2.12E-18	2.3E-18 ± 4.7E-20	-3.2E-19 ± 4.5E-19	4.97E-19 ± 1.39E-19	97%	3.2236	16.17 ± 0.15
5.3	1.14E-14 ± 8.80E-18	3.36E-15 ± 1.26E-17	7.0E-18 ± 5.2E-20	2.3E-19 ± 4.5E-19	1.70E-18 ± 1.78E-19	96%	3.2276	16.19 ± 0.10
5.5	1.17E-14 ± 8.80E-18	3.52E-15 ± 7.00E-18	7.7E-18 ± 7.4E-20	2.3E-19 ± 3.8E-19	1.62E-18 ± 9.51E-20	96%	3.1906	16.01 ± 0.05
5.8	1.17E-15 ± 5.35E-18	3.51E-16 ± 8.28E-19	7.0E-19 ± 3.8E-20	-6.6E-20 ± 4.2E-19	1.70E-19 ± 8.32E-20	96%	3.2009	16.06 ± 0.36
6.0	3.64E-16 ± 2.11E-18	1.05E-16 ± 9.21E-19	3.9E-19 ± 6.5E-20	1.7E-19 ± 3.4E-19	-5.42E-20 ± -8.43E-20	104%	3.6244	18.17 ± 1.21
6.5	7.57E-18 ± 2.12E-18	1.50E-18 ± 4.70E-19	4.1E-19 ± 1.8E-19	-3.5E-19 ± 4.2E-19	-8.96E-20 ± -9.11E-20	450%	22.7664	111.22 ± 92
7.0	2.72E-17 ± 2.58E-18	6.74E-18 ± 4.21E-19	6.1E-20 ± 1.0E-19	-3.4E-19 ± 3.9E-19	-1.29E-19 ± -9.06E-20	240%	9.6663	48.06 ± 19
8.0	7.49E-18 ± 2.08E-18	7.54E-19 ± 3.71E-19	2.4E-19 ± 1.9E-19	1.8E-19 ± 4.0E-19	-4.52E-20 ± -8.42E-20	279%	27.6782	134.34 ± 167
9.0	7.24E-18 ± 1.90E-18	1.80E-18 ± 4.92E-19	1.6E-19 ± 1.9E-19	-3.2E-19 ± 3.5E-19	-1.17E-19 ± -8.53E-20	578%	23.2122	113.33 ± 73
10.0	9.97E-18 ± 2.29E-18	-3.40E-19 ± -4.38E-19	-6.7E-21 ± -1.3E-19	-4.0E-19 ± 3.8E-19	-3.44E-19 ± -1.42E-19	1121%	-329.1044	-4538.78 ± -5618

Irradiation filename: au5.1a.adl.ih5

%P	40Ar(*±atm)	39Ar(K)	38Ar(Cl±atm)	37Ar(Ca)	36Ar(Atm)	%Rad	R	Age (Ma)
3.0	1.16E-15 ± 3.57E-18	4.26E-18 ± 3.49E-19	7.7E-19 ± 2.1E-19	-8.3E-19 ± 3.8E-19	4.07E-18 ± 1.51E-19	-3%	-9.4739	-48.38 ± -173
3.3	4.26E-16 ± 3.41E-18	8.81E-17 ± 8.09E-19	4.3E-19 ± 5.5E-20	5.1E-21 ± 4.8E-19	5.74E-19 ± 1.50E-19	60%	2.9068	14.59 ± 2.54
3.6	6.43E-16 ± 4.31E-18	1.65E-16 ± 8.15E-19	1.7E-19 ± 1.9E-20	1.6E-19 ± 4.9E-19	3.91E-19 ± 1.49E-19	82%	3.1958	16.03 ± 1.35
4.0	3.21E-15 ± 6.72E-18	9.35E-16 ± 3.31E-18	1.8E-18 ± 5.0E-20	-5.1E-19 ± 4.3E-19	6.90E-19 ± 1.42E-19	94%	3.2185	16.15 ± 0.24
4.3	8.16E-15 ± 6.66E-18	2.34E-15 ± 4.74E-18	5.9E-18 ± 1.2E-19	-1.3E-18 ± 5.7E-19	2.25E-18 ± 1.61E-19	92%	3.2007	16.06 ± 0.11
4.5	2.02E-14 ± 2.01E-17	6.02E-15 ± 1.01E-17	1.5E-17 ± 1.2E-19	4.1E-19 ± 4.2E-19	2.65E-18 ± 1.11E-19	96%	3.2254	16.18 ± 0.04
4.8	3.55E-15 ± 4.17E-18	1.08E-15 ± 4.72E-18	2.1E-18 ± 4.4E-20	-2.5E-19 ± 3.9E-19	3.49E-19 ± 8.42E-20	97%	3.1935	16.02 ± 0.14
5.0	4.10E-16 ± 2.89E-18	1.21E-16 ± 1.05E-18	-8.1E-20 ± -1.7E-20	5.3E-19 ± 3.5E-19	-1.69E-19 ± -1.12E-19	112%	3.7820	18.96 ± 1.38
5.3	1.83E-16 ± 2.76E-18	5.44E-17 ± 7.19E-19	-4.1E-19 ± -6.2E-19	1.7E-19 ± 3.3E-19	-1.38E-19 ± -1.17E-19	122%	4.1078	20.58 ± 3.21
5.5	8.98E-17 ± 1.99E-18	2.69E-17 ± 5.03E-19	-7.5E-20 ± -8.3E-20	1.3E-19 ± 3.4E-19	-7.54E-20 ± -7.73E-20	125%	4.1659	20.87 ± 4.28
5.8	2.40E-17 ± 2.04E-18	6.69E-18 ± 3.47E-19	-2.0E-19 ± -3.1E-19	3.2E-19 ± 4.0E-19	-2.56E-19 ± -1.38E-19	416%	14.9177	73.64 ± 30.38
6.0	8.97E-17 ± 2.66E-18	2.41E-17 ± 3.53E-19	4.3E-20 ± 2.4E-20	-4.1E-19 ± 3.8E-19	-3.22E-20 ± -8.67E-20	111%	4.1162	20.62 ± 5.36
6.5	3.93E-17 ± 2.51E-18	1.01E-17 ± 3.89E-19	-5.1E-20 ± -2.4E-19	-5.4E-19 ± 2.7E-19	-3.45E-19 ± -1.08E-19	359%	14.0192	69.29 ± 15
7.0	1.84E-17 ± 2.11E-18	5.09E-18 ± 2.49E-19	4.7E-20 ± 7.7E-20	-2.2E-19 ± 4.2E-19	-5.61E-22 ± -8.28E-20	101%	3.6509	18.30 ± 24
8.0	1.12E-17 ± 1.71E-18	1.28E-18 ± 3.01E-19	-6.6E-20 ± -2.0E-19	-3.4E-19 ± 2.8E-19	-3.74E-19 ± -1.45E-19	1082%	95.1714	425.26 ± 175
9.0	8.19E-18 ± 2.46E-18	1.03E-18 ± 3.87E-19	-3.2E-19 ± -1.8E-19	-9.4E-19 ± 2.5E-19	-4.46E-20 ± -7.88E-20	261%	20.8243	101.99 ± 115

New Alma deposit step heating increments for 5 single adularia crystals (14-20 mesh size, 1.2-0.75 mm) of sample: HCN-2
Irradiation filename: au5.1c.adl.ih1

%P	40Ar(*±atm)	39Ar(K)	38Ar(Cl±atm)	37Ar(Ca)	36Ar(Atm)	%Rad	R	Age (Ma)
3.0	3.28E-16 ± 3.00E-18	1.12E-17 ± 5.82E-19	7.1E-20 ± 8.3E-20	1.4E-19 ± 5.3E-19	8.79E-19 ± 9.08E-20	21%	6.0812	30.38 ± 15
3.3	4.65E-16 ± 3.23E-18	9.45E-17 ± 4.94E-19	-1.1E-19 ± -2.8E-20	9.5E-20 ± 5.0E-19	3.27E-19 ± 8.60E-20	79%	3.8939	19.52 ± 1.37
3.6	5.85E-16 ± 2.78E-18	1.78E-16 ± 1.13E-18	3.4E-19 ± 4.0E-20	2.6E-19 ± 5.3E-19	-1.67E-19 ± -7.80E-20	108%	3.5533	17.82 ± 0.66
4.0	2.99E-15 ± 3.57E-18	8.02E-16 ± 2.62E-18	1.6E-18 ± 4.6E-20	5.7E-20 ± 5.2E-19	1.38E-18 ± 9.96E-20	86%	3.2184	16.14 ± 0.20
4.3	1.84E-15 ± 4.82E-18	5.64E-16 ± 1.92E-18	1.5E-18 ± 6.6E-20	-3.6E-19 ± 5.0E-19	1.01E-19 ± 8.17E-20	98%	3.2020	16.06 ± 0.23
4.5	1.60E-15 ± 4.23E-18	4.91E-16 ± 1.29E-18	7.4E-19 ± 2.5E-20	3.0E-19 ± 4.7E-19	2.33E-20 ± 1.88E-19	100%	3.2437	16.27 ± 0.57
4.8	6.14E-15 ± 3.72E-18	1.91E-15 ± 4.17E-18	4.7E-18 ± 9.6E-20	1.7E-19 ± 4.6E-19	4.05E-19 ± 1.54E-19	98%	3.1588	15.85 ± 0.13
5.0	4.97E-15 ± 4.31E-18	1.56E-15 ± 2.86E-18	3.6E-18 ± 6.2E-20	8.8E-20 ± 5.2E-19	3.40E-19 ± 1.64E-19	98%	3.1290	15.70 ± 0.16
5.3	4.73E-15 ± 4.89E-18	1.49E-15 ± 7.61E-18	2.8E-18 ± 4.8E-20	-1.6E-19 ± 4.5E-19	3.42E-19 ± 1.59E-19	98%	3.1021	15.56 ± 0.18
5.5	1.41E-14 ± 8.95E-18	4.40E-15 ± 6.11E-18	9.7E-18 ± 9.1E-20	1.4E-18 ± 4.4E-19	4.81E-19 ± 1.54E-19	99%	3.1627	15.87 ± 0.06
5.8	4.24E-15 ± 3.65E-18	1.32E-15 ± 3.00E-18	3.1E-18 ± 5.4E-20	5.1E-19 ± 4.8E-19	1.08E-19 ± 9.18E-20	99%	3.1740	15.92 ± 0.11
6.0	2.45E-15 ± 5.37E-18	7.60E-16 ± 1.87E-18	1.9E-18 ± 3.6E-20	-3.3E-20 ± 2.9E-19	1.89E-19 ± 1.45E-19	98%	3.1424	15.76 ± 0.29
6.5	1.73E-15 ± 5.44E-18	5.29E-16 ± 1.51E-18	1.5E-18 ± 7.3E-20	3.8E-19 ± 3.6E-19	2.80E-19 ± 1.43E-19	95%	3.1097	15.60 ± 0.41
7.0	1.09E-16 ± 2.13E-18	3.29E-17 ± 5.16E-19	-1.6E-19 ± -1.7E-19	-2.3E-19 ± 3.7E-19	3.61E-19 ± 1.39E-19	2%	0.0806	0.41 ± 6.33
8.0	1.86E-16 ± 2.45E-18	5.69E-17 ± 6.94E-19	1.1E-19 ± 4.3E-20	3.4E-20 ± 3.4E-19	2.12E-19 ± 1.43E-19	66%	2.1607	10.86 ± 3.74
9.0	2.00E-17 ± 2.07E-18	5.28E-18 ± 6.39E-19	-1.8E-19 ± -2.1E-19	1.7E-18 ± 5.7E-19	2.57E-19 ± 1.37E-19	-280%	-10.6002	-54.22 ± -40

Irradiation filename: au5.1c.adl.ih2

%P	40Ar(*±atm)	39Ar(K)	38Ar(Cl±atm)	37Ar(Ca)	36Ar(Atm)	%Rad	R	Age (Ma)
3.0	3.05E-16 ± 2.56E-18	3.48E-18 ± 3.62E-19	4.2E-19 ± 1.7E-19	2.1E-19 ± 5.5E-19	1.02E-18 ± 9.37E-20	1%	0.9187	4.62 ± 76
3.3	2.67E-16 ± 2.73E-18	3.80E-17 ± 5.13E-19	6.2E-19 ± 1.3E-19	-2.9E-19 ± 4.6E-19	3.81E-19 ± 7.78E-20	58%	4.0590	20.34 ± 3.09
3.6	6.61E-16 ± 3.70E-18	1.61E-16 ± 1.07E-18	1.1E-18 ± 7.5E-20	4.9E-19 ± 4.6E-19	7.59E-20 ± 1.38E-19	97%	3.9583	19.84 ± 1.28
4.0	2.15E-15 ± 5.38E-18	6.43E-16 ± 1.80E-18	1.5E-18 ± 4.3E-20	2.7E-19 ± 5.0E-19	2.23E-19 ± 9.79E-20	97%	3.2444	16.27 ± 0.23
4.3	1.05E-15 ± 5.51E-18	3.21E-16 ± 1.69E-18	9.6E-19 ± 5.2E-20	4.3E-19 ± 4.2E-19	2.06E-20 ± 8.58E-20	99%	3.2363	16.23 ± 0.41
4.5	1.12E-16 ± 2.09E-18	3.32E-17 ± 4.75E-19	3.9E-19 ± 1.2E-19	-4.2E-19 ± 4.7E-19	-3.14E-19 ± -1.36E-19	183%	6.1637	30.79 ± 6.05
4.8	6.32E-16 ± 2.87E-18	1.94E-16 ± 7.52E-19	4.9E-19 ± 5.3E-20	-3.9E-19 ± 4.8E-19	1.17E-19 ± 7.82E-20	95%	3.0715	15.41 ± 0.60
5.0	8.05E-16 ± 5.01E-18	2.53E-16 ± 1.54E-18	9.1E-19 ± 5.7E-20	-4.3E-19 ± 4.4E-19	-5.11E-20 ± -9.00E-20	102%	3.2311	16.21 ± 0.54
5.3	1.42E-15 ± 5.39E-18	4.37E-16 ± 1.11E-18	1.3E-18 ± 6.0E-20	3.4E-19 ± 5.5E-19	2.15E-19 ± 8.79E-20	96%	3.0960	15.53 ± 0.31
5.5	2.31E-15 ± 5.40E-18	7.15E-16 ± 2.36E-18	1.9E-18 ± 6.6E-20	-4.7E-19 ± 5.1E-19	7.60E-20 ± 8.93E-20	99%	3.1918	16.01 ± 0.20
5.8	4.69E-15 ± 8.01E-18	1.45E-15 ± 3.51E-18	3.5E-18 ± 5.2E-20	-4.0E-19 ± 3.6E-19	1.39E-19 ± 8.58E-20	99%	3.1963	16.03 ± 0.10
6.0	6.70E-15 ± 4.16E-18	2.07E-15 ± 3.35E-18	4.2E-18 ± 5.8E-20	-2.6E-19 ± 4.5E-19	2.50E-19 ± 7.79E-20	99%	3.1948	16.03 ± 0.06
6.5	1.72E-14 ± 1.94E-17	5.31E-15 ± 6.74E-18	1.2E-17 ± 1.3E-19	2.6E-19 ± 5.5E-19	4.18E-19 ± 8.48E-20	99%	3.2065	16.09 ± 0.04
7.0	1.56E-14 ± 1.10E-17	4.85E-15 ± 9.08E-18	1.2E-17 ± 6.5E-20	-4.4E-19 ± 5.0E-19	5.03E-19 ± 7.83E-20	99%	3.1806	15.96 ± 0.04
8.0	1.12E-14 ± 9.60E-18	3.50E-15 ± 3.97E-18	7.9E-18 ± 1.0E-19	3.2E-19 ± 4.8E-19	1.58E-21 ± 1.13E-19	100%	3.2101	16.10 ± 0.05
9.0	1.55E-15 ± 4.91E-18	4.81E-16 ± 1.51E-18	9.1E-19 ± 3.0E-20	4.4E-19 ± 5.1E-19	2.13E-19 ± 8.15E-20	96%	3.0990	15.55 ± 0.26

Irradiation filename: au5.1c.adl.ih3

%P	40Ar(*±atm)	39Ar(K)	38Ar(Cl±atm)	37Ar(Ca)	36Ar(Atm)	%Rad	R	Age (Ma)
3.0	6.37E-17 ± 1.87E-18	2.57E-18 ± 2.85E-19	-7.1E-20 ± -4.5E-19	-5.1E-19 ± 3.9E-19	1.56E-19 ± 9.05E-20	28%	6.8747	34.31 ± 54
3.3	9.80E-17 ± 2.41E-18	1.30E-17 ± 4.35E-19	-6.4E-20 ± -2.7E-19	-5.0E-19 ± 4.2E-19	1.40E-19 ± 8.19E-20	58%	4.3335	21.70 ± 9.44
3.6	8.52E-16 ± 3.66E-18	2.18E-16 ± 7.00E-19	5.9E-19 ± 5.9E-20	-5.1E-19 ± 3.0E-19	-2.27E-20 ± -1.56E-19	101%	3.9294	19.69 ± 1.07
4.0	2.02E-15 ± 3.81E-18	6.16E-16 ± 2.26E-18	1.6E-18 ± 6.3E-20	-5.2E-19 ± 3.6E-19	9.88E-20 ± 8.28E-20	99%	3.2252	16.18 ± 0.21
4.3	2.80E-15 ± 3.69E-18	8.75E-16 ± 3.19E-18	2.2E-18 ± 7.9E-20	-6.9E-19 ± 3.5E-19	3.28E-20 ± 7.30E-20	100%	3.1895	16.00 ± 0.14
4.5	5.17E-15 ± 5.20E-18	1.62E-15 ± 4.87E-18	3.7E-18 ± 7.0E-20	3.4E-19 ± 4.3E-19	1.15E-19 ± 8.91E-20	99%	3.1662	15.88 ± 0.10
4.8	1.32E-14 ± 1.59E-17	4.09E-15 ± 5.67E-18	1.1E-17 ± 6.0E-20	3.1E-19 ± 4.3E-19	2.29E-19 ± 8.82E-20	99%	3.2093	16.10 ± 0.04
5.0	9.16E-15 ± 5.47E-18	2.84E-15 ± 4.02E-18	6.9E-18 ± 6.7E-20	-1.3E-19 ± 3.6E-19	2.87E-19 ± 7.51E-20	99%	3.1944	16.03 ± 0.05
5.3	7.33E-15 ± 7.03E-18	2.29E-15 ± 5.71E-18	5.1E-18 ± 8.2E-20	6.4E-20 ± 3.3E-19	-5.07E-20 ± -7.93E-20	100%	3.2079	16.09 ± 0.07
5.5	1.99E-15 ± 5.36E-18	6.22E-16 ± 3.68E-18	1.2E-18 ± 5.0E-20	1.6E-20 ± 3.9E-19	-4.60E-19 ± -1.39E-19	107%	3.4109	17.11 ± 0.35
5.8	2.68E-16 ± 2.74E-18	8.37E-17 ± 5.98E-19	1.3E-20 ± 3.3E-21	-2.5E-19 ± 4.1E-19	-1.40E-19 ± -7.87E-20	115%	3.6948	18.52 ± 1.41
6.0	3.35E-16 ± 2.64E-18	1.03E-16 ± 4.79E-19	3.4E-19 ± 5.2E-20	3.8E-19 ± 4.1E-19	1.32E-19 ± 1.59E-19	88%	2.8732	14.42 ± 2.29
6.5	1.46E-16 ± 2.51E-18	4.46E-17 ± 5.07E-19	-4.0E-20 ± -1.7E-20	7.8E-19 ± 4.2E-19	9.29E-20 ± 1.61E-19	81%	2.6616	13.36 ± 5.36
7.0	8.63E-17 ± 2.06E-18	2.69E-17 ± 2.60E-19	-6.4E-20 ± -6.2E-20	5.3E-19 ± 4.4E-19	1.69E-19 ± 1.71E-19	42%	1.3479	6.78 ± 9.48
8.0	2.33E-17 ± 1.99E-18	7.11E-18 ± 2.63E-19	6.6E-20 ± 9.1E-20	8.0E-19 ± 4.4E-19	4.30E-19 ± 1.25E-19	-445%	-14.5843	-75.03 ± -26
9.0	8.04E-18 ± 2.28E-18	2.21E-18 ± 3.07E-19	-4.0E-19 ± -1.6E-19	7.5E-19 ± 4.5E-19	9.99E-20 ± 1.57E-19	-267%	-9.7113	-49.61 ± -108

Irradiation filename: au5.1c.adl.ih4

%P	40Ar(*±atm)	39Ar(K)	38Ar(Cl±atm)	37Ar(Ca)	36Ar(Atm)	%Rad	R	Age (Ma)
3.0	3.73E-16 ± 3.14E-18	7.01E-18 ± 2.73E-19	4.2E-19 ± 1.7E-19	1.5E-19 ± 3.9E-19	1.28E-18 ± 8.64E-20	-1%	-0.5311	-2.68 ± -23
3.3	1.21E-16 ± 2.43E-18	1.62E-17 ± 3.93E-19	1.5E-19 ± 9.0E-20	-5.1E-19 ± 4.3E-19	3.12E-19 ± 7.09E-20	24%	1.7779	8.94 ± 6.66
3.6	3.37E-16 ± 3.63E-18	7.84E-17 ± 1.24E-18	-1.4E-19 ± -3.5E-20	9.2E-20 ± 3.5E-19	3.11E-19 ± 8.18E-20	73%	3.1235	15.67 ± 1.60
4.0	5.48E-16 ± 3.55E-18	1.55E-16 ± 6.79E-19	1.1E-19 ± 1.1E-20	-2.5E-19 ± 5.0E-19	1.69E-19 ± 8.17E-20	91%	3.2058	16.08 ± 0.79
4.3	3.86E-16 ± 3.71E-18	1.14E-16 ± 9.86E-19	-9.2E-19 ± -1.3E-18	-7.5E-19 ± 4.5E-19	1.44E-19 ± 7.97E-20	89%	3.0169	15.14 ± 1.06
4.5	4.85E-15 ± 3.51E-18	1.49E-15 ± 3.19E-18	3.4E-18 ± 6.4E-20	-2.2E-19 ± 3.3E-19	7.94E-20 ± 1.49E-19	100%	3.2422	16.26 ± 0.15
4.8	9.97E-15 ± 1.15E-17	3.11E-15 ± 7.34E-18	7.6E-18 ± 5.3E-20	-6.0E-20 ± 4.0E-19	8.98E-19 ± 1.63E-19	97%	3.1201	15.65 ± 0.09
5.0	9.39E-15 ± 1.30E-17	2.93E-15 ± 9.90E-18	6.7E-18 ± 7.9E-20	-3.1E-19 ± 3.5E-19	6.89E-19 ± 1.17E-19	98%	3.1381	15.74 ± 0.08
5.3	4.47E-15 ± 4.04E-18	1.39E-15 ± 6.26E-18	3.3E-18 ± 5.8E-20	-3.7E-19 ± 3.7E-19	5.27E-19 ± 1.18E-19	97%	3.1052	15.58 ± 0.15
5.5	8.53E-15 ± 5.81E-18	2.63E-15 ± 3.02E-18	5.7E-18 ± 5.4E-20	6.7E-20 ± 2.8E-19	5.98E-19 ± 1.19E-19	98%	3.1717	15.91 ± 0.07
5.8	6.08E-15 ± 7.13E-18	1.88E-15 ± 1.55E-18	3.9E-18 ± 7.7E-20	3.4E-19 ± 3.7E-19	5.49E-19 ± 1.15E-19	97%	3.1505	15.81 ± 0.09
6.0	7.44E-15 ± 5.03E-18	2.29E-15 ± 2.81E-18	6.5E-18 ± 1.2E-19	-3.2E-19 ± 3.3E-19	4.67E-21 ± 1.36E-19	100%	3.2424	16.26 ± 0.09
6.5	6.94E-15 ± 7.28E-18	2.16E-15 ± 6.04E-18	4.9E-18 ± 7.6E-20	-3.2E-19 ± 3.1E-19	2.86E-19 ± 7.82E-20	99%	3.1704	15.91 ± 0.07
7.0	4.79E-15 ± 3.24E-18	1.47E-15 ± 2.48E-18	3.5E-18 ± 5.6E-20	-4.1E-20 ± 3.3E-19	2.29E-19 ± 8.10E-20	99%	3.2116	16.11 ± 0.09
8.0	4.20E-15 ± 1.01E-17	1.31E-15 ± 3.39E-18	3.0E-18 ± 4.1E-20	-3.4E-19 ± 4.5E-19	-1.50E-19 ± -1.49E-19	101%	3.2482	16.29 ± 0.18
9.0	8.17E-15 ± 1.06E-17	2.54E-15 ± 6.07E-18	5.9E-18 ± 8.7E-20	1.3E-20 ± 3.2E-19	1.77E-19 ± 7.94E-20	99%	3.1905	16.01 ± 0.06

Irradiation filename: au5.1c.adl.ih5

%P	40Ar(*±atm)	39Ar(K)	38Ar(Cl±atm)	37Ar(Ca)	36Ar(Atm)	%Rad	R	Age (Ma)
3.0	9.16E-17 ± 2.06E-18	5.74E-18 ± 4.26E-19	-9.6E-21 ± -4.0E-20	-3.1E-19 ± 4.0E-19	1.69E-19 ± 9.19E-20	46%	7.2856	36.34 ± 24
3.3	4.27E-16 ± 3.54E-18	9.66E-17 ± 6.90E-19	-8.5E-20 ± -2.0E-20	-1.1E-18 ± 5.4E-19	2.03E-19 ± 9.08E-20	86%	3.7914	19.00 ± 1.41
3.6	4.82E-16 ± 3.71E-18	1.43E-16 ± 8.08E-19	1.9E-19 ± 2.1E-20	-8.5E-19 ± 3.7E-19	-1.40E-19 ± -9.32E-20	109%	3.6616	18.36 ± 0.98
4.0	7.47E-16 ± 6.83E-18	2.28E-16 ± 7.34E-19	6.4E-19 ± 5.0E-20	-1.0E-18 ± 3.9E-19	-1.44E-19 ± -8.44E-20	106%	3.4572	17.34 ± 0.57
4.3	2.62E-16 ± 2.46E-18	8.05E-17 ± 6.85E-19	3.7E-19 ± 6.6E-20	-8.1E-19 ± 4.3E-19	-8.65E-20 ± -8.55E-20	110%	3.5655	17.88 ± 1.59
4.5	4.28E-15 ± 5.12E-18	1.34E-15 ± 5.22E-18	3.1E-18 ± 4.0E-20	2.9E-19 ± 2.9E-19	-1.82E-20 ± -1.17E-19	100%	3.1994	16.05 ± 0.15
4.8	7.36E-15 ± 5.17E-18	2.31E-15 ± 5.49E-18	5.0E-18 ± 7.2E-20	-2.2E-19 ± 3.4E-19	2.96E-19 ± 7.16E-20	99%	3.1469	15.79 ± 0.06
5.0	2.32E-15 ± 6.12E-18	7.20E-16 ± 2.41E-18	2.0E-18 ± 7.6E-20	-3.5E-19 ± 3.5E-19	1.39E-19 ± 6.50E-20	98%	3.1647	15.88 ± 0.15
5.3	4.24E-15 ± 7.99E-18	1.33E-15 ± 2.14E-18	3.1E-18 ± 5.0E-20	-3.3E-19 ± 3.6E-19	7.78E-20 ± 7.00E-20	99%	3.1828	15.97 ± 0.09
5.5	2.80E-15 ± 4.32E-18	8.73E-16 ± 3.25E-18	2.4E-18 ± 8.5E-20	1.7E-19 ± 3.7E-19	3.92E-20 ± 6.57E-20	100%	3.1870	15.99 ± 0.13
5.8	1.40E-14 ± 8.98E-18	4.31E-15 ± 1.08E-17	9.8E-18 ± 1.0E-19	6.1E-21 ± 5.1E-19	9.67E-19 ± 8.06E-20	98%	3.1776	15.94 ± 0.05
6.0	1.99E-14 ± 3.39E-17	6.18E-15 ± 2.13E-17	1.6E-17 ± 2.3E-19	3.0E-19 ± 4.0E-19	7.74E-19 ± 8.65E-20	99%	3.1783	15.94 ± 0.07
6.5	8.88E-15 ± 1.11E-17	2.76E-15 ± 3.86E-18	6.7E-18 ± 5.6E-20	5.7E-19 ± 4.5E-19	1.03E-19 ± 6.28E-20	100%	3.2025	16.07 ± 0.05
7.0	1.67E-15 ± 5.73E-18	5.15E-16 ± 1.83E-18	1.1E-18 ± 4.6E-20	1.4E-18 ± 4.5E-19	-1.03E-19 ± -7.84E-20	102%	3.2907	16.51 ± 0.24
8.0	2.21E-15 ± 5.37E-18	6.85E-16 ± 2.01E-18	1.7E-18 ± 7.1E-20	-1.7E-19 ± 5.0E-19	8.89E-20 ± 7.69E-20	99%	3.1807	15.96 ± 0.18
9.0	8.74E-16 ± 3.28E-18	2.71E-16 ± 8.29E-19	8.0E-19 ± 5.3E-20	6.5E-19 ± 4.2E-19	7.32E-20 ± 7.99E-20	98%	3.1426	15.77 ± 0.44

Jumbo deposit step heating increments for 5 single adularia crystals (14-20 mesh size, 1.2-0.75 mm) of sample: HCN-3RE
Irradiation filename: au5.1f.adl.ih.1

%P	40Ar(*±atm)	39Ar(K)	38Ar(Cl±atm)	37Ar(Ca)	36Ar(Atm)	%Rad	R	Age (Ma)
3.0	3.42E-16 ± 3.70E-18	2.67E-18 ± 3.79E-19	4.4E-19 ± 1.7E-19	-5.2E-19 ± 3.5E-19	5.20E-19 ± 1.47E-19	55%	70.4089	323.89 ± 118
3.3	2.22E-16 ± 2.15E-18	2.79E-17 ± 4.13E-19	2.5E-19 ± 7.7E-20	1.0E-19 ± 4.5E-19	4.40E-19 ± 8.07E-20	42%	3.3163	16.63 ± 4.37
3.6	8.23E-16 ± 3.82E-18	2.19E-16 ± 9.69E-19	4.1E-19 ± 3.5E-20	-3.1E-19 ± 3.5E-19	2.00E-19 ± 8.55E-20	93%	3.4825	17.46 ± 0.59
4.0	2.14E-15 ± 3.81E-18	6.31E-16 ± 2.25E-18	1.8E-18 ± 5.1E-20	4.2E-19 ± 3.6E-19	-3.61E-21 ± -7.62E-20	100%	3.3862	16.98 ± 0.19
4.3	1.11E-15 ± 4.51E-18	3.38E-16 ± 2.04E-18	1.1E-18 ± 5.5E-20	4.3E-20 ± 3.2E-19	-9.26E-20 ± -8.16E-20	102%	3.3633	16.87 ± 0.38
4.5	3.77E-15 ± 4.57E-18	1.12E-15 ± 2.68E-18	2.8E-18 ± 8.0E-20	-4.5E-19 ± 2.8E-19	4.15E-19 ± 1.44E-19	97%	3.2498	16.30 ± 0.20
4.8	1.79E-14 ± 1.72E-17	5.36E-15 ± 1.30E-17	1.4E-17 ± 1.0E-19	-3.5E-19 ± 2.9E-19	7.39E-19 ± 1.82E-19	99%	3.2991	16.55 ± 0.07
5.0	8.10E-15 ± 1.07E-17	2.37E-15 ± 5.27E-18	5.6E-18 ± 7.4E-20	4.1E-19 ± 3.4E-19	1.09E-18 ± 1.42E-19	96%	3.2855	16.48 ± 0.10
5.3	7.53E-15 ± 6.49E-18	2.24E-15 ± 4.06E-18	5.2E-18 ± 8.3E-20	-9.7E-20 ± 3.5E-19	5.51E-19 ± 1.56E-19	98%	3.2919	16.51 ± 0.11
5.5	7.50E-15 ± 5.94E-18	2.23E-15 ± 6.30E-18	4.6E-18 ± 5.3E-20	-3.9E-19 ± 2.9E-19	3.00E-19 ± 8.96E-20	99%	3.3135	16.62 ± 0.08
5.8	7.33E-15 ± 5.94E-18	2.19E-15 ± 5.86E-18	5.2E-18 ± 9.9E-20	1.4E-19 ± 3.4E-19	3.42E-19 ± 8.94E-20	99%	3.2930	16.52 ± 0.08
6.0	1.09E-14 ± 8.21E-18	3.22E-15 ± 5.64E-18	6.8E-18 ± 7.9E-20	-5.8E-20 ± 4.3E-19	1.52E-19 ± 8.41E-20	100%	3.3527	16.82 ± 0.05
6.5	6.22E-15 ± 3.52E-17	1.81E-15 ± 4.42E-18	4.5E-18 ± 7.7E-20	-2.9E-19 ± 4.1E-19	1.35E-19 ± 7.33E-20	99%	3.4020	17.06 ± 0.12
7.0	1.09E-14 ± 8.21E-18	3.22E-15 ± 5.64E-18	6.8E-18 ± 7.9E-20	-5.8E-20 ± 4.3E-19	1.52E-19 ± 8.41E-20	100%	3.3527	16.82 ± 0.05
8.0	6.66E-16 ± 3.61E-18	1.95E-16 ± 1.16E-18	2.2E-19 ± 1.6E-20	-5.9E-19 ± 3.9E-19	-8.19E-20 ± -8.37E-20	104%	3.5297	17.70 ± 0.65
9.0	7.72E-17 ± 1.90E-18	2.09E-17 ± 4.63E-19	-3.1E-19 ± -7.3E-19	-6.7E-19 ± 3.9E-19	-4.70E-20 ± -7.73E-20	118%	4.3562	21.82 ± 5.51

Irradiation filename: au5.1f.adl.ih.2

%P	40Ar(*±atm)	39Ar(K)	38Ar(Cl±atm)	37Ar(Ca)	36Ar(Atm)	%Rad	R	Age (Ma)
3.0	1.87E-16 ± 1.85E-18	2.99E-18 ± 4.15E-19	1.6E-19 ± 1.7E-19	-5.1E-19 ± 4.0E-19	6.31E-19 ± 8.29E-20	0%	0.1822	0.92 ± 74
3.3	1.49E-16 ± 2.23E-18	3.17E-17 ± 6.09E-19	2.9E-19 ± 1.0E-19	2.6E-19 ± 4.4E-19	4.75E-20 ± 8.46E-20	91%	4.2523	21.30 ± 3.99
3.6	2.39E-16 ± 3.12E-18	6.32E-17 ± 5.75E-19	7.8E-20 ± 2.2E-20	1.6E-18 ± 5.6E-19	1.35E-22 ± 1.94E-20	100%	3.7795	18.94 ± 0.55
4.0	3.24E-16 ± 1.81E-18	9.57E-17 ± 9.17E-19	2.2E-19 ± 3.0E-20	-2.4E-20 ± 4.4E-19	7.43E-21 ± 7.95E-20	99%	3.3576	16.84 ± 1.25
4.3	3.79E-16 ± 3.18E-18	1.10E-16 ± 9.66E-19	1.8E-19 ± 3.3E-20	5.0E-19 ± 5.1E-19	-1.14E-19 ± -1.17E-19	109%	3.7612	18.85 ± 1.59
4.5	1.91E-15 ± 5.08E-18	5.73E-16 ± 1.97E-18	2.0E-18 ± 6.3E-20	-2.8E-19 ± 4.0E-19	1.29E-19 ± 8.04E-20	98%	3.2721	16.41 ± 0.22
4.8	8.10E-15 ± 5.62E-18	2.46E-15 ± 4.50E-18	7.6E-18 ± 1.2E-19	1.6E-19 ± 3.9E-19	3.91E-19 ± 7.71E-20	99%	3.2393	16.25 ± 0.06
5.0	9.38E-15 ± 5.05E-18	2.84E-15 ± 1.07E-17	7.2E-18 ± 8.4E-20	-3.3E-19 ± 4.4E-19	2.95E-19 ± 7.44E-20	99%	3.2674	16.39 ± 0.07
5.3	9.81E-15 ± 7.07E-18	2.97E-15 ± 7.74E-18	6.7E-18 ± 6.6E-20	-7.0E-20 ± 3.5E-19	2.52E-19 ± 8.96E-20	99%	3.2803	16.45 ± 0.06
5.5	6.45E-15 ± 5.49E-18	1.95E-15 ± 7.14E-18	4.4E-18 ± 3.4E-20	-9.9E-20 ± 3.7E-19	6.40E-20 ± 6.72E-20	100%	3.2990	16.55 ± 0.08
5.8	5.33E-15 ± 4.41E-18	1.61E-15 ± 4.79E-18	4.0E-18 ± 5.7E-20	-5.3E-21 ± 4.3E-19	-2.03E-19 ± -1.42E-19	101%	3.3413	16.76 ± 0.14
6.0	3.55E-15 ± 4.91E-18	1.07E-15 ± 4.62E-18	1.8E-18 ± 4.3E-20	-3.7E-19 ± 4.6E-19	-5.75E-20 ± -8.04E-20	100%	3.3316	16.71 ± 0.13
6.5	6.32E-15 ± 3.74E-18	1.91E-15 ± 6.50E-18	4.2E-18 ± 4.9E-20	2.0E-19 ± 4.2E-19	2.19E-20 ± 8.60E-20	100%	3.3062	16.58 ± 0.09
7.0	6.02E-15 ± 5.12E-18	1.81E-15 ± 3.28E-18	4.1E-18 ± 5.4E-20	-4.2E-20 ± 3.5E-19	-5.67E-20 ± -8.26E-20	100%	3.3409	16.76 ± 0.08
8.0	6.47E-15 ± 4.56E-18	1.96E-15 ± 5.19E-18	3.7E-18 ± 5.8E-20	-1.3E-19 ± 3.1E-19	-2.37E-19 ± -1.40E-19	101%	3.3418	16.76 ± 0.12
9.0	5.34E-15 ± 3.71E-18	1.60E-15 ± 2.43E-18	4.6E-18 ± 1.5E-19	1.2E-19 ± 3.7E-19	1.01E-19 ± 8.90E-20	99%	3.3062	16.58 ± 0.09

Irradiation filename: au5.1f.adl.ih.3

%P	40Ar(*±atm)	39Ar(K)	38Ar(Cl±atm)	37Ar(Ca)	36Ar(Atm)	%Rad	R	Age (Ma)
3.0	2.24E-16 ± 2.03E-18	3.64E-18 ± 3.86E-19	-8.6E-20 ± -2.9E-19	-1.0E-18 ± 3.9E-19	8.82E-19 ± 1.36E-19	-16%	-10.1138	-51.70 ± -76
3.3	1.60E-16 ± 2.65E-18	3.76E-17 ± 4.21E-19	-3.2E-19 ± -8.6E-19	-3.7E-19 ± 4.0E-19	2.09E-19 ± 1.41E-19	61%	2.6192	13.15 ± 5.59
3.6	3.37E-16 ± 2.42E-18	9.36E-17 ± 4.84E-19	1.6E-19 ± 2.9E-20	-5.0E-19 ± 4.6E-19	1.90E-19 ± 1.40E-19	83%	2.9954	15.03 ± 2.22
4.0	6.85E-16 ± 3.50E-18	2.00E-16 ± 8.73E-19	5.3E-19 ± 5.0E-20	-7.1E-19 ± 3.6E-19	1.35E-19 ± 1.35E-19	94%	3.2295	16.20 ± 1.01
4.3	6.09E-16 ± 3.74E-18	1.81E-16 ± 7.92E-19	4.7E-19 ± 5.0E-20	-9.9E-20 ± 3.9E-19	2.29E-19 ± 8.59E-20	89%	2.9821	14.96 ± 0.71
4.5	2.15E-15 ± 6.01E-18	6.56E-16 ± 3.51E-18	1.2E-18 ± 2.8E-20	-5.5E-19 ± 5.3E-19	-9.35E-20 ± -1.40E-19	101%	3.3245	16.67 ± 0.33
4.8	1.04E-14 ± 9.46E-18	3.14E-15 ± 5.79E-18	7.4E-18 ± 7.8E-20	-5.5E-19 ± 5.0E-19	1.84E-19 ± 8.57E-20	99%	3.2994	16.55 ± 0.05
5.0	1.17E-14 ± 8.86E-18	3.51E-15 ± 4.67E-18	8.0E-18 ± 1.0E-19	-1.0E-18 ± 4.8E-19	5.08E-19 ± 9.80E-20	99%	3.2894	16.50 ± 0.05
5.3	4.97E-15 ± 3.68E-18	1.50E-15 ± 2.27E-18	3.6E-18 ± 5.7E-20	4.7E-19 ± 4.9E-19	1.18E-19 ± 8.36E-20	99%	3.2889	16.50 ± 0.09
5.5	3.27E-15 ± 3.31E-18	9.81E-16 ± 2.18E-18	1.8E-18 ± 5.3E-20	-2.0E-18 ± 6.2E-19	-5.22E-20 ± -1.07E-19	100%	3.3492	16.80 ± 0.17
5.8	1.83E-15 ± 5.94E-18	5.46E-16 ± 1.71E-18	1.0E-18 ± 3.7E-20	-1.5E-19 ± 4.8E-19	-2.78E-19 ± -1.35E-19	104%	3.4882	17.49 ± 0.37
6.0	1.80E-15 ± 7.03E-18	5.36E-16 ± 1.70E-18	1.3E-18 ± 5.3E-20	-5.4E-19 ± 4.9E-19	4.95E-21 ± 8.89E-20	100%	3.3566	16.83 ± 0.26
6.5	8.96E-15 ± 1.35E-17	2.71E-15 ± 5.48E-18	6.1E-18 ± 8.1E-20	-2.0E-19 ± 5.0E-19	1.32E-19 ± 9.07E-20	100%	3.2848	16.48 ± 0.06
7.0	1.59E-15 ± 7.24E-18	4.73E-16 ± 1.91E-18	1.0E-18 ± 3.3E-20	-9.3E-19 ± 4.0E-19	-1.35E-20 ± -1.01E-19	100%	3.3729	16.92 ± 0.33
8.0	2.76E-16 ± 2.28E-18	8.01E-17 ± 7.56E-19	-5.9E-20 ± -1.4E-20	-4.0E-19 ± 4.3E-19	-2.77E-19 ± -1.37E-19	130%	4.4644	22.36 ± 2.55
9.0	6.44E-17 ± 2.47E-18	1.90E-17 ± 4.72E-19	-6.7E-20 ± -1.0E-19	-4.2E-19 ± 4.5E-19	1.33E-20 ± 9.30E-20	94%	3.1824	15.96 ± 7.31

Irradiation filename: au5.1f.adl.ih.4

%P	40Ar(*±atm)	39Ar(K)	38Ar(Cl±atm)	37Ar(Ca)	36Ar(Atm)	%Rad	R	Age (Ma)
3.0	5.96E-16 ± 2.72E-18	7.03E-18 ± 3.25E-19	5.8E-19 ± 2.5E-19	-1.8E-19 ± 4.1E-19	2.18E-18 ± 1.62E-19	-8%	-6.8368	-34.78 ± -45
3.3	2.31E-16 ± 3.44E-18	5.40E-17 ± 5.26E-19	6.8E-20 ± 2.9E-20	-5.0E-19 ± 4.2E-19	4.54E-19 ± 1.52E-19	42%	1.7858	8.98 ± 4.19
3.6	9.08E-16 ± 4.71E-18	2.61E-16 ± 6.33E-19	3.7E-19 ± 3.8E-20	5.2E-22 ± 5.6E-19	4.31E-19 ± 1.54E-19	86%	2.9841	14.97 ± 0.88
4.0	7.60E-15 ± 3.66E-18	2.24E-15 ± 3.64E-18	4.5E-18 ± 4.7E-20	-2.1E-19 ± 5.6E-19	3.76E-19 ± 1.84E-19	99%	3.3360	16.73 ± 0.12
4.3	1.02E-14 ± 9.73E-18	2.97E-15 ± 4.53E-18	8.8E-18 ± 1.3E-19	-4.3E-19 ± 3.7E-19	1.54E-18 ± 1.70E-19	96%	3.2932	16.52 ± 0.09
4.5	3.69E-15 ± 8.96E-18	1.04E-15 ± 3.58E-18	2.9E-18 ± 8.1E-20	1.1E-18 ± 6.5E-19	1.21E-18 ± 1.51E-19	90%	3.2146	16.13 ± 0.23
4.8	5.06E-15 ± 7.31E-18	1.45E-15 ± 3.89E-18	3.9E-18 ± 6.6E-20	1.0E-18 ± 6.2E-19	1.10E-18 ± 1.49E-19	94%	3.2738	16.42 ± 0.16
5.0	3.78E-15 ± 6.31E-18	1.11E-15 ± 3.95E-18	3.0E-18 ± 8.8E-20	1.3E-18 ± 6.6E-19	3.34E-19 ± 1.85E-19	97%	3.3162	16.63 ± 0.26
5.3	4.53E-15 ± 7.08E-18	1.33E-15 ± 4.24E-18	3.1E-18 ± 5.2E-20	1.3E-18 ± 6.2E-19	4.26E-19 ± 1.44E-19	97%	3.3041	16.57 ± 0.17
5.5	7.21E-15 ± 6.34E-18	2.13E-15 ± 2.48E-18	6.4E-18 ± 1.3E-19	5.3E-19 ± 6.4E-19	5.05E-19 ± 1.46E-19	98%	3.3111	16.61 ± 0.10
5.8	2.69E-15 ± 5.74E-18	7.97E-16 ± 2.74E-18	1.7E-18 ± 4.3E-20	1.6E-18 ± 7.1E-19	4.17E-19 ± 1.43E-19	95%	3.2223	16.16 ± 0.27
6.0	2.22E-15 ± 2.96E-18	6.48E-16 ± 2.09E-18	2.1E-18 ± 7.3E-20	-6.7E-19 ± 4.2E-19	-2.14E-19 ± -1.27E-19	103%	3.5212	17.66 ± 0.30
6.5	8.73E-16 ± 4.13E-18	2.60E-16 ± 1.63E-18	3.5E-19 ± 2.1E-20	-4.5E-19 ± 4.1E-19	3.91E-20 ± 7.93E-20	99%	3.3078	16.59 ± 0.47
7.0	2.76E-16 ± 2.68E-18	8.01E-17 ± 9.28E-19	7.0E-20 ± 1.3E-20	-5.7E-19 ± 4.7E-19	-1.22E-19 ± -7.32E-20	113%	3.9008	19.55 ± 1.38
8.0	5.40E-17 ± 1.90E-18	1.57E-17 ± 4.09E-19	-7.4E-20 ± -1.4E-19	-6.0E-19 ± 4.0E-19	-1.75E-19 ± -7.40E-20	196%	6.7456	33.67 ± 7.02
9.0	2.73E-17 ± 1.41E-18	7.30E-18 ± 4.47E-19	-2.1E-19 ± -2.7E-19	-1.4E-18 ± 4.3E-19	-1.39E-19 ± -8.07E-20	251%	9.3775	46.64 ± 16

114

Irradiation filename: au5.1f.adl.ih.5

%P	40Ar(*±atm)	39Ar(K)	38Ar(Cl±atm)	37Ar(Ca)	36Ar(Atm)	%Rad	R	Age (Ma)
3.0	3.93E-16 ± 3.38E-18	2.17E-18 ± 3.35E-19	-5.6E-20 ± -2.9E-19	2.7E-19 ± 4.2E-19	1.48E-18 ± 8.28E-20	-11%	-20.3667	-105.66 ± -224
3.3	n/a ± n/a	3.49E-18 ± 2.88E-19	6.7E-19 ± 1.6E-19	-1.2E-19 ± 5.1E-19	3.94E-18 ± 1.10E-19	n/a	n/a	n/a ± n/a
3.6	3.49E-16 ± 2.56E-18	6.91E-17 ± 9.46E-19	6.5E-20 ± 1.4E-20	5.4E-19 ± 3.2E-19	3.67E-19 ± 6.80E-20	69%	3.4805	17.45 ± 1.51
4.0	7.37E-16 ± 4.45E-18	2.04E-16 ± 1.21E-18	4.9E-19 ± 3.9E-20	3.8E-19 ± 3.5E-19	1.20E-19 ± 7.23E-20	95%	3.4411	17.26 ± 0.55
4.3	6.31E-16 ± 5.03E-18	1.88E-16 ± 1.28E-18	2.9E-19 ± 3.4E-20	5.4E-19 ± 4.2E-19	8.86E-20 ± 8.60E-20	96%	3.2158	16.13 ± 0.70
4.5	6.81E-15 ± 9.27E-18	2.07E-15 ± 3.62E-18	4.7E-18 ± 9.3E-20	-4.1E-19 ± 3.0E-19	1.89E-19 ± 7.94E-20	99%	3.2541	16.32 ± 0.07
4.8	1.95E-14 ± 1.06E-17	5.86E-15 ± 1.07E-17	1.4E-17 ± 9.5E-20	1.1E-19 ± 2.7E-19	9.32E-19 ± 7.31E-20	99%	3.2768	16.44 ± 0.04
5.0	9.40E-15 ± 1.26E-17	2.79E-15 ± 4.59E-18	8.2E-18 ± 1.6E-19	7.2E-19 ± 2.8E-19	9.37E-19 ± 7.50E-20	97%	3.2690	16.40 ± 0.05
5.3	8.95E-15 ± 7.24E-18	2.65E-15 ± 3.83E-18	6.7E-18 ± 6.5E-20	5.0E-19 ± 3.6E-19	4.94E-19 ± 7.56E-20	98%	3.3222	16.66 ± 0.05
5.5	4.34E-15 ± 7.05E-18	1.32E-15 ± 3.23E-18	2.6E-18 ± 4.8E-20	2.7E-19 ± 4.3E-19	2.42E-19 ± 7.65E-20	98%	3.2245	16.17 ± 0.10
5.8	2.75E-15 ± 5.77E-18	8.18E-16 ± 2.25E-18	1.8E-18 ± 4.2E-20	-3.7E-19 ± 2.7E-19	1.83E-19 ± 9.13E-20	98%	3.2872	16.49 ± 0.18
6.0	4.24E-15 ± 7.29E-18	1.26E-15 ± 3.76E-18	1.9E-18 ± 3.2E-20	9.7E-20 ± 4.3E-19	4.07E-19 ± 8.43E-20	97%	3.2540	16.32 ± 0.11
6.5	7.69E-15 ± 1.06E-17	2.31E-15 ± 6.05E-18	6.0E-18 ± 1.3E-19	5.2E-19 ± 5.6E-19	3.00E-19 ± 7.10E-20	99%	3.2892	16.50 ± 0.07
7.0	1.02E-14 ± 8.61E-18	3.07E-15 ± 5.76E-18	9.0E-18 ± 2.0E-19	1.7E-18 ± 4.8E-19	1.09E-19 ± 8.65E-20	100%	3.3062	16.58 ± 0.05
8.0	1.07E-14 ± 1.21E-17	3.20E-15 ± 7.41E-18	5.6E-18 ± 8.3E-20	5.5E-19 ± 3.8E-19	-7.37E-20 ± -1.34E-19	100%	3.3336	16.72 ± 0.08
9.0	1.12E-15 ± 4.33E-18	3.35E-16 ± 1.21E-18	6.6E-19 ± 3.9E-20	7.8E-19 ± 4.9E-19	-6.30E-20 ± -1.27E-19	102%	3.3794	16.95 ± 0.57

Ten Mile deposit step heating increments for 5 single adularia crystals (14-20 mesh size, 1.2-0.75 mm) of sample: HCN-4
Irradiation filename: au5.1h.adl.ih1

%P	40Ar(*±atm)	39Ar(K)	38Ar(Cl±atm)	37Ar(Ca)	36Ar(Atm)	%Rad	R	Age (Ma)
3.0	3.30E-15 ± 4.23E-18	3.86E-18 ± 4.06E-19	2.0E-18 ± 1.5E-19	-6.9E-19 ± 3.3E-19	1.11E-17 ± 1.58E-19	0%	2.3137	11.62 ± 640
3.3	3.19E-15 ± 5.21E-18	2.28E-17 ± 6.49E-19	1.8E-18 ± 1.6E-19	-4.5E-19 ± 4.2E-19	1.02E-17 ± 1.26E-19	5%	7.4235	37.02 ± 28
3.6	1.88E-15 ± 2.69E-18	1.19E-16 ± 7.25E-19	1.2E-18 ± 7.9E-20	2.8E-19 ± 4.0E-19	4.19E-18 ± 1.98E-19	34%	5.3753	26.88 ± 2.54
4.0	2.02E-15 ± 4.68E-18	3.19E-16 ± 1.23E-18	1.1E-18 ± 5.5E-20	-1.9E-19 ± 4.3E-19	2.94E-18 ± 1.05E-19	57%	3.6060	18.08 ± 0.51
4.3	1.04E-15 ± 1.68E-18	2.02E-16 ± 1.66E-18	4.9E-19 ± 4.5E-20	-1.0E-20 ± 3.6E-19	1.14E-18 ± 9.53E-20	67%	3.4610	17.36 ± 0.74
4.5	1.34E-15 ± 3.96E-18	2.42E-16 ± 1.45E-18	1.0E-18 ± 5.9E-20	1.2E-19 ± 3.2E-19	1.60E-18 ± 9.21E-20	65%	3.5858	17.98 ± 0.60
4.8	8.89E-16 ± 3.59E-18	2.25E-16 ± 2.51E-18	5.3E-19 ± 3.8E-20	3.4E-19 ± 4.3E-19	3.29E-19 ± 8.39E-20	89%	3.5184	17.64 ± 0.60
5.0	1.10E-15 ± 4.13E-18	2.41E-16 ± 1.26E-18	1.2E-18 ± 6.8E-20	4.5E-19 ± 4.5E-19	9.86E-19 ± 9.27E-20	74%	3.3659	16.88 ± 0.59
5.3	3.23E-15 ± 3.78E-18	7.71E-16 ± 2.18E-18	2.7E-18 ± 6.1E-20	4.4E-19 ± 4.4E-19	2.27E-18 ± 8.65E-20	79%	3.3143	16.62 ± 0.18
5.5	1.01E-14 ± 9.27E-18	2.78E-15 ± 2.71E-18	7.1E-18 ± 8.3E-20	-1.3E-19 ± 4.6E-19	2.98E-18 ± 1.03E-19	91%	3.3229	16.67 ± 0.06
5.8	1.91E-14 ± 2.07E-17	5.63E-15 ± 1.55E-17	1.3E-17 ± 1.4E-19	1.1E-19 ± 4.0E-19	1.63E-18 ± 1.00E-19	97%	3.2967	16.54 ± 0.06
6.0	1.54E-14 ± 1.15E-17	4.61E-15 ± 8.85E-18	1.2E-17 ± 1.1E-19	-4.8E-19 ± 3.4E-19	8.99E-19 ± 8.33E-20	98%	3.2815	16.46 ± 0.04
6.5	7.57E-15 ± 8.82E-18	2.27E-15 ± 2.61E-18	4.5E-18 ± 6.2E-20	-4.1E-19 ± 3.5E-19	2.81E-19 ± 7.93E-20	99%	3.2985	16.54 ± 0.06
7.0	1.94E-15 ± 3.32E-18	5.77E-16 ± 2.75E-18	7.5E-19 ± 3.3E-20	-1.3E-19 ± 3.5E-19	2.09E-19 ± 7.51E-20	97%	3.2547	16.33 ± 0.21
8.0	1.35E-15 ± 3.43E-18	4.00E-16 ± 3.34E-18	4.9E-19 ± 2.3E-20	-8.2E-20 ± 3.6E-19	8.42E-20 ± 7.71E-20	98%	3.3041	16.57 ± 0.32
9.0	1.95E-15 ± 5.89E-18	5.86E-16 ± 3.54E-18	1.5E-18 ± 5.4E-20	-2.9E-19 ± 4.2E-19	3.76E-20 ± 8.97E-20	99%	3.3115	16.61 ± 0.25

Irradiation filename: au5.1h.adl.ih2

%P	40Ar(*±atm)	39Ar(K)	38Ar(Cl±atm)	37Ar(Ca)	36Ar(Atm)	%Rad	R	Age (Ma)
3.0	9.51E-16 ± 2.68E-18	1.66E-19 ± 4.10E-19	1.2E-18 ± 2.9E-19	-6.9E-19 ± 4.0E-19	3.11E-18 ± 8.97E-20	3%	196.9579	790.78 ± 7936
3.3	4.08E-15 ± 7.99E-18	6.26E-18 ± 3.49E-19	3.2E-18 ± 3.2E-19	-3.0E-19 ± 3.4E-19	1.36E-17 ± 1.75E-19	1%	7.1064	35.46 ± 258
3.6	1.79E-15 ± 4.37E-18	6.84E-17 ± 1.36E-18	1.8E-18 ± 2.1E-19	-5.1E-19 ± 3.3E-19	5.19E-18 ± 1.20E-19	14%	3.7373	18.73 ± 4.33
4.0	1.37E-15 ± 2.72E-18	2.57E-16 ± 1.75E-18	1.4E-18 ± 1.1E-19	-4.8E-19 ± 3.8E-19	1.71E-18 ± 9.43E-20	63%	3.3759	16.93 ± 0.58
4.3	1.04E-15 ± 5.16E-18	1.54E-16 ± 7.69E-19	6.0E-19 ± 1.1E-19	-7.7E-19 ± 4.5E-19	1.47E-18 ± 1.73E-19	58%	3.8997	19.54 ± 1.68
4.5	1.60E-14 ± 2.12E-17	4.16E-15 ± 4.77E-18	1.2E-17 ± 1.3E-19	5.6E-19 ± 4.4E-19	8.04E-18 ± 1.31E-19	85%	3.2781	16.44 ± 0.06
4.8	1.75E-14 ± 1.57E-17	5.28E-15 ± 6.13E-18	1.2E-17 ± 6.5E-20	4.3E-19 ± 4.4E-19	1.03E-18 ± 8.71E-20	98%	3.2636	16.37 ± 0.03
5.0	1.21E-14 ± 9.48E-18	3.66E-15 ± 8.29E-18	8.6E-18 ± 6.7E-20	3.9E-19 ± 4.3E-19	2.64E-19 ± 7.64E-20	99%	3.2892	16.50 ± 0.05
5.3	3.57E-15 ± 5.45E-18	1.08E-15 ± 3.09E-18	2.4E-18 ± 4.0E-20	2.9E-20 ± 3.9E-19	4.42E-20 ± 8.69E-20	100%	3.2934	16.52 ± 0.13
5.5	1.50E-15 ± 2.69E-18	4.50E-16 ± 2.93E-18	7.9E-19 ± 2.3E-20	1.2E-19 ± 3.6E-19	-8.97E-20 ± -7.58E-20	102%	3.3922	17.01 ± 0.27
5.8	1.24E-15 ± 3.62E-18	3.66E-16 ± 1.80E-18	9.3E-19 ± 4.7E-20	1.8E-19 ± 4.3E-19	-5.46E-20 ± -7.37E-20	101%	3.4145	17.12 ± 0.31
6.0	6.17E-16 ± 5.11E-18	1.85E-16 ± 9.80E-19	2.0E-19 ± 1.7E-20	-8.8E-21 ± 4.0E-19	-3.02E-20 ± -7.22E-20	101%	3.3880	16.99 ± 0.60
6.5	8.43E-16 ± 4.48E-18	2.49E-16 ± 1.52E-18	4.2E-19 ± 3.5E-20	-2.2E-19 ± 3.9E-19	-2.39E-20 ± -8.07E-20	101%	3.4113	17.11 ± 0.50
7.0	4.63E-16 ± 4.71E-18	1.38E-16 ± 9.96E-19	-4.2E-20 ± -6.6E-21	-5.7E-19 ± 4.1E-19	-2.53E-19 ± -1.02E-19	116%	3.8842	19.47 ± 1.11
8.0	7.72E-16 ± 4.89E-18	2.27E-16 ± 1.17E-18	3.3E-19 ± 2.9E-20	-3.9E-20 ± 3.6E-19	-5.00E-20 ± -7.56E-20	102%	3.4576	17.34 ± 0.51
9.0	4.70E-16 ± 2.68E-18	1.43E-16 ± 1.23E-18	1.9E-20 ± 2.2E-21	-4.2E-19 ± 3.5E-19	-8.42E-21 ± -8.33E-20	101%	3.3012	16.56 ± 0.88

%P	40Ar(*±atm)	39Ar(K)	38Ar(Cl±atm)	37Ar(Ca)	36Ar(Atm)	%Rad	R	Age (Ma)
3.0	1.23E-15 ± 3.42E-18	2.62E-18 ± 3.39E-19	9.6E-19 ± 1.2E-19	5.6E-19 ± 4.3E-19	4.22E-18 ± 1.06E-19	-1%	-5.6097	-28.49 ± -444
3.3	8.08E-16 ± 3.77E-18	4.59E-17 ± 4.85E-19	5.9E-19 ± 9.5E-20	7.8E-19 ± 4.9E-19	2.21E-18 ± 1.10E-19	19%	3.3909	17.01 ± 3.76
3.6	1.20E-15 ± 2.58E-18	2.66E-16 ± 2.23E-18	6.6E-19 ± 4.5E-20	3.2E-19 ± 4.3E-19	1.10E-18 ± 9.37E-20	73%	3.2899	16.50 ± 0.56
4.0	1.65E-14 ± 1.47E-17	4.67E-15 ± 7.83E-18	1.1E-17 ± 1.0E-19	-1.0E-19 ± 5.0E-19	4.28E-18 ± 1.15E-19	92%	3.2577	16.34 ± 0.05
4.3	9.17E-15 ± 9.73E-18	2.76E-15 ± 5.99E-18	6.1E-18 ± 8.7E-20	6.5E-19 ± 4.5E-19	1.74E-19 ± 1.43E-19	99%	3.3001	16.55 ± 0.09
4.5	2.09E-15 ± 4.96E-18	6.20E-16 ± 1.67E-18	1.5E-18 ± 5.9E-20	-5.8E-19 ± 3.7E-19	-3.68E-20 ± -7.39E-20	101%	3.3913	17.01 ± 0.19
4.8	6.91E-16 ± 2.70E-18	2.08E-16 ± 1.05E-18	2.5E-19 ± 2.1E-20	-7.4E-19 ± 3.0E-19	-6.18E-20 ± -7.80E-20	103%	3.4070	17.09 ± 0.57
5.0	4.18E-16 ± 2.37E-18	1.22E-16 ± 9.79E-19	-4.0E-19 ± -1.1E-19	-1.9E-20 ± 4.4E-19	-4.93E-20 ± -7.66E-20	103%	3.5326	17.71 ± 0.94
5.3	5.62E-17 ± 2.46E-18	1.62E-17 ± 3.48E-19	1.2E-19 ± 1.0E-19	-5.1E-19 ± 3.4E-19	-1.23E-20 ± -8.18E-20	106%	3.7019	18.56 ± 7.55
5.5	5.77E-18 ± 1.81E-18	1.29E-19 ± 3.57E-19	6.0E-21 ± 1.6E-19	-8.3E-19 ± 4.1E-19	-1.00E-19 ± -7.69E-20	613%	274.8279	1027.65 ± 2516
5.8	4.91E-18 ± 1.75E-18	-8.98E-20 ± -2.80E-19	4.9E-20 ± 2.1E-19	-4.8E-19 ± 3.8E-19	3.73E-20 ± 8.34E-20	-124%	68.7209	316.77 ± 2312
6.0	7.96E-19 ± 2.26E-18	8.72E-20 ± 3.07E-19	-1.1E-19 ± -2.0E-19	3.7E-19 ± 3.5E-19	1.57E-19 ± 1.99E-19	-5747%	-525.8438	n/a ± n/a
6.5	3.42E-18 ± 1.97E-18	1.14E-19 ± 2.31E-19	-1.1E-19 ± -2.2E-19	3.9E-19 ± 4.4E-19	4.35E-19 ± 1.28E-19	-3661%	-1096.3408	n/a ± n/a
7.0	1.51E-18 ± 2.15E-18	-9.21E-19 ± -4.27E-19	-4.0E-20 ± -1.9E-19	3.5E-19 ± 4.5E-19	5.05E-19 ± 1.33E-19	-9807%	160.3184	667.56 ± 359
8.0	1.36E-18 ± 1.97E-18	-3.16E-19 ± -3.06E-19	-1.8E-19 ± -2.0E-19	-1.4E-19 ± 4.4E-19	3.50E-19 ± 1.33E-19	-7479%	323.4493	1161.19 ± 1226
9.0	1.31E-18 ± 2.08E-18	6.47E-20 ± 2.61E-19	-2.6E-19 ± -2.1E-19	-2.9E-19 ± 3.5E-19	4.10E-19 ± 1.32E-19	-9125%	-1852.5235	n/a ± na

Irradiation filename: au5.1h.adl.ih4

%P	40Ar(*±atm)	39Ar(K)	38Ar(Cl±atm)	37Ar(Ca)	36Ar(Atm)	%Rad	R	Age (Ma)
3.0	1.25E-15 ± 7.03E-18	2.82E-18 ± 3.21E-19	6.2E-19 ± 1.7E-19	-7.5E-19 ± 4.9E-19	4.12E-18 ± 1.12E-19	3%	12.1610	60.26 ± 353
3.3	4.87E-16 ± 3.11E-18	2.07E-17 ± 4.11E-19	3.4E-19 ± 6.4E-20	-1.1E-18 ± 3.8E-19	1.29E-18 ± 8.56E-20	22%	5.1477	25.75 ± 6.83
3.6	3.89E-16 ± 3.20E-18	7.82E-17 ± 5.83E-19	8.3E-20 ± 1.7E-20	-1.1E-18 ± 4.1E-19	-1.58E-20 ± -1.34E-19	101%	5.0290	25.16 ± 2.55
4.0	1.97E-15 ± 3.75E-18	2.14E-16 ± 1.15E-18	1.2E-18 ± 4.4E-20	-7.7E-19 ± 4.0E-19	3.50E-18 ± 1.88E-19	47%	4.3608	21.84 ± 1.33
4.3	3.18E-15 ± 3.14E-18	4.33E-16 ± 1.06E-18	2.2E-18 ± 9.7E-20	1.5E-18 ± 5.1E-19	5.92E-18 ± 1.11E-19	45%	3.3074	16.59 ± 0.40
4.5	2.01E-14 ± 1.95E-17	5.78E-15 ± 9.83E-18	1.2E-17 ± 9.6E-20	3.1E-19 ± 4.6E-19	3.61E-18 ± 1.05E-19	95%	3.2837	16.47 ± 0.04
4.8	2.02E-14 ± 9.99E-18	6.12E-15 ± 6.81E-18	1.4E-17 ± 1.4E-19	1.2E-19 ± 5.4E-19	5.73E-20 ± 1.39E-19	100%	3.3043	16.57 ± 0.04
5.0	3.72E-15 ± 2.63E-18	1.11E-15 ± 2.80E-18	2.9E-18 ± 4.7E-20	-1.6E-19 ± 4.8E-19	-5.66E-20 ± -8.24E-20	100%	3.3622	16.86 ± 0.12
5.3	1.50E-15 ± 4.72E-18	4.46E-16 ± 1.03E-18	2.2E-18 ± 1.4E-19	-6.7E-20 ± 5.2E-19	-1.94E-19 ± -1.33E-19	104%	3.4894	17.50 ± 0.45
5.5	9.26E-16 ± 3.80E-18	2.80E-16 ± 2.01E-18	3.2E-19 ± 2.4E-20	1.6E-19 ± 5.2E-19	-4.29E-19 ± -1.28E-19	114%	3.7588	18.84 ± 0.69
5.8	7.19E-16 ± 3.91E-18	2.15E-16 ± 1.13E-18	2.9E-19 ± 2.7E-20	-3.9E-19 ± 4.7E-19	6.04E-20 ± 8.10E-20	98%	3.2603	16.35 ± 0.57
6.0	5.12E-16 ± 3.08E-18	1.54E-16 ± 8.13E-19	3.0E-19 ± 3.6E-20	-2.5E-19 ± 3.9E-19	8.50E-20 ± 8.41E-20	95%	3.1658	15.88 ± 0.82
6.5	8.34E-16 ± 2.86E-18	2.47E-16 ± 1.42E-18	4.8E-19 ± 4.8E-20	-5.5E-19 ± 5.2E-19	6.75E-21 ± 8.31E-20	100%	3.3682	16.89 ± 0.51
7.0	8.71E-16 ± 4.67E-18	2.57E-16 ± 1.06E-18	-1.7E-19 ± -1.8E-20	-2.9E-19 ± 2.6E-19	-6.10E-20 ± -8.05E-20	102%	3.4496	17.30 ± 0.48
8.0	8.60E-16 ± 2.72E-18	2.53E-16 ± 1.25E-18	6.2E-19 ± 3.9E-20	-2.7E-19 ± 3.7E-19	-2.94E-19 ± -1.02E-19	110%	3.7359	18.73 ± 0.60
9.0	2.62E-16 ± 2.41E-18	7.60E-17 ± 6.55E-19	2.0E-19 ± 3.7E-20	-3.0E-19 ± 3.8E-19	5.95E-20 ± 8.46E-20	93%	3.2063	16.08 ± 1.66

Irradiation filename: au5.1h.adl.ih5

%P	40Ar(*±atm)	39Ar(K)	38Ar(Cl±atm)	37Ar(Ca)	36Ar(Atm)	%Rad	R	Age (Ma)
3.0	1.17E-15 ± 5.06E-18	3.26E-18 ± 2.13E-19	1.1E-18 ± 1.6E-19	-4.1E-20 ± 4.0E-19	3.69E-18 ± 1.08E-19	7%	24.6500	120.12 ± 163
3.3	7.90E-16 ± 3.56E-18	5.45E-17 ± 6.40E-19	8.6E-19 ± 1.3E-19	-1.9E-20 ± 4.3E-19	2.09E-18 ± 9.81E-20	22%	3.1822	15.96 ± 2.90
3.6	2.72E-16 ± 3.46E-18	5.22E-17 ± 5.08E-19	5.5E-19 ± 9.9E-20	-6.6E-19 ± 4.0E-19	3.23E-19 ± 7.71E-20	65%	3.3737	16.92 ± 2.23
4.0	5.44E-17 ± 3.00E-18	1.53E-17 ± 3.56E-19	9.2E-19 ± 2.3E-19	6.5E-19 ± 7.1E-19	7.68E-22 ± 6.47E-20	100%	3.5449	17.77 ± 6.36
4.3	5.96E-16 ± 3.01E-18	1.11E-16 ± 1.17E-18	7.7E-19 ± 8.6E-20	3.6E-19 ± 3.6E-19	7.48E-19 ± 8.56E-20	63%	3.3899	17.00 ± 1.20
4.5	1.60E-16 ± 2.79E-18	4.43E-17 ± 5.87E-19	3.4E-19 ± 8.0E-20	4.4E-20 ± 3.3E-19	-1.09E-19 ± -1.24E-19	120%	4.3303	21.69 ± 4.16
4.8	5.79E-16 ± 3.63E-18	1.50E-16 ± 6.80E-19	1.4E-19 ± 2.1E-20	-8.3E-19 ± 4.2E-19	-2.57E-20 ± -1.27E-19	101%	3.9086	19.59 ± 1.27
5.0	1.12E-14 ± 1.13E-17	3.17E-15 ± 4.85E-18	8.2E-18 ± 8.8E-20	-3.1E-19 ± 4.2E-19	2.23E-18 ± 2.01E-19	94%	3.3241	16.67 ± 0.10
5.3	1.44E-14 ± 2.14E-17	4.30E-15 ± 8.94E-18	1.1E-17 ± 7.1E-20	-5.7E-19 ± 4.0E-19	9.13E-19 ± 8.72E-20	98%	3.2771	16.44 ± 0.05
5.5	7.34E-15 ± 6.24E-18	2.20E-15 ± 4.53E-18	6.8E-18 ± 2.1E-19	-2.7E-20 ± 4.2E-19	1.18E-20 ± 1.33E-19	100%	3.3338	16.72 ± 0.10
5.8	1.67E-15 ± 4.45E-18	4.96E-16 ± 1.83E-18	1.8E-18 ± 1.2E-19	-4.0E-19 ± 3.6E-19	2.61E-19 ± 8.58E-20	95%	3.2087	16.10 ± 0.27
6.0	2.36E-15 ± 3.54E-18	7.08E-16 ± 2.51E-18	1.1E-18 ± 5.3E-20	-6.7E-19 ± 3.4E-19	1.87E-19 ± 8.74E-20	98%	3.2571	16.34 ± 0.19
6.5	2.13E-16 ± 2.32E-18	6.26E-17 ± 4.90E-19	3.7E-19 ± 7.8E-20	6.9E-19 ± 3.9E-19	2.44E-19 ± 1.33E-19	66%	2.2546	11.33 ± 3.16
7.0	1.45E-17 ± 1.81E-18	3.81E-18 ± 2.93E-19	1.4E-19 ± 1.6E-19	2.1E-19 ± 3.5E-19	3.56E-19 ± 1.32E-19	-623%	-23.7740	-123.96 ± -54
8.0	1.55E-17 ± 1.46E-18	2.93E-18 ± 2.82E-19	1.7E-19 ± 1.7E-19	2.6E-19 ± 3.4E-19	-1.23E-19 ± -1.69E-19	334%	17.7467	87.28 ± 83
9.0	7.61E-18 ± 1.68E-18	1.08E-18 ± 3.78E-19	5.8E-20 ± 1.9E-19	2.6E-19 ± 3.5E-19	3.17E-19 ± 1.35E-19	-1131%	-79.9909	-456.17 ± -274
10.0	5.54E-18 ± 2.32E-18	2.07E-19 ± 3.26E-19	8.8E-20 ± 1.8E-19	9.6E-19 ± 3.5E-19	-1.28E-19 ± -1.68E-19	780%	209.5503	831.25 ± 1487

Oro Fino deposit step heating increments for 5 single adularia crystals (14-20, 1.2-0.75 mm) of sample: OF-1
Irradiation filename:au8.adl.31

%P	40Ar(*±atm)	39Ar(K)	38Ar(Cl±atm)	37Ar(Ca)	36Ar(Atm)	%Rad	R	Age (Ma)
6.0	1.43E-14 ± 4.23E-17	8.16E-16 ± 2.96E-18	8.8E-18 ± 1.4E-19	-4.9E-19 ± 8.2E-19	3.47E-17 ± 4.91E-19	28%	4.9117	17.17 ± 0.70
6.5	8.58E-15 ± 1.85E-17	1.76E-15 ± 3.81E-18	5.0E-18 ± 1.0E-19	1.0E-19 ± 8.5E-19	1.45E-18 ± 7.08E-20	95%	4.6209	16.16 ± 0.07
7.0	6.97E-15 ± 6.66E-18	1.41E-15 ± 5.14E-18	4.1E-18 ± 6.7E-20	6.0E-20 ± 7.5E-19	1.01E-18 ± 1.19E-19	96%	4.7254	16.52 ± 0.11
7.5	2.73E-15 ± 3.27E-18	5.38E-16 ± 1.33E-18	1.9E-18 ± 5.2E-20	1.4E-18 ± 1.0E-18	5.91E-19 ± 8.24E-20	94%	4.7521	16.61 ± 0.17
8.0	4.47E-15 ± 4.10E-18	7.27E-16 ± 2.75E-18	2.6E-18 ± 6.3E-20	-4.6E-19 ± 7.8E-19	3.61E-18 ± 9.50E-20	76%	4.6754	16.35 ± 0.16
8.5	2.25E-15 ± 6.62E-18	3.86E-16 ± 1.71E-18	1.3E-18 ± 4.6E-20	-7.2E-19 ± 9.6E-19	1.53E-18 ± 8.22E-20	80%	4.6679	16.32 ± 0.25
9.0	3.04E-15 ± 4.77E-18	5.40E-16 ± 3.33E-18	1.4E-18 ± 3.3E-20	-5.8E-19 ± 1.1E-18	1.70E-18 ± 8.42E-20	83%	4.6990	16.43 ± 0.21
9.3	5.32E-15 ± 7.19E-18	1.01E-15 ± 2.09E-18	2.9E-18 ± 5.3E-20	-2.1E-19 ± 9.6E-19	2.04E-18 ± 9.68E-20	89%	4.6827	16.37 ± 0.11
9.5	4.35E-15 ± 8.66E-18	8.81E-16 ± 1.79E-18	2.1E-18 ± 4.0E-20	-3.2E-19 ± 1.1E-18	8.00E-19 ± 7.69E-20	95%	4.6648	16.31 ± 0.10
9.8	4.85E-15 ± 1.11E-17	9.89E-16 ± 3.58E-18	2.1E-18 ± 5.1E-20	-9.1E-19 ± 9.8E-19	7.29E-19 ± 6.69E-20	96%	4.6841	16.38 ± 0.10
10.0	2.97E-15 ± 3.40E-18	6.21E-16 ± 2.45E-18	1.6E-18 ± 4.2E-20	-1.9E-18 ± 7.1E-19	2.38E-19 ± 5.95E-20	98%	4.6756	16.35 ± 0.12
10.3	9.17E-15 ± 9.00E-18	1.90E-15 ± 4.32E-18	4.6E-18 ± 8.2E-20	-9.5E-19 ± 7.2E-19	1.03E-18 ± 5.98E-20	97%	4.6697	16.33 ± 0.05
10.5	3.70E-15 ± 2.71E-18	7.78E-16 ± 1.80E-18	1.7E-18 ± 2.7E-20	-8.5E-19 ± 7.0E-19	2.37E-19 ± 6.24E-20	98%	4.6607	16.29 ± 0.09
11.0	1.09E-15 ± 3.04E-18	2.31E-16 ± 1.12E-18	2.3E-19 ± 1.5E-20	-8.5E-19 ± 7.5E-19	1.41E-19 ± 6.40E-20	96%	4.5295	15.84 ± 0.30
11.5	5.76E-16 ± 2.94E-18	1.20E-16 ± 6.27E-19	3.5E-19 ± 3.6E-20	-1.2E-18 ± 7.9E-19	-1.12E-19 ± -1.01E-19	106%	5.0730	17.73 ± 0.88
12.5	2.39E-16 ± 2.62E-18	4.94E-17 ± 4.52E-19	1.3E-19 ± 3.8E-20	1.8E-19 ± 6.7E-19	-1.29E-20 ± -6.99E-20	102%	4.9217	17.20 ± 1.48
13.5	1.85E-16 ± 2.64E-18	3.76E-17 ± 3.87E-19	6.5E-20 ± 2.3E-20	2.5E-19 ± 3.7E-19	-1.82E-19 ± -1.08E-19	129%	6.3528	22.17 ± 2.97

Irradiation filename:au8.adl.32

%P	40Ar(*±atm)	39Ar(K)	38Ar(Cl±atm)	37Ar(Ca)	36Ar(Atm)	%Rad	R	Age (Ma)
5.0	2.57E-14 ± 1.39E-17	5.54E-17 ± 8.61E-19	1.7E-17 ± 2.9E-19	5.1E-19 ± 5.5E-19	8.50E-17 ± 3.52E-19	2%	10.8934	37.86 ± 35
6.0	8.06E-15 ± 9.79E-18	6.86E-16 ± 2.12E-18	4.6E-18 ± 1.3E-19	2.7E-18 ± 8.3E-19	1.57E-17 ± 1.20E-19	42%	4.9821	17.41 ± 0.24
6.3	3.19E-15 ± 3.13E-18	6.27E-16 ± 1.80E-18	1.7E-18 ± 3.3E-20	1.0E-19 ± 4.0E-19	8.43E-19 ± 7.59E-20	92%	4.6891	16.39 ± 0.14
6.7	6.30E-15 ± 7.11E-18	1.15E-15 ± 3.92E-18	3.2E-18 ± 7.5E-20	-6.8E-20 ± 5.6E-19	3.45E-18 ± 1.60E-19	84%	4.5819	16.02 ± 0.16
7.0	6.26E-15 ± 5.09E-18	1.30E-15 ± 3.41E-18	3.4E-18 ± 5.2E-20	8.3E-20 ± 4.7E-19	8.59E-19 ± 7.17E-20	96%	4.6184	16.15 ± 0.07
7.5	1.92E-14 ± 2.16E-17	2.85E-15 ± 6.81E-18	1.1E-17 ± 9.7E-20	1.5E-18 ± 5.7E-19	2.03E-17 ± 1.59E-19	69%	4.6478	16.25 ± 0.09
8.0	7.55E-15 ± 1.40E-17	1.35E-15 ± 3.78E-18	3.5E-18 ± 6.4E-20	1.2E-18 ± 6.6E-19	4.54E-18 ± 9.00E-20	82%	4.6099	16.12 ± 0.10
8.5	1.07E-14 ± 1.29E-17	1.77E-15 ± 7.71E-18	5.2E-18 ± 8.0E-20	-7.9E-19 ± 7.9E-19	8.31E-18 ± 1.12E-19	77%	4.6515	16.26 ± 0.12
9.0	1.01E-14 ± 1.35E-17	1.86E-15 ± 4.43E-18	5.3E-18 ± 4.5E-20	-6.1E-19 ± 7.1E-19	4.75E-18 ± 1.04E-19	86%	4.6770	16.35 ± 0.08
9.3	8.16E-15 ± 9.36E-18	1.53E-15 ± 3.92E-18	4.2E-18 ± 9.0E-20	-1.2E-18 ± 8.3E-19	3.25E-18 ± 8.58E-20	88%	4.6910	16.40 ± 0.08
9.5	4.26E-15 ± 2.68E-18	8.13E-16 ± 1.85E-18	2.0E-18 ± 5.5E-20	-1.1E-18 ± 8.8E-19	1.54E-18 ± 8.50E-20	89%	4.6721	16.33 ± 0.12
9.7	3.97E-15 ± 3.74E-18	7.55E-16 ± 3.52E-18	2.3E-18 ± 5.2E-20	-1.5E-18 ± 6.6E-19	1.57E-18 ± 9.19E-20	88%	4.6360	16.21 ± 0.15
10.0	6.18E-15 ± 9.83E-18	1.20E-15 ± 2.07E-18	3.1E-18 ± 6.9E-20	-5.6E-19 ± 9.1E-19	1.95E-18 ± 7.29E-20	91%	4.6829	16.37 ± 0.08
10.2	1.00E-14 ± 1.00E-17	1.98E-15 ± 5.30E-18	5.2E-18 ± 6.1E-20	-1.2E-18 ± 7.9E-19	2.63E-18 ± 6.62E-20	92%	4.6640	16.31 ± 0.06
10.5	9.67E-15 ± 4.95E-18	1.79E-15 ± 3.14E-18	4.9E-18 ± 6.0E-20	-1.2E-18 ± 7.1E-19	4.20E-18 ± 1.07E-19	87%	4.6966	16.42 ± 0.07
11.0	3.89E-15 ± 3.90E-18	7.94E-16 ± 2.10E-18	1.9E-18 ± 4.5E-20	1.0E-18 ± 9.0E-19	6.95E-19 ± 8.21E-20	95%	4.6360	16.21 ± 0.12
11.5	1.31E-15 ± 4.21E-18	2.74E-16 ± 1.03E-18	9.8E-19 ± 4.7E-20	-8.0E-19 ± 7.1E-19	1.81E-19 ± 6.86E-20	96%	4.5959	16.07 ± 0.27
12.5	1.25E-15 ± 3.06E-18	2.48E-16 ± 1.19E-18	7.1E-19 ± 3.7E-20	-4.2E-19 ± 1.1E-18	2.49E-19 ± 8.68E-20	94%	4.7585	16.63 ± 0.37
13.5	1.18E-16 ± 2.43E-18	2.41E-17 ± 5.46E-19	5.6E-20 ± 3.7E-20	3.1E-19 ± 1.1E-18	7.51E-20 ± 7.60E-20	81%	3.9678	13.88 ± 3.31
15.0	6.00E-17 ± 2.65E-18	1.25E-17 ± 5.47E-19	3.9E-19 ± 1.4E-19	-5.9E-19 ± 1.0E-18	-2.28E-19 ± -1.15E-19	212%	10.2384	35.60 ± 9.56
17.0	2.25E-17 ± 2.32E-18	5.45E-18 ± 5.51E-19	-1.5E-19 ± -3.4E-19	2.0E-18 ± 8.5E-19	-2.25E-19 ± -1.15E-19	395%	16.3227	56.43 ± 22

Irradiation filename:au8.adl.33

%P	40Ar(*±atm)	39Ar(K)	38Ar(Cl±atm)	37Ar(Ca)	36Ar(Atm)	%Rad	R	Age (Ma)
5.0	1.77E-14 ± 1.73E-17	4.94E-16 ± 6.43E-19	1.1E-17 ± 2.0E-19	-2.6E-19 ± 6.8E-19	5.08E-17 ± 3.28E-19	15%	5.4937	19.19 ± 0.73
6.0	7.37E-15 ± 2.13E-17	1.51E-15 ± 5.95E-18	3.7E-18 ± 9.2E-20	3.3E-19 ± 6.8E-19	1.43E-18 ± 7.66E-20	94%	4.6136	16.13 ± 0.10
6.3	4.98E-15 ± 1.11E-17	9.36E-16 ± 1.22E-18	2.4E-18 ± 7.3E-20	4.7E-20 ± 4.6E-19	2.11E-18 ± 9.85E-20	87%	4.6494	16.25 ± 0.12
6.7	7.54E-15 ± 4.90E-18	1.37E-15 ± 3.17E-18	4.2E-18 ± 6.7E-20	2.5E-18 ± 1.0E-18	4.04E-18 ± 8.53E-20	84%	4.6385	16.22 ± 0.08
7.0	5.04E-15 ± 4.05E-18	8.90E-16 ± 2.66E-18	2.7E-18 ± 7.1E-20	2.4E-18 ± 9.9E-19	3.17E-18 ± 7.14E-20	81%	4.6094	16.12 ± 0.10
7.5	2.04E-14 ± 1.80E-17	3.51E-15 ± 1.11E-17	1.1E-17 ± 8.9E-20	5.5E-18 ± 1.5E-18	1.41E-17 ± 1.40E-19	80%	4.6347	16.20 ± 0.08
8.0	2.68E-15 ± 4.32E-18	4.56E-16 ± 1.32E-18	1.3E-18 ± 4.2E-20	3.3E-18 ± 1.0E-18	1.88E-18 ± 7.77E-20	79%	4.6644	16.31 ± 0.19
8.5	1.35E-14 ± 7.00E-18	2.29E-15 ± 3.35E-18	7.7E-18 ± 1.2E-19	6.9E-19 ± 6.7E-19	9.53E-18 ± 1.48E-19	79%	4.6565	16.28 ± 0.07
9.0	4.23E-15 ± 1.57E-17	7.27E-16 ± 2.09E-18	2.3E-18 ± 6.7E-20	5.3E-19 ± 5.7E-19	2.91E-18 ± 1.20E-19	80%	4.6356	16.21 ± 0.20
9.3	1.79E-15 ± 3.18E-18	3.22E-16 ± 8.50E-19	8.7E-19 ± 3.8E-20	-3.9E-19 ± 7.9E-19	1.23E-18 ± 1.18E-19	80%	4.4158	15.44 ± 0.38
9.5	1.68E-15 ± 3.90E-18	3.03E-16 ± 1.38E-18	6.5E-19 ± 3.4E-20	5.6E-19 ± 7.8E-19	1.23E-18 ± 1.10E-19	78%	4.3458	15.20 ± 0.39
9.7	5.42E-16 ± 4.09E-18	9.67E-17 ± 5.69E-19	2.0E-19 ± 2.7E-20	4.3E-19 ± 6.2E-19	6.48E-19 ± 1.07E-19	65%	3.6213	12.67 ± 1.16
10.0	1.28E-16 ± 1.62E-18	2.00E-17 ± 4.43E-19	-1.7E-19 ± -1.4E-18	6.7E-19 ± 8.3E-19	3.02E-19 ± 9.60E-20	30%	1.9513	6.84 ± 5.03

Irradiation filename:au8.adl.34

%P	40Ar(*±atm)	39Ar(K)	38Ar(Cl±atm)	37Ar(Ca)	36Ar(Atm)	%Rad	R	Age (Ma)
5.0	1.46E-14 ± 9.17E-18	3.53E-16 ± 7.64E-19	9.3E-18 ± 1.4E-19	-6.5E-19 ± 8.2E-19	4.23E-17 ± 2.40E-19	14%	5.8679	20.49 ± 0.82
6.0	4.03E-15 ± 3.63E-18	6.91E-16 ± 2.67E-18	2.5E-18 ± 6.8E-20	5.0E-19 ± 7.2E-19	2.74E-18 ± 8.27E-20	80%	4.6647	16.31 ± 0.15
6.3	2.24E-15 ± 5.19E-18	4.53E-16 ± 1.26E-18	1.3E-18 ± 6.6E-20	4.3E-19 ± 8.2E-19	5.44E-19 ± 8.11E-20	93%	4.5904	16.05 ± 0.20
6.7	3.73E-15 ± 3.65E-18	7.93E-16 ± 2.13E-18	8.0E-19 ± 2.8E-20	2.6E-19 ± 7.0E-19	4.41E-19 ± 8.24E-20	97%	4.5323	15.85 ± 0.12
7.0	2.64E-15 ± 4.70E-18	5.40E-16 ± 8.78E-19	9.1E-19 ± 4.4E-20	1.2E-18 ± 9.9E-19	4.63E-19 ± 8.13E-20	95%	4.6294	16.19 ± 0.16
7.5	7.93E-15 ± 1.04E-17	1.55E-15 ± 3.94E-18	2.6E-18 ± 8.3E-20	1.2E-18 ± 1.1E-18	2.70E-18 ± 1.03E-19	90%	4.6074	16.11 ± 0.09
8.0	1.51E-14 ± 1.87E-17	2.55E-15 ± 4.16E-18	8.1E-18 ± 9.5E-20	3.7E-18 ± 1.1E-18	1.16E-17 ± 1.26E-19	77%	4.5747	15.99 ± 0.07
8.5	2.17E-15 ± 6.89E-18	2.58E-16 ± 1.28E-18	1.1E-18 ± 7.7E-20	1.5E-19 ± 1.1E-18	3.28E-18 ± 1.37E-19	55%	4.6727	16.34 ± 0.58
9.0	6.22E-15 ± 1.05E-17	8.65E-16 ± 3.17E-18	3.1E-18 ± 4.8E-20	-3.7E-19 ± 8.3E-19	7.49E-18 ± 1.48E-19	64%	4.6298	16.19 ± 0.21
9.3	3.31E-15 ± 2.98E-18	4.90E-16 ± 1.33E-18	1.3E-18 ± 3.8E-20	8.8E-19 ± 7.7E-19	3.56E-18 ± 1.37E-19	68%	4.6128	16.13 ± 0.30
9.5	1.82E-15 ± 5.82E-18	2.66E-16 ± 7.82E-19	9.4E-19 ± 5.9E-20	6.5E-20 ± 7.1E-19	2.17E-18 ± 1.28E-19	65%	4.4091	15.42 ± 0.51
9.7	5.65E-16 ± 3.64E-18	7.83E-17 ± 6.80E-19	1.4E-19 ± 3.0E-20	5.0E-19 ± 8.1E-19	7.87E-19 ± 1.28E-19	59%	4.2381	14.82 ± 1.71
10.0	2.31E-15 ± 7.42E-18	3.55E-16 ± 6.94E-19	1.1E-18 ± 4.0E-20	5.3E-19 ± 7.4E-19	1.99E-18 ± 1.53E-19	75%	4.8465	16.94 ± 0.45
10.2	2.54E-15 ± 6.05E-18	3.54E-16 ± 1.30E-18	1.5E-18 ± 5.3E-20	-5.3E-20 ± 5.3E-19	3.04E-18 ± 7.14E-20	65%	4.6401	16.22 ± 0.24
10.5	8.60E-16 ± 3.22E-18	1.31E-16 ± 8.32E-19	2.3E-19 ± 3.2E-20	8.8E-20 ± 6.9E-19	8.17E-19 ± 7.18E-20	72%	4.7411	16.57 ± 0.59
11.0	2.63E-15 ± 2.94E-18	4.27E-16 ± 1.19E-18	1.1E-18 ± 3.8E-20	3.5E-19 ± 8.6E-19	2.19E-18 ± 8.31E-20	75%	4.6427	16.23 ± 0.21
11.5	5.29E-15 ± 3.95E-18	8.83E-16 ± 2.99E-18	2.9E-18 ± 3.3E-20	-2.2E-18 ± 1.1E-18	3.79E-18 ± 1.07E-19	79%	4.7121	16.47 ± 0.15
12.5	3.87E-15 ± 3.50E-18	6.49E-16 ± 2.29E-18	1.9E-18 ± 5.6E-20	1.7E-19 ± 6.8E-19	2.97E-18 ± 1.60E-19	77%	4.6095	16.12 ± 0.27
13.5	3.03E-15 ± 2.12E-18	5.20E-16 ± 1.54E-18	9.6E-19 ± 3.1E-20	-1.8E-20 ± 6.9E-19	2.25E-18 ± 1.16E-19	78%	4.5401	15.87 ± 0.24
15.0	5.25E-16 ± 1.95E-18	7.99E-17 ± 6.37E-19	1.6E-19 ± 2.4E-20	1.6E-19 ± 6.3E-19	7.48E-19 ± 1.13E-19	58%	3.8094	13.33 ± 1.48
17.0	4.25E-17 ± 1.86E-18	7.01E-18 ± 3.90E-19	-2.2E-19 ± -2.3E-19	-4.6E-19 ± 8.2E-19	2.28E-19 ± 1.38E-19	-59%	-3.5524	-12.52 ± -20

Irradiation filename:au8.adl.35

%P	40Ar(*±atm)	39Ar(K)	38Ar(Cl±atm)	37Ar(Ca)	36Ar(Atm)	%Rad	R	Age (Ma)
5.0	2.10E-14 ± 3.78E-17	1.34E-15 ± 1.76E-18	1.5E-17 ± 2.4E-19	1.8E-19 ± 6.4E-19	5.06E-17 ± 5.02E-19	29%	4.5522	15.92 ± 0.41
6.0	1.26E-14 ± 1.70E-17	2.50E-15 ± 6.53E-18	7.5E-18 ± 7.3E-20	1.4E-19 ± 6.3E-19	3.68E-18 ± 8.69E-20	91%	4.5951	16.07 ± 0.06
6.3	2.32E-15 ± 6.93E-18	3.84E-16 ± 9.54E-19	1.9E-18 ± 7.4E-20	-2.5E-19 ± 6.7E-19	1.86E-18 ± 8.40E-20	76%	4.6159	16.14 ± 0.24
6.7	5.93E-15 ± 2.86E-18	9.62E-16 ± 2.26E-18	3.0E-18 ± 3.3E-20	2.2E-18 ± 1.3E-18	5.11E-18 ± 1.45E-19	75%	4.5915	16.05 ± 0.16
7.0	5.87E-15 ± 7.25E-18	1.13E-15 ± 3.27E-18	2.4E-18 ± 4.1E-20	-9.2E-19 ± 8.3E-19	2.38E-18 ± 1.40E-19	88%	4.5865	16.04 ± 0.14
7.5	7.85E-15 ± 9.05E-18	1.49E-15 ± 1.64E-18	4.1E-18 ± 5.4E-20	-1.3E-18 ± 7.7E-19	3.42E-18 ± 1.39E-19	87%	4.5853	16.03 ± 0.10
8.0	4.02E-15 ± 2.62E-18	7.78E-16 ± 2.18E-18	2.0E-18 ± 4.7E-20	1.4E-18 ± 7.2E-19	1.43E-18 ± 8.79E-20	89%	4.6167	16.14 ± 0.13
8.5	2.81E-15 ± 7.74E-18	5.72E-16 ± 3.17E-18	1.5E-18 ± 5.3E-20	1.3E-18 ± 8.0E-19	6.01E-19 ± 6.48E-20	94%	4.5999	16.08 ± 0.16
9.0	2.34E-15 ± 3.54E-18	4.45E-16 ± 1.40E-18	1.1E-18 ± 5.1E-20	9.9E-19 ± 7.6E-19	8.58E-19 ± 8.59E-20	89%	4.7009	16.43 ± 0.21
9.3	8.79E-16 ± 2.13E-18	1.79E-16 ± 1.08E-18	5.2E-19 ± 4.2E-20	3.6E-18 ± 1.4E-18	1.50E-19 ± 7.34E-20	95%	4.6617	16.30 ± 0.44
9.5	3.60E-16 ± 3.07E-18	7.07E-17 ± 6.31E-19	3.0E-19 ± 4.4E-20	8.7E-19 ± 7.6E-19	1.31E-19 ± 6.51E-20	89%	4.5417	15.88 ± 0.98
9.7	7.71E-17 ± 2.53E-18	1.54E-17 ± 2.76E-19	2.9E-19 ± 1.1E-19	1.0E-18 ± 7.5E-19	-1.05E-19 ± -1.09E-19	140%	7.0162	24.47 ± 7.32

War Eagle Mountain site 3 deposit step heating increments for 5 single crystals (14-20 mesh size, 1.2-0.75 mm) of sample: WEMS3-1
Irradiation filename: au8.2c.adl.41.

%P	40Ar(*±atm)	39Ar(K)	38Ar(Cl±atm)	37Ar(Ca)	36Ar(Atm)	%Rad	R	Age (Ma)
6.00	7.53E-15 ± 9.52E-18	5.40E-17 ± 9.45E-19	4.6E-18 ± 1.7E-19	-1.1E-18 ± 1.2E-18	2.45E-17 ± 2.13E-19	4%	5.5793	19.49 ± 12
6.50	2.87E-15 ± 5.27E-18	4.44E-16 ± 9.84E-19	8.8E-19 ± 3.3E-20	-1.7E-18 ± 7.3E-19	3.06E-18 ± 1.06E-19	68%	4.4193	15.45 ± 0.26
7.00	2.26E-16 ± 2.17E-18	4.14E-17 ± 4.35E-19	9.2E-20 ± 2.7E-20	-3.0E-18 ± 1.5E-18	1.71E-19 ± 8.30E-20	78%	4.2256	14.78 ± 2.09
7.50	1.42E-15 ± 2.44E-18	3.09E-16 ± 1.58E-18	8.2E-19 ± 3.5E-20	-5.3E-20 ± 6.5E-19	1.51E-19 ± 6.23E-20	97%	4.4426	15.53 ± 0.23
8.00	1.31E-15 ± 6.16E-18	2.87E-16 ± 1.93E-18	8.1E-19 ± 5.1E-20	-2.4E-19 ± 7.7E-19	3.24E-19 ± 6.65E-20	93%	4.2443	14.84 ± 0.27
8.50	1.87E-14 ± 1.24E-17	3.29E-15 ± 5.47E-18	1.0E-17 ± 6.4E-20	7.4E-19 ± 8.3E-19	1.38E-17 ± 1.57E-19	78%	4.4271	15.48 ± 0.06
9.00	1.49E-14 ± 2.33E-17	2.50E-15 ± 4.89E-18	8.1E-18 ± 7.6E-20	-1.0E-19 ± 7.8E-19	1.24E-17 ± 1.17E-19	75%	4.4789	15.66 ± 0.07
9.25	3.24E-15 ± 2.31E-18	5.81E-16 ± 1.68E-18	1.6E-18 ± 7.2E-20	-6.5E-19 ± 6.7E-19	2.39E-18 ± 1.21E-19	78%	4.3512	15.22 ± 0.22
9.50	6.15E-15 ± 9.56E-18	1.15E-15 ± 2.71E-18	2.8E-18 ± 4.6E-20	-4.1E-19 ± 7.2E-19	3.47E-18 ± 1.29E-19	83%	4.4664	15.62 ± 0.13
9.75	4.65E-15 ± 4.07E-18	9.14E-16 ± 2.71E-18	2.5E-18 ± 5.6E-20	-1.6E-18 ± 9.8E-19	1.89E-18 ± 1.65E-19	88%	4.4782	15.66 ± 0.19
10.00	2.69E-15 ± 4.19E-18	5.32E-16 ± 1.11E-18	1.0E-18 ± 4.0E-20	-8.2E-19 ± 5.4E-19	1.11E-18 ± 1.72E-19	88%	4.4315	15.50 ± 0.34
10.25	1.23E-15 ± 6.14E-18	2.48E-16 ± 8.71E-19	3.0E-20 ± 2.8E-21	-3.3E-19 ± 6.8E-19	3.48E-19 ± 9.18E-20	92%	4.5200	15.80 ± 0.40
10.50	5.95E-15 ± 8.19E-18	1.10E-15 ± 5.48E-18	3.3E-18 ± 5.8E-20	6.6E-19 ± 9.6E-19	3.59E-18 ± 9.73E-20	82%	4.4411	15.53 ± 0.13
11.00	3.58E-15 ± 6.87E-18	6.66E-16 ± 2.79E-18	1.9E-18 ± 5.7E-20	4.2E-19 ± 8.3E-19	1.98E-18 ± 8.80E-20	84%	4.4853	15.68 ± 0.16
11.50	5.06E-16 ± 2.67E-18	9.35E-17 ± 5.36E-19	2.8E-19 ± 4.3E-20	-1.7E-19 ± 7.0E-19	3.00E-19 ± 7.51E-20	83%	4.4666	15.62 ± 0.84
12.50	1.56E-16 ± 1.83E-18	2.97E-17 ± 4.58E-19	3.4E-19 ± 1.2E-19	-1.8E-18 ± 1.2E-18	-2.29E-19 ± -1.24E-19	143%	7.5409	26.29 ± 4.32
13.50	3.57E-17 ± 1.30E-18	5.77E-18 ± 6.80E-19	2.9E-19 ± 1.2E-19	-6.5E-20 ± 7.4E-19	2.32E-20 ± 7.66E-20	81%	4.9959	17.46 ± 13
15.00	1.65E-16 ± 2.92E-18	3.14E-17 ± 3.68E-19	1.2E-19 ± 3.9E-20	3.4E-19 ± 6.6E-19	7.83E-20 ± 1.84E-19	86%	4.5313	15.84 ± 6.08
17.00	1.55E-16 ± 1.46E-18	1.73E-17 ± 2.56E-19	1.3E-19 ± 7.1E-20	-1.5E-18 ± 5.8E-19	4.14E-19 ± 1.95E-19	21%	1.8704	6.56 ± 11
20.00	5.35E-17 ± 1.46E-18	7.70E-18 ± 1.97E-19	2.2E-20 ± 3.5E-20	1.6E-18 ± 6.9E-19	4.40E-19 ± 1.77E-19	-143%	-9.9315	-35.22 ± -24
24.00	1.04E-16 ± 2.23E-18	1.23E-17 ± 3.87E-19	2.4E-19 ± 1.2E-19	1.1E-18 ± 4.8E-19	2.82E-19 ± 1.97E-19	20%	1.7384	6.09 ± 16

Irradiation filename: au8.2c.adl.42.

%P	40Ar(*±atm)	39Ar(K)	38Ar(Cl±atm)	37Ar(Ca)	36Ar(Atm)	%Rad	R	Age (Ma)
6.00	2.69E-15 ± 3.66E-18	9.49E-17 ± 4.85E-19	1.3E-18 ± 1.3E-19	-7.1E-19 ± 8.1E-19	7.85E-18 ± 1.61E-19	14%	3.8536	13.48 ± 1.89
6.50	7.77E-15 ± 6.86E-18	1.56E-15 ± 3.15E-18	3.7E-18 ± 4.4E-20	2.6E-18 ± 1.2E-18	2.62E-18 ± 1.46E-19	90%	4.4808	15.67 ± 0.10
7.00	5.28E-15 ± 6.07E-18	1.14E-15 ± 3.14E-18	2.8E-18 ± 5.1E-20	-2.2E-19 ± 6.4E-19	8.52E-19 ± 1.41E-19	95%	4.4157	15.44 ± 0.14
7.50	3.83E-15 ± 2.50E-18	8.06E-16 ± 1.89E-18	2.4E-18 ± 5.6E-20	6.8E-20 ± 4.6E-19	9.33E-19 ± 1.31E-19	93%	4.4098	15.42 ± 0.17
8.00	4.45E-15 ± 3.86E-18	9.19E-16 ± 1.80E-18	2.5E-18 ± 5.1E-20	5.2E-19 ± 6.2E-19	1.14E-18 ± 1.34E-19	92%	4.4751	15.65 ± 0.16
8.50	1.16E-14 ± 1.11E-17	2.40E-15 ± 3.60E-18	5.7E-18 ± 6.8E-20	9.8E-19 ± 4.9E-19	2.84E-18 ± 1.48E-19	93%	4.4837	15.68 ± 0.07
9.00	1.58E-14 ± 1.81E-17	3.16E-15 ± 4.78E-18	7.5E-18 ± 5.6E-20	1.4E-18 ± 6.7E-19	5.59E-18 ± 1.52E-19	90%	4.4695	15.63 ± 0.06
9.25	7.80E-15 ± 5.74E-18	1.48E-15 ± 5.08E-18	4.2E-18 ± 3.4E-20	-4.2E-20 ± 7.6E-19	3.84E-18 ± 9.26E-20	85%	4.5072	15.76 ± 0.09
9.50	3.50E-15 ± 6.81E-18	6.85E-16 ± 1.61E-18	1.6E-18 ± 2.9E-20	-1.4E-18 ± 7.3E-19	1.44E-18 ± 9.08E-20	88%	4.4860	15.69 ± 0.15
9.75	1.29E-15 ± 4.07E-18	2.33E-16 ± 9.26E-19	6.3E-19 ± 2.9E-20	-2.0E-19 ± 7.9E-19	7.66E-19 ± 8.33E-20	82%	4.5584	15.94 ± 0.38
10.00	2.71E-15 ± 4.94E-18	4.64E-16 ± 1.67E-18	1.3E-18 ± 5.7E-20	4.9E-21 ± 6.9E-19	2.04E-18 ± 9.86E-20	78%	4.5440	15.89 ± 0.23
10.25	4.44E-16 ± 3.28E-18	8.05E-17 ± 7.98E-19	2.3E-19 ± 2.8E-20	-7.1E-20 ± 8.7E-19	2.05E-19 ± 7.54E-20	86%	4.7558	16.62 ± 1.00
10.50	7.99E-16 ± 5.14E-18	1.34E-16 ± 5.33E-19	6.3E-19 ± 6.3E-20	-3.3E-19 ± 7.3E-19	7.75E-19 ± 7.95E-20	71%	4.2638	14.91 ± 0.64
11.00	3.17E-15 ± 4.67E-18	5.01E-16 ± 2.88E-18	1.8E-18 ± 3.9E-20	5.4E-20 ± 8.3E-19	2.97E-18 ± 9.19E-20	72%	4.5651	15.96 ± 0.23
11.50	1.23E-15 ± 4.39E-18	2.24E-16 ± 9.13E-19	6.5E-19 ± 5.4E-20	-1.0E-18 ± 8.1E-19	7.45E-19 ± 8.46E-20	82%	4.4799	15.66 ± 0.40
12.50	2.84E-15 ± 3.18E-18	5.04E-16 ± 5.61E-19	2.0E-18 ± 7.0E-20	1.1E-18 ± 7.5E-19	1.83E-18 ± 9.84E-20	81%	4.5538	15.92 ± 0.20
13.50	3.75E-15 ± 3.87E-18	6.85E-16 ± 1.33E-18	2.5E-18 ± 6.5E-20	1.1E-18 ± 8.8E-19	2.07E-18 ± 1.00E-19	84%	4.5714	15.98 ± 0.16
15.00	1.58E-15 ± 4.74E-18	3.03E-16 ± 1.39E-18	1.0E-18 ± 4.9E-20	-6.1E-19 ± 7.7E-19	8.39E-19 ± 7.54E-20	84%	4.4009	15.39 ± 0.28
17.00	3.21E-15 ± 3.20E-18	5.95E-16 ± 1.21E-18	1.8E-18 ± 5.4E-20	-1.9E-19 ± 7.2E-19	1.76E-18 ± 9.72E-20	84%	4.5120	15.78 ± 0.17
20.00	8.65E-16 ± 4.27E-18	1.54E-16 ± 5.83E-19	2.8E-19 ± 3.0E-20	-2.9E-19 ± 8.0E-19	9.22E-19 ± 7.82E-20	69%	3.8405	13.44 ± 0.54
24.00	7.57E-16 ± 2.82E-18	1.49E-16 ± 7.32E-19	3.1E-19 ± 3.3E-20	-1.4E-18 ± 7.1E-19	4.39E-19 ± 8.18E-20	83%	4.1926	14.66 ± 0.58

Irradiation filename: au8.2c.adl.43.

%P	40Ar(*±atm)	39Ar(K)	38Ar(Cl±atm)	37Ar(Ca)	36Ar(Atm)	%Rad	R	Age (Ma)
6.00	2.69E-15 ± 3.66E-18	9.49E-17 ± 4.85E-19	1.3E-18 ± 1.3E-19	-7.1E-19 ± 8.1E-19	7.85E-18 ± 1.61E-19	14%	3.8536	13.48 ± 1.89
6.50	5.53E-15 ± 7.68E-18	1.21E-15 ± 4.27E-18	3.0E-18 ± 5.7E-20	-2.6E-18 ± 1.6E-18	4.64E-19 ± 8.57E-20	98%	4.4452	15.54 ± 0.09
7.00	8.18E-15 ± 8.28E-18	1.74E-15 ± 4.37E-18	4.6E-18 ± 7.5E-20	1.6E-18 ± 9.3E-19	1.57E-18 ± 7.87E-20	94%	4.4292	15.49 ± 0.06
7.50	5.16E-15 ± 5.60E-18	1.02E-15 ± 3.98E-18	2.4E-18 ± 4.8E-20	1.4E-18 ± 1.1E-18	2.17E-18 ± 8.41E-20	88%	4.4305	15.49 ± 0.11
8.00	1.95E-15 ± 4.75E-18	4.00E-16 ± 1.47E-18	9.6E-19 ± 3.7E-20	-5.7E-19 ± 1.0E-18	5.96E-19 ± 7.84E-20	91%	4.4264	15.48 ± 0.22
8.50	7.08E-15 ± 5.67E-18	1.23E-15 ± 1.94E-18	3.8E-18 ± 6.8E-20	-5.6E-19 ± 1.0E-18	5.04E-18 ± 9.45E-20	79%	4.5218	15.81 ± 0.09
9.00	6.60E-15 ± 9.80E-18	1.38E-15 ± 3.57E-18	3.1E-18 ± 3.7E-20	-5.8E-19 ± 8.2E-19	1.41E-18 ± 1.31E-19	94%	4.4723	15.64 ± 0.11
9.25	1.81E-15 ± 4.06E-18	3.77E-16 ± 1.14E-18	1.0E-18 ± 4.2E-20	-6.3E-19 ± 9.4E-19	5.82E-19 ± 1.17E-19	91%	4.3498	15.21 ± 0.33
9.50	4.40E-15 ± 5.57E-18	8.92E-16 ± 1.87E-18	1.9E-18 ± 3.9E-20	1.2E-18 ± 9.2E-19	1.50E-18 ± 1.21E-19	90%	4.4348	15.51 ± 0.15
9.75	5.46E-15 ± 8.82E-18	1.18E-15 ± 4.01E-18	2.4E-18 ± 4.8E-20	1.7E-19 ± 7.7E-19	6.50E-19 ± 1.18E-19	96%	4.4460	15.55 ± 0.12
10.00	1.81E-15 ± 3.21E-18	3.90E-16 ± 5.11E-19	1.1E-18 ± 4.7E-20	-4.7E-19 ± 8.0E-19	2.27E-19 ± 1.16E-19	96%	4.4613	15.60 ± 0.31
10.25	1.02E-15 ± 4.13E-18	2.20E-16 ± 1.12E-18	3.4E-19 ± 2.0E-20	5.3E-19 ± 9.2E-19	2.61E-19 ± 1.12E-19	92%	4.3056	15.06 ± 0.54
10.50	2.19E-15 ± 4.50E-18	4.72E-16 ± 2.47E-18	1.0E-18 ± 4.0E-20	-1.9E-18 ± 8.5E-19	5.38E-19 ± 1.31E-19	93%	4.3026	15.05 ± 0.30
11.00	2.18E-15 ± 8.85E-18	4.70E-16 ± 1.17E-18	1.1E-18 ± 5.4E-20	5.8E-19 ± 7.9E-19	4.63E-19 ± 1.31E-19	94%	4.3352	15.16 ± 0.30
11.50	2.65E-16 ± 2.88E-18	5.62E-17 ± 4.77E-19	-5.5E-19 ± -8.5E-18	-6.6E-19 ± 9.6E-19	2.61E-19 ± 1.30E-19	71%	3.3395	11.69 ± 2.40
12.50	6.14E-16 ± 3.21E-18	1.33E-16 ± 8.94E-19	1.8E-19 ± 2.0E-20	-1.2E-18 ± 6.8E-19	2.03E-19 ± 1.26E-19	90%	4.1716	14.59 ± 0.99
13.50	2.77E-16 ± 2.95E-18	6.06E-17 ± 9.70E-19	1.4E-20 ± 5.0E-21	-1.2E-18 ± 7.7E-19	2.14E-19 ± 1.26E-19	77%	3.5147	12.30 ± 2.18

Irradiation filename: au8.2c.adl.44.

%P	40Ar(*±atm)	39Ar(K)	38Ar(Cl±atm)	37Ar(Ca)	36Ar(Atm)	%Rad	R	Age (Ma)
6.00	2.79E-15 ± 1.76E-18	2.16E-16 ± 7.97E-19	1.6E-18 ± 9.6E-20	3.9E-19 ± 7.8E-19	6.15E-18 ± 9.33E-20	35%	4.4991	15.73 ± 0.49
6.50	7.05E-15 ± 1.46E-17	1.50E-15 ± 3.98E-18	3.9E-18 ± 6.4E-20	6.3E-19 ± 7.3E-19	1.13E-18 ± 8.43E-20	95%	4.4917	15.71 ± 0.08
7.00	8.37E-15 ± 6.00E-18	1.71E-15 ± 3.50E-18	3.7E-18 ± 6.0E-20	1.8E-18 ± 1.1E-18	2.44E-18 ± 8.66E-20	91%	4.4675	15.62 ± 0.06
7.50	6.27E-15 ± 9.66E-18	1.27E-15 ± 4.30E-18	3.7E-18 ± 7.7E-20	9.1E-19 ± 1.0E-18	1.93E-18 ± 1.74E-19	91%	4.5005	15.74 ± 0.16
8.00	1.27E-15 ± 4.93E-18	2.31E-16 ± 8.79E-19	6.4E-19 ± 2.7E-20	-1.4E-18 ± 6.8E-19	9.75E-19 ± 1.10E-19	77%	4.2193	14.76 ± 0.50
8.50	6.86E-15 ± 3.15E-18	1.31E-15 ± 2.50E-18	3.6E-18 ± 5.9E-20	5.7E-19 ± 9.2E-19	3.21E-18 ± 1.05E-19	86%	4.4960	15.72 ± 0.09
9.00	9.42E-15 ± 1.16E-17	1.79E-15 ± 2.14E-18	5.1E-18 ± 6.0E-20	2.8E-18 ± 1.1E-18	4.57E-18 ± 1.22E-19	86%	4.4907	15.70 ± 0.08
9.25	5.68E-15 ± 1.79E-17	1.17E-15 ± 3.71E-18	2.2E-18 ± 4.1E-20	1.3E-18 ± 7.6E-19	1.46E-18 ± 1.58E-19	92%	4.4963	15.72 ± 0.16
9.50	1.77E-15 ± 6.97E-18	3.73E-16 ± 1.66E-18	3.0E-19 ± 1.6E-20	5.4E-19 ± 9.0E-19	3.24E-19 ± 1.47E-19	95%	4.4913	15.70 ± 0.42
9.75	5.58E-18 ± 1.21E-18	1.21E-18 ± 3.38E-19	-4.5E-19 ± -1.6E-19	-9.8E-19 ± 1.1E-18	-1.60E-19 ± -1.80E-19	945%	43.6593	147.16 ± 153
10.00	1.80E-16 ± 1.57E-18	3.75E-17 ± 4.09E-19	-3.2E-19 ± -1.2E-18	1.4E-18 ± 8.8E-19	1.56E-19 ± 1.46E-19	74%	3.5604	12.46 ± 4.03
10.25	3.80E-16 ± 3.69E-18	8.15E-17 ± 5.73E-19	-3.5E-19 ± -1.5E-19	1.0E-18 ± 7.9E-19	1.12E-19 ± 1.46E-19	91%	4.2514	14.87 ± 1.86
10.50	4.38E-16 ± 2.37E-18	9.09E-17 ± 6.51E-19	1.5E-19 ± 2.9E-20	-1.1E-19 ± 5.4E-19	4.41E-19 ± 1.69E-19	70%	3.3767	11.82 ± 1.93
11.00	1.25E-16 ± 2.37E-18	2.52E-17 ± 2.85E-19	5.7E-20 ± 3.8E-20	-3.8E-19 ± 5.5E-19	7.44E-20 ± 1.78E-19	82%	4.0925	14.32 ± 7.30
11.50	4.48E-17 ± 1.94E-18	9.35E-18 ± 2.54E-19	-7.8E-20 ± -1.0E-18	-8.5E-19 ± 5.3E-19	4.09E-19 ± 1.65E-19	-170%	-8.1284	-28.77 ± -18
12.50	1.36E-17 ± 1.37E-18	1.17E-18 ± 3.04E-19	1.6E-19 ± 1.8E-19	-1.9E-19 ± 7.7E-19	3.48E-19 ± 1.67E-19	-654%	-76.4863	-290.84 ± -183
13.50	9.90E-18 ± 1.55E-18	1.93E-18 ± 3.01E-19	1.0E-20 ± 6.7E-20	-7.2E-20 ± 3.4E-19	4.72E-19 ± 1.66E-19	-1310%	-67.1113	-252.57 ± -104

Irradiation filename: au8.2c.adl.45.

%P	40Ar(*±atm)	39Ar(K)	38Ar(Cl±atm)	37Ar(Ca)	36Ar(Atm)	%Rad	R	Age (Ma)
6.00	2.24E-15 ± 6.20E-18	1.79E-16 ± 1.27E-18	1.4E-18 ± 1.1E-19	1.8E-18 ± 6.9E-19	4.59E-18 ± 1.20E-19	40%	4.9697	17.37 ± 0.79
6.50	4.91E-15 ± 9.14E-18	1.05E-15 ± 2.80E-18	2.9E-18 ± 4.6E-20	2.1E-18 ± 9.9E-19	5.09E-19 ± 9.40E-20	97%	4.5106	15.77 ± 0.11
7.00	1.42E-15 ± 4.33E-18	3.08E-16 ± 2.98E-18	1.0E-18 ± 3.8E-20	-3.6E-19 ± 8.1E-19	5.32E-20 ± 7.79E-20	99%	4.5621	15.95 ± 0.31
7.50	1.24E-15 ± 2.96E-18	2.69E-16 ± 1.24E-18	6.8E-19 ± 4.1E-20	4.2E-20 ± 8.4E-19	1.49E-19 ± 8.71E-20	96%	4.4685	15.62 ± 0.35
8.00	2.85E-15 ± 3.02E-18	5.67E-16 ± 1.68E-18	1.9E-18 ± 8.0E-20	-1.4E-18 ± 8.1E-19	9.10E-19 ± 8.69E-20	91%	4.5561	15.93 ± 0.17
8.50	1.53E-15 ± 3.08E-18	3.27E-16 ± 1.49E-18	8.3E-19 ± 3.5E-20	-3.4E-19 ± 9.4E-19	1.62E-19 ± 9.70E-20	97%	4.5469	15.90 ± 0.32
9.00	4.21E-15 ± 8.14E-18	9.09E-16 ± 2.58E-18	2.2E-18 ± 3.1E-20	-1.3E-18 ± 7.6E-19	2.08E-19 ± 7.63E-20	99%	4.5611	15.95 ± 0.10
9.25	2.96E-15 ± 4.29E-18	6.43E-16 ± 4.60E-18	1.3E-18 ± 3.9E-20	-4.0E-19 ± 6.6E-19	2.32E-19 ± 6.42E-20	98%	4.4876	15.69 ± 0.16
9.50	3.78E-15 ± 5.93E-18	8.29E-16 ± 1.92E-18	1.2E-18 ± 4.3E-20	-4.7E-19 ± 7.8E-19	1.59E-19 ± 7.37E-20	99%	4.4967	15.72 ± 0.10
9.75	2.07E-15 ± 4.57E-18	4.49E-16 ± 1.94E-18	8.3E-19 ± 3.8E-20	-6.5E-19 ± 8.7E-19	2.28E-19 ± 7.37E-20	97%	4.4512	15.56 ± 0.19
10.00	1.42E-15 ± 4.27E-18	3.11E-16 ± 1.11E-18	3.7E-19 ± 3.1E-20	2.1E-19 ± 7.6E-19	1.76E-19 ± 6.74E-20	96%	4.4109	15.42 ± 0.24
10.25	7.68E-16 ± 3.17E-18	1.69E-16 ± 7.01E-19	-3.1E-20 ± -3.6E-21	-2.4E-19 ± 7.8E-19	1.00E-19 ± 7.13E-20	96%	4.3806	15.32 ± 0.45
10.50	2.91E-16 ± 2.53E-18	6.22E-17 ± 8.97E-19	5.6E-20 ± 1.1E-20	1.2E-19 ± 6.0E-19	-1.31E-19 ± -7.38E-20	113%	5.3033	18.53 ± 1.26
11.00	2.14E-16 ± 2.63E-18	4.61E-17 ± 5.00E-19	-1.7E-19 ± -9.1E-20	2.5E-18 ± 7.6E-19	-7.23E-21 ± -8.45E-20	101%	4.7022	16.44 ± 1.91
11.50	1.53E-16 ± 1.76E-18	3.29E-17 ± 5.08E-19	2.0E-20 ± 8.8E-21	-1.5E-19 ± 4.6E-19	-6.46E-20 ± -7.34E-20	112%	5.2295	18.27 ± 2.32

APPENDIX 3
Monitor and Air Data

Monitor Data

Sample	%P	40Ar(*+atm)	39Ar(K)	38Ar(Cl+atm)	37Ar(Ca)	36Ar(Atm)	%Rad	R	J-Value
au5.1e.san.a	27	6.94E-14 ± 5.91E-17	1.23E-14 ± 1.22E-17	3.6E-17 ± 2.5E-19	1.9E-18 ± 4.1E-19	1.14E-20 ± 1.33E-19	1.000	5.6258	0.002782 ± 3.97E-06
b	27	4.03E-14 ± 2.18E-17	7.03E-15 ± 1.22E-17	1.8E-17 ± 1.2E-19	1.8E-18 ± 3.6E-19	3.61E-18 ± 1.10E-19	0.974	5.5850	0.002803 ± 5.73E-06
c	27	5.21E-14 ± 4.01E-17	9.26E-15 ± 1.14E-17	8.4E-17 ± 1.0E-18	1.9E-18 ± 3.4E-19	9.00E-19 ± 8.08E-20	0.995	5.5994	0.002795 ± 4.27E-06
d	27	5.94E-14 ± 1.39E-16	1.06E-14 ± 2.69E-17	2.7E-17 ± 1.3E-19	1.5E-18 ± 3.6E-19	9.58E-19 ± 8.70E-20	0.995	5.6010	0.002795 ± 9.79E-06
e	27	8.36E-14 ± 1.82E-16	1.49E-14 ± 2.97E-17	3.6E-17 ± 2.4E-19	1.2E-18 ± 3.0E-19	1.03E-18 ± 8.95E-20	0.996	5.6098	0.002790 ± 8.33E-06
au8.3k.san.21	21	3.09E-14 ± 2.96E-17	3.82E-15 ± 4.40E-18	9.4E-18 ± 1.2E-19	2.6E-17 ± 1.5E-18	4.74E-19 ± 1.09E-19	0.995	8.0516	0.001944 ± 3.57E-06
22	22	1.89E-14 ± 3.10E-17	2.33E-15 ± 2.35E-18	6.1E-18 ± 9.1E-20	1.1E-17 ± 8.6E-19	5.12E-19 ± 1.34E-19	0.992	8.0194	0.001952 ± 5.60E-06
23	23	1.15E-13 ± 1.32E-16	1.43E-14 ± 2.26E-17	7.2E-17 ± 4.6E-19	8.9E-17 ± 2.5E-18	1.76E-18 ± 1.20E-19	0.995	8.0043	0.001956 ± 3.88E-06
24	24	4.90E-14 ± 5.32E-17	6.04E-15 ± 1.85E-17	1.6E-17 ± 1.1E-19	3.6E-17 ± 1.4E-18	5.69E-19 ± 1.13E-19	0.997	8.0815	0.001937 ± 6.46E-06
25	25	6.01E-14 ± 6.31E-17	7.43E-15 ± 9.49E-18	1.9E-17 ± 1.8E-19	4.8E-17 ± 1.3E-18	8.33E-19 ± 1.11E-19	0.996	8.0487	0.001945 ± 3.40E-06
au8.1g.san.a	27	1.18E-13 ± 9.46E-17	1.48E-14 ± 2.49E-17	4.3E-17 ± 1.9E-19	1.1E-16 ± 7.8E-19	2.17E-18 ± 1.15E-19	0.995	7.9670	0.001965 ± 3.73E-06
b	27	3.47E-14 ± 6.55E-17	4.35E-15 ± 1.36E-17	1.1E-17 ± 1.2E-19	3.0E-17 ± 6.8E-19	1.96E-19 ± 7.08E-20	0.998	7.9769	0.001962 ± 7.26E-06
c	27	1.46E-13 ± 2.99E-17	1.82E-14 ± 1.99E-17	5.0E-17 ± 5.0E-19	1.4E-16 ± 1.5E-18	4.67E-18 ± 1.25E-19	0.991	7.9351	0.001973 ± 2.27E-06
d	27	8.82E-14 ± 1.16E-16	1.10E-14 ± 1.75E-17	2.5E-17 ± 1.8E-19	9.1E-17 ± 1.1E-18	4.66E-19 ± 7.10E-20	0.998	8.0062	0.001955 ± 4.07E-06
e	27	4.80E-14 ± 9.11E-17	5.79E-15 ± 1.16E-17	1.5E-17 ± 1.3E-19	7.1E-17 ± 7.9E-19	5.84E-18 ± 1.13E-19	0.964	8.0023	0.001956 ± 5.78E-06
au8.2j.san.a	27	6.65E-14 ± 5.26E-17	8.19E-15 ± 1.14E-17	2.1E-17 ± 1.9E-19	5.5E-17 ± 8.2E-19	2.39E-18 ± 9.27E-20	0.989	8.0229	0.001951 ± 3.26E-06
b	27	9.97E-14 ± 5.78E-17	1.13E-14 ± 5.53E-18	3.4E-17 ± 1.5E-19	7.4E-17 ± 8.6E-19	2.82E-17 ± 2.50E-19	0.917	8.0492	0.001945 ± 2.25E-06
c	27	5.05E-14 ± 1.78E-17	6.26E-15 ± 4.85E-18	1.5E-17 ± 7.8E-20	4.1E-17 ± 6.0E-19	5.02E-19 ± 9.27E-20	0.997	8.0359	0.001948 ± 1.97E-06
d	27	7.01E-14 ± 4.17E-17	8.49E-15 ± 1.59E-17	2.3E-17 ± 7.0E-20	5.5E-17 ± 1.0E-18	5.82E-18 ± 1.17E-19	0.975	8.0555	0.001943 ± 4.04E-06
e	27	6.13E-14 ± 2.91E-17	7.58E-15 ± 1.26E-17	1.8E-17 ± 1.4E-19	4.8E-17 ± 6.4E-19	2.25E-18 ± 1.13E-19	0.989	7.9960	0.001958 ± 3.58E-06
au8.3k.san.a	27	1.05E-13 ± 5.05E-16	1.34E-14 ± 2.20E-17	3.4E-17 ± 1.4E-19	8.4E-17 ± 8.3E-19	7.06E-20 ± 7.72E-20	1.000	7.8654	0.001933 ± 3.25E-06
b	27	4.18E-14 ± 2.82E-17	5.15E-15 ± 8.55E-18	1.3E-17 ± 8.2E-20	3.5E-17 ± 5.8E-19	2.15E-19 ± 9.03E-20	0.998	8.1084	0.001930 ± 3.68E-06
c	27	1.06E-13 ± 6.49E-17	1.31E-14 ± 2.09E-17	3.5E-17 ± 1.8E-19	8.2E-17 ± 1.1E-18	5.16E-19 ± 9.24E-20	0.999	8.0809	0.001937 ± 3.36E-06
d	27	6.06E-14 ± 3.80E-17	7.46E-15 ± 1.05E-17	1.8E-17 ± 1.8E-19	5.3E-17 ± 8.7E-19	6.20E-20 ± 7.33E-20	1.000	8.1241	0.001927 ± 3.05E-06
e	27	4.33E-14 ± 2.30E-17	5.35E-15 ± 6.78E-18	1.3E-17 ± 8.5E-20	3.1E-17 ± 5.1E-19	1.03E-19 ± 8.72E-20	0.999	8.0821	0.001937 ± 2.90E-06
au8.4a.san.a	27	3.64E-14 ± 2.35E-17	4.37E-15 ± 5.54E-18	1.2E-17 ± 5.2E-20	9.9E-17 ± 1.3E-18	3.25E-18 ± 1.17E-19	0.974	8.1142	0.001929 ± 3.39E-06
b	27	4.13E-14 ± 3.59E-17	5.11E-15 ± 1.19E-17	1.3E-17 ± 1.1E-19	3.4E-17 ± 7.5E-19	4.07E-19 ± 9.22E-20	0.997	8.0652	0.001941 ± 5.01E-06

Monitor Data (*cont.*)

Sample	%P	40Ar(*+atm)	39Ar(K)	38Ar(Cl+atm)	37Ar(Ca)	36Ar(Atm)	%Rad	R	J-Value
c	27	1.23E-13 ± 5.34E-17	1.52E-14 ± 1.43E-17	3.9E-17 ± 2.2E-19	1.0E-16 ± 1.1E-18	8.60E-19 ± 1.06E-19	0.998	8.0789	0.001937 ± 2.07E-06
d	27	1.38E-13 ± 5.38E-17	1.71E-14 ± 1.52E-17	4.3E-17 ± 2.1E-19	1.1E-16 ± 1.8E-18	1.10E-18 ± 1.16E-19	0.998	8.0691	0.001940 ± 1.95E-06
e	27	1.04E-13 ± 4.89E-17	1.24E-14 ± 1.01E-17	3.7E-17 ± 2.1E-19	2.4E-16 ± 1.5E-18	2.18E-18 ± 1.32E-19	0.994	8.3307	0.001879 ± 1.91E-06
au8.5i.san.a	27	3.31E-14 ± 2.11E-16	4.17E-15 ± 2.93E-17	9.7E-18 ± 8.0E-20	3.2E-17 ± 4.6E-19	4.30E-19 ± 1.06E-19	0.996	7.9014	0.001981 ± 1.90E-05
b	27	9.01E-14 ± 7.81E-17	1.13E-14 ± 2.04E-17	2.9E-17 ± 1.1E-19	7.2E-17 ± 1.4E-18	8.37E-19 ± 1.12E-19	0.997	7.9461	0.001970 ± 4.01E-06
c	27	3.70E-14 ± 3.03E-17	4.66E-15 ± 7.99E-18	1.1E-17 ± 1.0E-19	2.8E-17 ± 6.6E-19	7.22E-19 ± 1.10E-19	0.994	7.8992	0.001982 ± 4.18E-06
d	27	2.78E-14 ± 2.44E-17	3.49E-15 ± 1.00E-17	8.4E-18 ± 1.1E-19	2.5E-17 ± 7.4E-19	5.03E-19 ± 1.08E-19	0.995	7.9197	0.001976 ± 6.40E-06
e	27	4.14E-14 ± 3.95E-17	5.17E-15 ± 7.32E-18	1.5E-17 ± 1.9E-19	3.6E-17 ± 7.4E-19	5.67E-19 ± 1.07E-19	0.996	7.9804	0.001961 ± 3.68E-06

Air Standard Data

Date	40Ar(*+atm)	39Ar(K)	38Ar(Cl+atm)	37Ar(Ca)	36Ar(Atm)	(40/36)m	(40/38)m	M. Fract
1/26/07 a	1.15E-13 ± 4.92E-17	-5.79E-18 ± 4.86E-19	7.29E-17 ± 4.94E-19	5.00E-19 ± 1.37E-19	3.85E-16 ± 1.94E-18	298.7	1577	1.0027
b	1.12E-13 ± 7.40E-17	-4.56E-18 ± 7.28E-19	7.37E-17 ± 9.71E-19	-1.17E-19 ± 2.02E-19	3.76E-16 ± 1.59E-18	297.8	1519	1.0019
c	8.58E-14 ± 3.71E-17	-3.07E-18 ± 7.53E-19	5.42E-17 ± 5.75E-19	-1.64E-19 ± 1.84E-19	2.85E-16 ± 1.32E-18	300.7	1583	1.0044
1/27/07 b	1.11E-13 ± 5.77E-17	-7.68E-18 ± 5.35E-19	7.08E-17 ± 6.73E-19	4.91E-20 ± 2.03E-19	3.77E-16 ± 1.76E-18	295.7	1573	1.0002
1/28/07 a	1.16E-13 ± 1.00E-16	-3.90E-19 ± 3.10E-19	7.40E-17 ± 6.67E-19	8.32E-19 ± 1.81E-19	3.83E-16 ± 1.50E-18	301.7	1561.5	1.0052
b	1.15E-13 ± 1.41E-16	-5.93E-20 ± 2.57E-19	7.33E-17 ± 5.21E-19	9.75E-19 ± 1.63E-19	3.84E-16 ± 1.73E-18	299.1	1564.7	1.0
1/29/07 a	1.17E-13 ± 1.93E-16	-7.26E-18 ± 4.42E-19	7.39E-17 ± 7.39E-19	5.34E-19 ± 2.82E-19	3.91E-16 ± 9.14E-19	300.2	1590.1	1.0
b	1.14E-13 ± 7.18E-17	-6.75E-18 ± 4.47E-19	7.20E-17 ± 5.67E-19	2.04E-19 ± 1.35E-19	3.80E-16 ± 8.96E-19	299.6	1579.9	1.0
1/30/07 a	1.15E-13 ± 8.00E-17	-6.15E-18 ± 4.25E-19	7.30E-17 ± 7.83E-19	3.17E-19 ± 1.62E-19	3.85E-16 ± 6.52E-19	299.0	1577.0	1.0
b	1.14E-13 ± 1.70E-16	-7.03E-18 ± 4.07E-19	7.23E-17 ± 5.32E-19	2.22E-19 ± 1.82E-19	3.81E-16 ± 6.63E-19	299.0	1576.4	1.0
c	1.08E-13 ± 3.69E-17	-6.53E-18 ± 3.94E-19	6.95E-17 ± 5.41E-19	-1.19E-20 ± 1.91E-19	3.63E-16 ± 6.05E-19	298.9	1561.6	1.0
1/31/07 a	1.19E-13 ± 1.17E-16	-6.46E-18 ± 4.38E-19	7.80E-17 ± 1.34E-18	4.86E-20 ± 2.11E-19	4.00E-16 ± 1.98E-18	298.5	1531.6	1.0
b	1.16E-13 ± 3.39E-17	-6.37E-18 ± 4.98E-19	7.35E-17 ± 5.82E-19	4.41E-20 ± 1.26E-19	3.88E-16 ± 7.57E-19	297.8	1572.4	1.0
2/2/07 a	1.13E-13 ± 5.44E-17	-6.45E-18 ± 4.66E-19	7.22E-17 ± 4.95E-19	7.23E-20 ± 1.56E-19	3.77E-16 ± 7.86E-19	300.1	1568.4	1.0
2/4/07 a	1.17E-13 ± 4.41E-17	-6.22E-18 ± 3.06E-19	7.34E-17 ± 5.88E-19	1.86E-19 ± 2.04E-19	3.89E-16 ± 8.17E-19	299.3	1586.2	1.0
3/3/07 a	1.17E-13 ± 1.37E-16	-4.04E-18 ± 5.60E-19	7.50E-17 ± 6.70E-19	9.16E-20 ± 1.82E-19	4.02E-16 ± 1.60E-18	290.5	1558	0.9958
b	1.18E-13 ± 1.15E-16	-7.11E-18 ± 4.24E-19	7.68E-17 ± 7.26E-19	6.57E-19 ± 2.20E-19	4.06E-16 ± 1.10E-18	291.7	1542	0.9968
c	1.17E-13 ± 2.22E-16	-5.93E-18 ± 8.00E-19	7.76E-17 ± 1.40E-18	-9.92E-20 ± 3.17E-19	4.02E-16 ± 1.78E-18	291.0	1509	0.9962
3/4/07 a	1.15E-13 ± 3.66E-16	-7.33E-18 ± 4.62E-19	7.47E-17 ± 6.25E-19	4.27E-19 ± 2.45E-19	3.95E-16 ± 2.27E-18	291.2	1540	0.9963
b	1.15E-13 ± 2.00E-17	-7.05E-18 ± 5.56E-19	7.51E-17 ± 1.04E-18	2.10E-19 ± 2.03E-19	3.97E-16 ± 7.37E-19	289.0	1528.0	0.9945
3/5/07 a	1.18E-13 ± 4.46E-17	-6.90E-18 ± 4.95E-19	7.59E-17 ± 6.03E-19	-1.48E-21 ± 1.79E-19	4.07E-16 ± 9.19E-19	290.2	1556.1	0.9956
b	1.20E-13 ± 6.23E-17	-7.77E-18 ± 2.89E-19	7.56E-17 ± 9.63E-19	-6.21E-20 ± 1.25E-19	4.15E-16 ± 9.72E-19	289.3	1589.6	0.9948
3/6/07 a	1.16E-13 ± 8.35E-17	-6.44E-18 ± 5.50E-19	7.49E-17 ± 9.55E-19	-2.27E-21 ± 1.74E-19	4.03E-16 ± 1.69E-18	287.9	1548.6	0.9936
b	1.16E-13 ± 8.35E-17	-1.50E-17 ± 3.85E-19	7.33E-17 ± 9.54E-19	-1.26E-18 ± 1.76E-19	4.02E-16 ± 1.69E-18	288.5	1581.2	0.9941
3/7/07 a	6.95E-14 ± 6.85E-17	-3.88E-18 ± 4.69E-19	4.43E-17 ± 3.51E-19	-4.36E-19 ± 1.62E-19	2.40E-16 ± 1.09E-18	289.1	1566.7	0.9946
3/8/07 a	1.15E-13 ± 6.88E-17	3.02E-18 ± 7.28E-19	7.58E-17 ± 3.26E-19	1.23E-18 ± 1.49E-19	3.93E-16 ± 9.16E-19	292.0	1513.1	0.9971
b	6.65E-14 ± 2.46E-17	-2.05E-18 ± 5.55E-19	4.28E-17 ± 4.17E-19	8.59E-21 ± 1.24E-19	2.28E-16 ± 6.15E-19	291.8	1554.7	0.9968
3/9/07 a	6.81E-14 ± 7.06E-17	-3.98E-18 ± 2.21E-19	4.36E-17 ± 2.80E-19	3.09E-19 ± 1.48E-19	2.33E-16 ± 4.67E-19	292.0	1560.5	0.9971